UNIVERSITY OF SOUTHAMPTON

FACULTY OF ENGINEERING AND APPLIED SCIENCE

INSTITUTE OF SOUND AND VIBRATION RESEARCH

Predicting Variability in Environmental Noise Measurements

by

Javier Alberola

A thesis submitted for the degree of

Doctor of Philosophy

April 2005

UNIVERSITY OF SOUTHAMPTON

ABSTRACT

Doctor of Philosophy

Predicting Variability in Environmental Noise Measurements

by Javier Alberola

The general subject of this thesis is the study and quantification of noise level variability. Environmental noise assessments focus on standard methods to calculate or present measured noise levels which pay no attention to the actual variability underlying in-situ field measurements. This often leads to output data which do not fully represent received noise levels in measurements, and which create a common source of misinterpretation when justifying planning, legal and compensatory decisions based on these results.

To tackle this problem, the thesis first investigates the statistical variability associated with a large measurement database acquired under field conditions. The results show a strong inverse relationship between measured variability (standard deviations) and mean noise levels. The investigation also reveals that the source-receiver distance and the meteorological conditions have strong effects on the measured standard deviations. Searching for a quantitative explanation of this relation, a flat ground acoustical propagation test was carried out under controlled conditions. The results provide a detailed breakdown of the different contributions that each variable has on the measured noise level variability. Another flat ground experiment was carried out in a different location and only over one day to account for the effect of short-term atmospheric turbulence. The experimental data obtained allowed understanding and adjusting the more significant parameters to develop a turbulence model within the Parabolic Equation sound propagation method.

All the obtained results give an insight of sound level variability in three different situations: when having multiple environmental sources (urban-residential areas) and in both mid-term and short-term atmospheric conditions. It is anticipated that this study may be of assistance when predicting environmental noise level variability or dimensioning the uncertainty in common calculated noise levels.

Table of Contents

List of Figures

List of Tables

Acknowledgements

List of notation

∇^2	Laplacian operator
A, B	Modulus of a sound pressure wave
A_{atm}	Absorption of sound in air
A_{div}	Geometrical spreading attenuation factor
A_E	Excess attenuation
A_{gr}	Ground attenuation
c	Sound speed (m/s)
C	Substituting variable in Delany's formula for calculating Z
C(s)	Autocorrelation function describing atmospheric turbulence
c_0	Reference sound speed (m/s)
C_{met}	ISO 9613-2 method's factor to take into account the meteorology
d	Distance defined in both Figure 3.16 and Figure 3.17
d', r	Distance from a noise source in metres
d_1	Distance from the source to the edge of the screening object
d_2	Distance from the edge of the screening object to the receiver
d_3	Direct distance from source to receiver
DI	Directivity index (dB)
d_x	Horizontal distance from source to receiver
D_z	Screening attenuation
E	Arbitrary scalar field
e	Unit vector perpendicular to a wavefront
F	Fourier transform
f	Frequency (Hz)
F	Mathematical expression related to the complex error function of w
F^{-1}	Inverse Fourier transform
F_N	Vibrational relaxation frequency of nitrogen
F_O	Vibrational relaxation frequency of oxygen
g	Sound-speed gradient
H	Molar concentration of water vapour (%)
$H_0^{(1)}$	Zeroth-order Hankel function of the first kind
$H_0^{(2)}$	Zeroth-order Hankel function of the second kind

h_i	Height from the ground at a certain point i in metres
H_n	Height at zenith of a sound ray with n reflections on the ground
h_r	Height of the receiver
h_s	Height of the source
I	Acoustic intensity (watts/m^2)
K	Constant ($=c_0/\cos\emptyset_0$)
k	Wavenumber
k_0	Reference wavenumber
k_T	Increase rate of the sound speed with height due to temperature
k_x	Wavenumer in the x direction
k_y	Wavenumer in the y direction
k_z	Wavenumer in the z direction
l	Correlation length
L	Monin-Obukhov length
$Lft(i)$	Sound level at the receiver fro each nominal frequency of the octave band
L_p	Sound pressure level (dB re $2\cdot10^{-5}$watts)
L_w	Sound power level (dB re 10^{-12}watts)
m	Number that stands for atmospheric stability
n	Refractive index
$\emptyset$	Angle of incidence
$\emptyset$	Angle of propagation referred to the horizontal
$\emptyset_0$	Launch angle
$p(r)$	Sound pressure at a radial distance r (N/m^2)
P, p	Acoustic pressure
P_d	Direct pressure contribution at the receiver
P_e	Environment atmospheric pressure in Pascal
p_i	Incident pressure wave
p_r	Reflected pressure wave
P_{ref}	$2\cdot10^{-5}$watts
P_{sat}	Air pressure at water saturation
P_{so}	Reference atmospheric pressure ($=101.325$ kPa)
P_{sr}	Specularly reflected pressure contribution at the receiver
P_t	Total pressure at the receiver
R	Plane-wave reflection coefficient. It can also denote receiver location

R'	Receiver location in the curved ground analogy
r_1	Incident sound ray path
r_2	Reflected sound ray path
R_c	Radius of curvature
RH	Relative humidity
s	Measure of the distance along a sound ray, that is, path length
S	Source location
S'	Source location in the curved ground analogy
T	Temperature (Kelvin)
T_0	Reference ambient temperature
T_{01}	Triple point isotherm temperature (T=273.16 Kelvin)
u	Intermediate substituting variable of Φ (= $u(r,z) \cdot v(r)$)
u'	Mean flow velocity
u_n	Normal particle velocity
v	Intermediate substituting variable of Φ (= $u(r,z) \cdot v(r)$)
v_h	Wind speed as a function of height
v_{ref}	Wind speed at a reference height
w	Numerical distance
W	Sound power level in watts
$W(k_1,k_2)$	Wavenumber spectrum
W_{ref}	10^{-12} watts
x	Coordinate denoting range
$x_{R'}$	x-coordinate at the receiver when using the curved ground analogy
z	Coordinate denoting height
Z	Normal acoustic impedance of the ground surface
z_0	Coordinate z for the source location
Z_0	$\rho_0 c_0$
z_{eq}	Equivalent distance for screening attenuation calculations
z_L	Surface roughness length
z_r	Coordinate z for the receiver location
$z_{R'}$	z-coordinate at the receiver when using the curved ground analogy
z_s	Coordinate z for the source location
α	Absorption coefficient of sound in air (in dB/100m)
β	Attenuation coefficient in dB/λ

γ_T	Increase rate of the sound speed with height
λ	Wavelength
μ	Fluctuations in the refractive-index representing atmospheric turbulence
μ_0	Root-mean-square fluctuation of $\mu(r,z)$
ρ_0	Ambient air density (=1.2 Kg m^{-3})
$\rho_0 c_0$	Acoustic impedance of air (415 rayls)
σ	Standard deviation
σ_{1h}	Standard deviation of 1hour LAeq values
σ_{1min}	Standard deviation of 1min LAeq values
σ_e	Effective flow resistivity (Pa·s/m^2)
σ_f	Flow resistivity
φ	Argument (phase) of a sound pressure wave
Φ	Sound wave field
ψ	Angle defined in Figure 3.16
ψ_m	Mathematical function depending on h and L
ω	Angular frequency

Chapter 1

Introduction

1.1. Problem and objectives

This thesis is about the understanding and prediction of sound level variability arising in the practical measurement of environmental noise. In recent years noise control policies have become a need for the society, as a result of searching for noise protection measures against the irrepressible increase of environmental noise sources such as aircraft and motor vehicles. It is claimed that around 20 per cent of the European Union's population (80 million people) are exposed to unacceptable noise levels (European Commission Green Paper). In addition, it is also claimed that a further 170 million Europeans live in so called grey areas, where noise levels are such as to cause serious annoyance during the day time. In sum, it is generally accepted that noise is one of the main local environmental problems and that the data currently available on environmental noise exposure is poor.

In that respect, government departments and local authorities are pursuing ways to identify and quantify the scale of noise problems, activate action plans to reduce noise and protect community areas from inappropriate noise exposure levels. Such aims are currently addressed by the creation of "state-of-the-art" noise maps, which are produced by using acoustic calculation methods adopted within specialised software, and are generally validated against a set of in-situ noise measurements.

The noise mapping technique can relatively easily provide predicted noise level contours in areas sizing from small residential neighbourhoods (see Figure 1.1) to the extension of cities. Regardless the measurement validation, generating a noise map of an existing or future environmental scenario is as simple as feeding a computer with geographical and noise-related data and clicking the start button. The flexibility of this technique, its low-cost and its capacity to cover extensive areas without requiring a substantial amount of in-situ noise measurements have made it specially attractive and popular.

Indeed the potential advantages of this modern mapping method have rapidly aroused much interest amongst noise professionals and government departments, which have seen this new technology as a suitable aid for the development of planning controls and action plans to reduce noise in both rural and urban areas – as shown by both European (European Commission directive) and national (DEFRA) proposals for assessing and managing environmental noise.
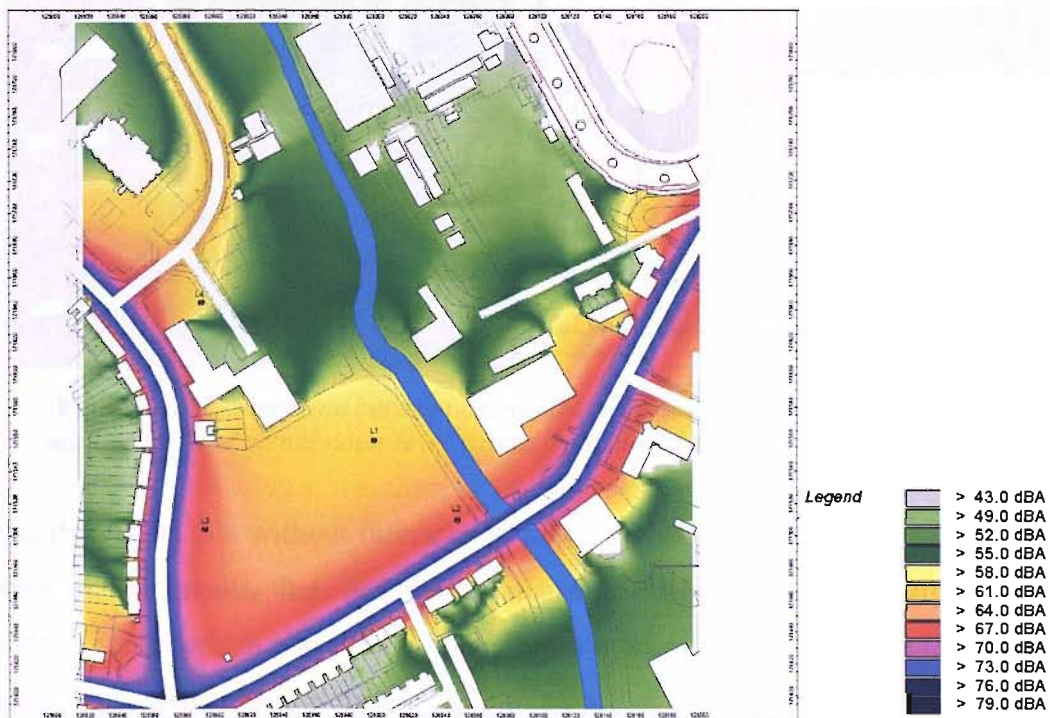
Figure 1.1 *Example of a 2D noise mapping of a small area in London.*

The promising capabilities and the success of current noise mapping methods might, however, provide a false impression of the limitations of their results. The noise map shown in Figure 1.1, for instance, looks professional and informative, but

when one wants to extract noise level information, one realises that the colour-noise conversion in which the noise map is presented is very ambiguous. Furthermore, when it comes to validating the output results against environmental noise measurements, one notices that received noise levels vary over time and space whereas predicted noise levels do not take into account this variation (see Figure 1.2). This ambiguity in both data presentation and validation might make the map reader fall into an error when interpreting results. This is especially the case when the public, politicians and acousticians fully rely on the calculated sound levels to justify planning, legal and compensatory decisions, ignoring the variability and the real representativeness of the output data generated by the models. To the extent that an incorrect interpretation could potentially result in the inefficiency of noise action plans, unfair applications of noise management restrictions, or adverse health or social consequences.
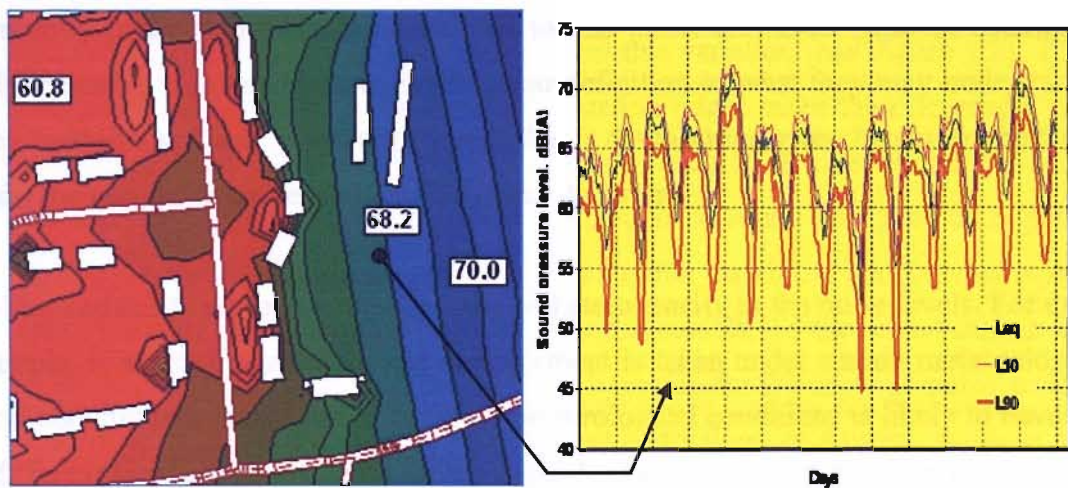
Figure 1.2 *Comparison between calculated noise levels by noise mapping techniques(left) and actual noise level values from in-situ noise measurements (right).*

It is then clear that without information on the variability arising in environmental noise measurements, there is a risk of misinterpretation of both measured and predicted results, which can lead to inappropriate noise management decisions being taken. The current procedure to tackle this problem is to represent the central tendency from a long-term environmental noise situation. In this respect, the (European Noise Directive), for example, specifies that the Lden, Lday, Levening, and Lnight noise indicators might be determined over a 'relevant year as regards the emission of sound and an average year as regards the meteorological conditions'.

While the intention is clear, that the indicators should be representative of long term average conditions, the Directive does not require any indication of the measured variability. This indication would provide the additional information needed to have a complete representation of any long-term environmental noise situation.

Additionally, given that it is not feasible to measure for such a long term and cover different locations, experienced acousticians tend to measure for a shorter, but still representative period and extend the results for a "relevant" or "average" year. However, this practical solution originates another type of uncertainty into the problem, as there is not a standard procedure to shorten the measurement either. In these terms, (Ten Wolde), as one of the chief architects of the European Noise Directive, has identified the problem and has already suggested that the estimation and management of uncertainties involved in noise measurement and prediction should be one of the priorities for future research. Inspired by this idea, other authors have recently made significant contributions to this issue. However, prior to detailing their results, it is important to have a clear definition of what they may understand by "uncertainty" and "variability", and what is the meaning given herein. In the thesis, the two terms are related but in essence different:

-The variability represents the diversity or heterogeneity in the noise levels. For example, if an environmental noise measurement is taken under certain meteorological conditions and repeated with other meteorological conditions is likely to have a different level which accounts for the natural variability of the environment. Using more measurements or increasing the precision of the measurements will not remove this variability, but it can provide a better indication of its magnitude.

-Uncertainty can be differentiated from variability because it refers to the lack of knowledge in the deviations of measured or calculated values from a "true or real value". There are at least two kinds: measuring and modelling uncertainties. For example, measuring uncertainty results when non-representative sampling (to measure the distribution of noise levels) gives sampling errors. Modelling uncertainty results, for example, from simplifications in the calculation methods or errors in the model input data (Alberola-Asensio, J. et al). In this context, measuring uncertainty should not be confused with 'inaccuracy'. Inaccuracy is a term which ap-

plies to the measurement process, whereas measuring uncertainty is a term which applies to the result of that measurement. Hence, it would be correct to describe a measurement process as being accurate or inaccurate, and incorrect to describe it as being certain or uncertain; however, the result of that measurement could be characterised, for example, as being uncertain. As another example, you can have an inaccurate measurement which is certain because the inaccuracy is known.

When referring to the work of others, they may be using 'variability' and 'uncertainty' in a different way. Some authors consider the central tendency of the environmental noise measurements as the "true or real value", and the actual variability of the measurements as the uncertainty (deviations from this "true" value). In contrast, the meaning adopted in this thesis is that any of the levels in an environmental measurement database are not deviations from an artificial "true" value, but true or real values in itself with their own associated measuring uncertainty (which arises from the lack of knowledge in the working accuracy of our equipment at the time of the measurement).

A clear example of how some authors tend to use the word uncertainty as a synonym for variability is the work presented by (Craven, et al). Craven's reference to uncertainty in environmental noise measurements is associated with "factors influencing the source and propagation path rather than instrumentation shortfalls" while in this thesis, Craven's definition stands more for the intrinsic environmental noise variation in the measurements. To keep the terminology uniform throughout the thesis, whenever the words uncertainty and variability appear in the text (even when discussing the work of others), they must be understood as terms with different meanings: Variability will always describe the heterogeneity in the received noise levels, and uncertainty will always refer to the lack of knowledge regarding the actual levels of a measurement (measuring uncertainties) or of a calculation method (modelling uncertainties).

Despite the difference in terminology, Craven's work is particularly relevant as it is one of the few contributions that tackles the problem of noise variability (in his work described as "uncertainty"). (Craven, et al) identifies and classifies in a clear way the different factors influencing environmental noise levels, and recommends a

method to estimate the overall noise level variability by aggregating the different contributions of each of the identified factors. His method has, however, a questionable validity as it applies an uncertainty estimation method to predict the variability, when, following conventional practice, it should be the other way round: variability should be used to predict uncertainty.

Other authors have focused on the estimation of modelling uncertainties. Both (Probst, W., et al) and (Manvell, D. et al) have recommended methods to quantify the uncertainty in noise mapping calculations through an uncertainty budget system, consisting in adding separate uncertainties associated with each of the variables affecting the calculated noise levels. Uncertainties in this case are mainly estimated by using a scientific judgement or a general knowledge rather than a repeated set of observations.

The investigation reported in this thesis follows a different approach. It is clear that the variability in measurements contributes to difficulties in finding the best way to represent measured data and also to compare predicted and measured noise levels. However, there are parts of the problem that can be solved, and that can serve as both a practical assistance for predicting variability with limited resources and a research line to achieve better environmental noise calculation methods in the future. The approach followed here is to study which input variables are most closely associated with (and hence predictive of) measured variability (as described by standard deviation), and then develop predictive models which could be used to estimate variability associated with future measurements or calculation exercises. To reach that objective, three different areas have been investigated:

First, based on a large measurement database consisted of 2 week's noise recordings at each of 50 separate locations (henceforth described as the 50 site database), different environmental variables were investigated as to how they have an influence on noise level variability. The study provides a general view of which are the main causes and their relationships to the overall noise level variability associated with common environmental noise measurements.

Second, having reviewed the conclusions of the 50 site database, the next step was to pursue a quantitative and deeper explanation of the meteorological effects on noise variability. Under such a goal, a flat ground acoustical propagation test was carried out under controlled conditions under the European Joule III project framework (henceforth named Joule database). The exercise was undertaken over a two week monitoring period to account for the diurnal and nocturnal meteorological variations, and for synoptic weather variations arising from passing pressure systems which occur typically over a few days.

Third, an additional and more detailed acoustical propagation exercise (henceforth described as Salisbury Plain database) was carried out to account for the effect of short-term atmospheric turbulence. The recording time comprised only 8 hours, but the acoustical test involved features which were not used in previous exercises, like tonal source signals, and audio recordings. All these features allowed analysing the rapid fluctuations in noise levels arising under a turbulent atmosphere and understanding the relationship between atmospheric turbulence and noise variability.

With these three case studies, the work reported here aims to assist in finding alternative and more efficient ways to estimate environmental noise variability: First, by understanding how fluctuations in environmental variables are related to noise level variability, and second, by developing predictive models which could be used to estimate variability arising: a) in mid-term practical measurements of environmental noise, b) under both mid-term and c) short-term (turbulence) meteorological conditions.

1.2. Outline of the thesis

The thesis is hence structured following the three main areas indicated above. Each of them includes its own literature review, its own experimental work and its own conclusions.

In Chapter 2 is tackled the problem of noise variability and uncertainties arising in practical environmental noise measurements. The chapter starts reviewing the current knowledge of the noise level variability estimation and its direct relation to the

uncertainty associated with output data predicted by current acoustical calculation models. This link is explained under the assumption that actual field measurements set an upper limit to the level of accuracy that computational prediction methods could reach in practice. The review also examines the causes and variables affecting road traffic as one of the predominant and most generalized noise sources in environmental noise.

All this information suggests that the lack of a standard procedure to take noise level variability into account is one of the main reasons why disagreements appear when applying regulations and specifications. Providing information on variability is essential for a correct noise measurement interpretation, and for facilitating suitable comparisons, either among measured levels or with predicted values produced by current calculation methods. The work presented in this chapter contributes to solve this general problem by investigating the statistical variability associated with a large measurement database acquired under field conditions. The database consists of 2 week's noise recordings at each of 50 separate locations in residential areas affected mainly by road traffic noise. The results show a strong inverse relationship between measured variability (standard deviations) and mean noise levels. The investigation also reveals that the meteorology and the source-receiver distance have a significant influence on the variability arising in the 50 measurement locations.

Developing a quantitative explanation of the meteorological and source-receiver distance influence on noise level variability, Chapter 3 studies the variation arising under long-term meteorological conditions through a flat ground sound propagation test (the Joule database). The beginning of this chapter examines some aspects of the current knowledge of outdoor sound propagation, especially the way in which both the atmospheric-acoustic scenario and the different physical phenomena affecting sound propagation are understood within current acoustical calculation methods. Amongst all these sound propagation methods, the text introduces the fundamentals and limitations of the current ray acoustics theory, as this will be essential to understand the key points of the work reported further. The chapter continues with the experimental description of the Joule database. The test was undertaken with the purpose of analysing the effects of mid-term meteorological conditions on

outdoor noise measurements in a series of different distances from a controlled point source.

The Joule database is on a much more minor scale and under a much simpler environmental scenario than the 50 site database, but this simplicity allowed a better monitoring of the relations between noise level variability and the measured environmental parameters. Subsequent theoretical modelling took into account predicted variability associated with small changes in source sound power output; changes in atmospheric absorption arising under different atmospheric conditions; and changes in upwards or downwards sound ray curvature arising under different vertical sound speed profiles. The effects of downwards sound ray curvature conditions were modelled by using a heuristic ray-tracing model. The effects of upwards sound ray curvature conditions were modelled by extending the existing curved ground analogy with the use of diffraction theory.

Chapter 4 deals with a more specific problem: The effects of atmospheric turbulence on the short-term noise level variability. In this case, a shorter but more detailed flat ground acoustic propagation test was carried out in Salisbury Plain under controlled conditions. The theoretical modelling for this exercise was based on the Parabolic Equation method, which was properly reviewed and compared against other numerical methods at the beginning of the chapter. Amongst the different PE solution techniques, the Fourier Split Step transform scheme, commonly used in underwater acoustics, was developed and adapted here for modelling our sound propagation test. Additionally, a turbulence model, based on a Gaussian autocorrelation function, was implemented within the PE algorithm. The Gaussian turbulence spectrum is in overall terms less realistic than other models, such as the von Kármán spectrum (Salomons, E.M), however its use is justified because the Gaussian spectrum, with proper values of its parameters, reaches a good agreement with the actual spectrum in the relevant wave number range for our acoustic experiment (1-30 m^{-1}) (Wilson DK, et al.). The comparison between the measured noise variability and the predicted variability was carried out by running 100 realizations of the turbulence model for each of the frequencies considered in the test.

Chapter 5 summarises all the different contributions to knowledge as compared to the knowledge currently available to provide a final conclusion and a generic view of the developed work. The chapter gathers all the findings described throughout the thesis, gives a meaning of the work as a whole, and suggests applications and additional research lines related to the prediction and use of environmental noise level variability.

1.3. Contributions to knowledge

Section 1.1 has made quite clear that outdoor sound levels can vary over a wide range under different environmental conditions. This can contribute to uncertainty when applying standards and regulations as they do not take this variation into account. As a significant input to this technical debate, this PhD contributes to knowledge by presenting which are the constituent elements of the problem and in which way it has to be managed in practice to minimise the effects of variability arising in practical measurements of environmental noise. The work reported in this thesis might help when developing procedures to provide a representative indication of measurement variability, so that results could be compared and be used as a testing reference against predicted noise levels obtained by new computational noise mapping tools. The thesis puts special emphasis on assisting in the construction of a readily implemented, easily understood and generally accepted procedure for characterising the representativeness of measured noise levels.

For achieving this main goal, a number of different measurement exercises have been undertaken. Each of these exercises has been designed for analysing the noise level variability underlying outdoor measurements, but each of them covering a specific area about environmental noise. Simultaneously, some theoretical modelling has helped in the measurement analysis, and has brought into play some technical contributions related to the application and implementation of sound calculation methods. All these contributions are listed in detail below, following the chapter structure of the thesis.

In Chapter 2, the study of the 50 site database reveals some useful correlations to estimate variability in practical measurements of environmental noise. The analysis

of this large database shows a strong inverse relationship between measured standard deviations of hourly LAeq levels and overall average noise levels measured in a variety of different situations. The measurement database is in itself a contribution to knowledge because of its extension over time and space, but the so-found trends are substantially more important with regard to the ultimate goal of the thesis. The measurement analysis also reveals that the measured noise variability is strongly linked to other variables, such as the meteorology or the source-receiver distance. The 50 site database did not contain meteorological and noise source data to a sufficient level of detail to justify a quantitative explanation of the found relationships, thereby they have been only explained qualitatively here. However, a quantitative and more detailed explanation of some of these relationships was obtained through the study of both the Joule and Salisbury Plain databases.

Chapter 3 investigates the noise variability arising under mid-term meteorological conditions over a number of different distances through the Joule database. A theoretical model was designed for developing the analysis: The effects of downwards sound ray curvature conditions were modelled by using a heuristic ray-tracing model, while the effects of upwards sound ray curvature conditions were modelled by expanding the existing curved ground analogy with the use of diffraction theory. The results showed good agreement between the theoretical predictions and the empirical data obtained under actual field conditions. Over the shorter source to receiver distances, the experienced small noise level variability arose mostly from changes in measured source sound power output and predicted changes in atmospheric absorption rates. At increasing source to receiver distances, the predicted effects of either upwards or downwards sound ray curvature became increasingly dominant as compared to other factors.

The Salisbury Plain database is described in Chapter 4. This loudspeaker test is shorter in time, but with a more detailed environment monitoring than the Joule database. The study pursues a better understanding of the effects of atmospheric-turbulence on noise level variability. The preliminary analysis of the measured data shows actual attenuation over long distances, and how the longer time average attenuations vary at different frequencies while the short time averages vary a lot and by an increasing amount at increasing distances even though the met data only var-

ies over a limited range. The theoretical modelling used for a further analysis is based on the Parabolic Equation. This numerical method is implemented with an additional turbulence model, based on a Gaussian autocorrelation function driven by two parameters (the correlation length and the magnitude of the fluctuations). The comparison between the turbulence model and the experimental data allows a better understanding of atmospheric turbulence and a possible adjustment between modelling parameters and reality.

The theoretical models of Chapter 3 and 4 were used as predictive tools for modelling noise level variability. They were not designed to predict noise levels, but the range of variation in measurements. However, the core of the models was based on noise calculation methods (mainly ISO 9613 for Chapter 3 – Joule database, and the PE method for Chapter 4 –Salisbury Plain database). This arises from the fact that any prediction of variability ranges must be fixed on a correct central tendency, otherwise the prediction would be of no use. In the predictions reported in Chapter 3 and 4, the procedure has been: First to calculate the central tendency by using the ISO and the PE methods respectively, then validate the calculated noise levels against the measured values, and finally develop additional theoretical modelling within the aforementioned methods to provide a prediction of the noise level variability.

Chapter 2

General Levels of Variability

2.1. Introduction

This section is about the study of noise level variability from the view of a practical and generic environmental noise survey. The investigation of this large and varied measurement database acts as a basis for identifying and exploring all the different causes, factors and variable interactions associated with the environmental noise level variability – specially that arising from road traffic. The knowledge acquired with this section assists further in the thesis with the selection of those variables which require a more detailed investigation and with the design of subsequent experimental work.

In the study presented here, our first task has been to analyse the statistical variability arising in the measurements. For this analysis, the measuring uncertainty has been neglected, as for environmental noise measurements the range of variation generated by factors influencing the source and propagation path rather is usually more significant than the range of uncertainty associated with instrumentation shortfalls. Nevertheless, for more detailed information about factors influencing the instrumentation, standards and specifications on uncertainties in laboratory-based measurements can be consulted.

2.2. Literature review

It is clear that environmental noise levels vary over time and space, but the lack of consensus as to how to take into account this variability can contribute to disagreement and dispute when applying standards and regulations. Measurements and calculations are necessarily expressed as single values, but often without reporting the representativeness of these single values as compared to the potential wide range of values that may occur in actual field measurements. Noise assessment based on measured or calculated data of unknown representativeness could lead to inappropriate noise management decisions. There is therefore a clear implication that this problem might compromise the overall effectiveness of current national (DEFRA) and EU noise policies (European Noise Directive), as discussed in Chapter 1.

Fortunately, the problem and its consequences have already been identified. (Wolde, T. T.), as one of the main architects of the current EU environmental noise policy, affirms that the estimation and management of uncertainties involved in noise measurement and prediction should be one of the priorities for future research. His suggestion seems to have had a reply, as some authors have recently made significant contributions to the subject:

Regarding predictions, (Manvell, D. et al) and (Probst, W. et al) have recommended a methodology to estimate modelling uncertainties. Their method involves breaking down the overall uncertainties into an uncertainty budget comprising a number of separate uncertainties associated with each of the input variables which have at least some effect on output levels. Then they estimate uncertainties associated with each of the separate input variables and eventually derive an overall or aggregated uncertainty from the separate uncertainty contributions. This approach is not, however, without problems, some of which are listed below:

-There are a large number of different input variables which may need to be taken into account. For example, Figure A.1 in the Appendix shows the vast amount of variables only affecting road traffic noise. The reader can have an idea, by looking at this figure, of how difficult might be to estimate the uncertainties of each single variable.

-The uncertainty values for each factor depend on the time and the particular circumstances of each site. For example, as described in Figure A.1, the road traffic noise variables are highly sensitive to random events (accidents), interactions with other variables (i.e. speed and traffic flow), seasonal trends, or even external factors like traffic lights.

Regarding measurements, (Craven, et al) also applies the same budget method for estimating variability. Given the vast amount of variables and situations involved in environmental noise, (Craven, et al) estimates variability using a scientific judgement or a general knowledge rather than a repeated set of observations. The use of this judgement for estimating uncertainties is valid and accepted by the "Guide to the expression of uncertainty in measurements" (ISO-GUM), but it is not clear to what extent is justified in the use of variability estimation. In addition, it is understandable that noise variation does need to reflect what it is happening in the measurements and that a professional judgement might be in error to a greater or lesser degree. Under this philosophy, other authors, like (Farrelly, et al), have attempted to estimate variability based on statistical analysis of real data from small data sets expanded to long tem. However, without adequate long term data, there still exists the uncertainty on whether or not any sampled data based on limited measurements is properly representative of long term average conditions over a wide range of different receiver conditions.

The investigation reported in this section follows a different approach. Since environmental noise variability can only be suitably studied through adequate long term noise data, a comprehensive measured noise level database has been investigated. Based on this large database, it has first been identified which input variables are most closely associated with (and hence predictive of) measured variability (as described by standard deviation), and then develop predictive models which could be used to estimate variability associated with future measurement or calculation exercises. It is anticipated that this work might help to enlarge the knowledge about the range of factors associated with environmental noise measurements and thereby also help those acoustic professionals who base their variability estimations on an expert judgement.

2.3. The 50 site database

Any representative statistical assessment of outdoor noise measurement variability requires a large amount of measured data which ideally should be collected by a large scale survey specifically designed for this task. For this analysis, the measured data was collected in a large scale survey comprising continuous noise monitoring for two weeks at each of 50 separate locations, where the main source of environmental noise was typically road traffic noise. The 50 measurements were recorded between the 26th of January and the 10th of May of 2001 as part of a large transport infrastructure project to investigate the potential for current noise mapping techniques to be able to extrapolate between sites at which actual noise measurement data exists; and to be able to assess future noise levels with a known degree of accuracy. The engineers in charge of the data collection belonged to Hayes McKenzie Partnership and were subcontracted by ISVR Consultancy Services, who provided the collected data to be used and analysed in this PhD thesis.

The 50 measurement locations were selected to be as generically representative as possible of a wide range of different types of suburban and rural residential areas at varying distances from main roads and other noise sources, but within the practical constraints imposed by accessibility and the need to obtain landowner consents for a relatively intrusive 2 week measurement survey period. There is no reason to suppose that these practical constraints have in fact had any effect on the spatial representativeness of the overall sample.

In terms of time representativeness, the 2 week measurement period is considered by a number of different authors (Craven, et al) or (Gaja, E. et al) as sufficiently representative for a long-term basis. However, it must be remarked that any time extrapolation of the further results outside the actual measurement period may be of dubious value. Hence, even if the measured data might provide a good indication of long-term levels according to the above authors, it is clear that long-term phenomena, like meteorological or road traffic seasonal variations, could not be encompassed by a 2 week measurement database.

To provide some assistance in separating out the different effects of variation at source from variation in acoustic propagation, the 50 measurement locations were clustered in 5 groups of 10, with simultaneous and time synchronised measurements over the continuous 2 week measurement periods across each cluster of 10 locations. For each cluster of 10, at least one noise monitoring system was deployed close to the edge of the nearside carriageway of the nearest main road passing through the general area. The remaining 8-9 locations in each cluster were selected to cover a representative range of distances on both the prevailing upwind and downwind sides of the main road. The main characteristics of the 50 locations are summarised in Table 2.1. The 5 clusters were distributed along the entire 40 km route of a new motorway route. The route passes through a representative mixture of suburban and rural settings.

The engineers responsible for sound level meter deployment and the data downloading at the end of each measurement period took comprehensive notes of all noise sources audible at each measurement location. A number of non-road traffic noise sources were identified by this means.

Each of the ten Larson Davis LD-820 data logging sound level meter systems was set up to record average L_{Aeq}, L_{A5}, L_{A10}, L_{A50}, L_{A90}, and L_{A95} for each consecutive hourly interval. In addition, each sound level meter system recorded a continuous sequence of $L_{Aeq,1min}$ sound levels for possible assistance in first identifying and then (if necessary) removing intermittent non-road traffic noise contributions from the overall measurement database. At three measurement locations within 100m of an existing railway line the time resolution of the continuous sequence recording was increased to 20s to support finer discrimination of separate railway noise events that might not have been discriminable using the 1 minute measurement interval. In accordance with the (EU Noise Directive), all microphones were mounted away from reflecting facades at a height of 4m above local ground level. A meteorological monitoring station was set up in a central location and recorded averaged wind speed and direction, temperature and humidity 10m above the ground and rainfall at ground level on an hourly basis throughout the entire 10 week measurement survey period.

Table 2.1 *Site characteristics and overall levels for each of the 50 monitoring points*

Group	Ref	Overall L_{Aeq}	Area type	Distance (m) to nearest main roads	Site characteristics
1	1	67.0	Suburban	60-150	-In a line back from the raised section of a motorway and parallel to a railway line.
	2	63.5	Suburban	≥150	
	3	56.7	Suburban		
	4	72.3	Semi-Rural	60-150	-Close to a busy roundabout. -Dominant source: motorway.
	5	66.1	Semi-Rural		
	6	62.8		30-60	-Situated on a hill that looks down 2 main roads. 6 and 7 also affected by noise coming from schools.
	7	66.9			
	8	60.4	Suburban	≥150	
	9	71.0		30-60	-Reference locations of the 2 main roads affecting 6, 7 and 8.
	10	71.0			
2	11	71.0	Semi-rural	≤30	-Fronts on to a main road.
	12	52.9	Semi-rural	60-150	-Further back from the ref. Road of 11.
	13	64.0	Suburban	30-60	-Between 2 major roads.
	14	55.2	Suburban		-Faces one of the roads affecting 13.
	15	59.7	Rural	60-150	-Between 2 main roads (1 with shielding).
	16	70.6	Semi-rural	≤30	-Close to 2 busy roads.
	17	54.9	Rural	≥150	-Further back from the ref. Road of 16.
	18	51.1	Rural		-Only local traffic noise and farm noises.
	19	62.9		60-150	-Dominant source: far busy road.
	20	48.5		≥150	-Only local traffic noise and farm noises.
3	21	53.8	Residential	≥150	-Quiet residential locations.
	22	53.0	Residential		
	23	60.5	Suburban	≤30	-Unobstructed view to a main road.
	24	54.9	Suburban	30-60	-Further back from the ref. Road of 23.
	25	52.6	Suburban		-Distant main roads and factory works.
	26	59.3	Suburban		-Traffic and temporary construction noise.
	27	55.4	Residential	60-150	-Quiet location with distant traffic noise.
	28	70.5	Semi-rural	≤30	-Faces towards a main road.
	29	53.2	Residential	60-150	-Quiet sites with distant traffic noise.
	30	53.2	Residential		
4	31	56.5	Suburban	≥150	-Local traffic and a 'hum' from a factory.
	32	59.8	Suburban	30-60	-Traffic noise but also audible factory works.
	33	74.3	Suburban	≤30	-Very close to a main road.
	34	62.2	Suburban	30-60	-Affected by two main roads.
	35	53.0	Residential	≥150	-Together with No. 40 do a line out from a main road.
	36	52.8	Residential	60-150	
	37	57.8	Suburban		-Traffic and school noise present.
	38	57.7	Suburban		-Between two main roads
	39	53.9	Residential	≥150	-Distant road traffic and light aircraft noise.
	40	54.1	Residential		-See 35-36
5	41	63.0	Semi-rural	60-150	-Dominant source: Motorway.
	42	68.3	Suburban	30-60	-Close to a main road but with shielding.
	43	52.1	Residential	60-150	-Distant traffic noise sources.
	44	54.0	Semi-rural		-Far main road and some construction noise.
	45	52.5	Rural	≥150	-Distant road traffic and light aircraft noise.
	46	54.8	Rural		-Medium distance away from a busy junction.
	47	56.1		60-150	-Between 3 main distant roads.
	48	58.4	Suburban	30-60	-Unobstructed view to a semi-busy street.
	49	58.8	Semi-rural		-Local and distant traffic noise sources.
	50	59.3	Suburban	≥150	-Dominant source: Motorway.

2.4. Results

2.4.1. Noise level versus standard deviation. – Overall data

Figure 2.1 (top and bottom) shows the observed relationships between the standard deviations and overall logarithmic and arithmetic mean daytime (6am-7pm) hourly L_{Aeq} values across all 50 measurement locations. This and all subsequent analyses were restricted to the 6am to 7pm period to avoid the additional variation caused by significantly reduced traffic flows at night.
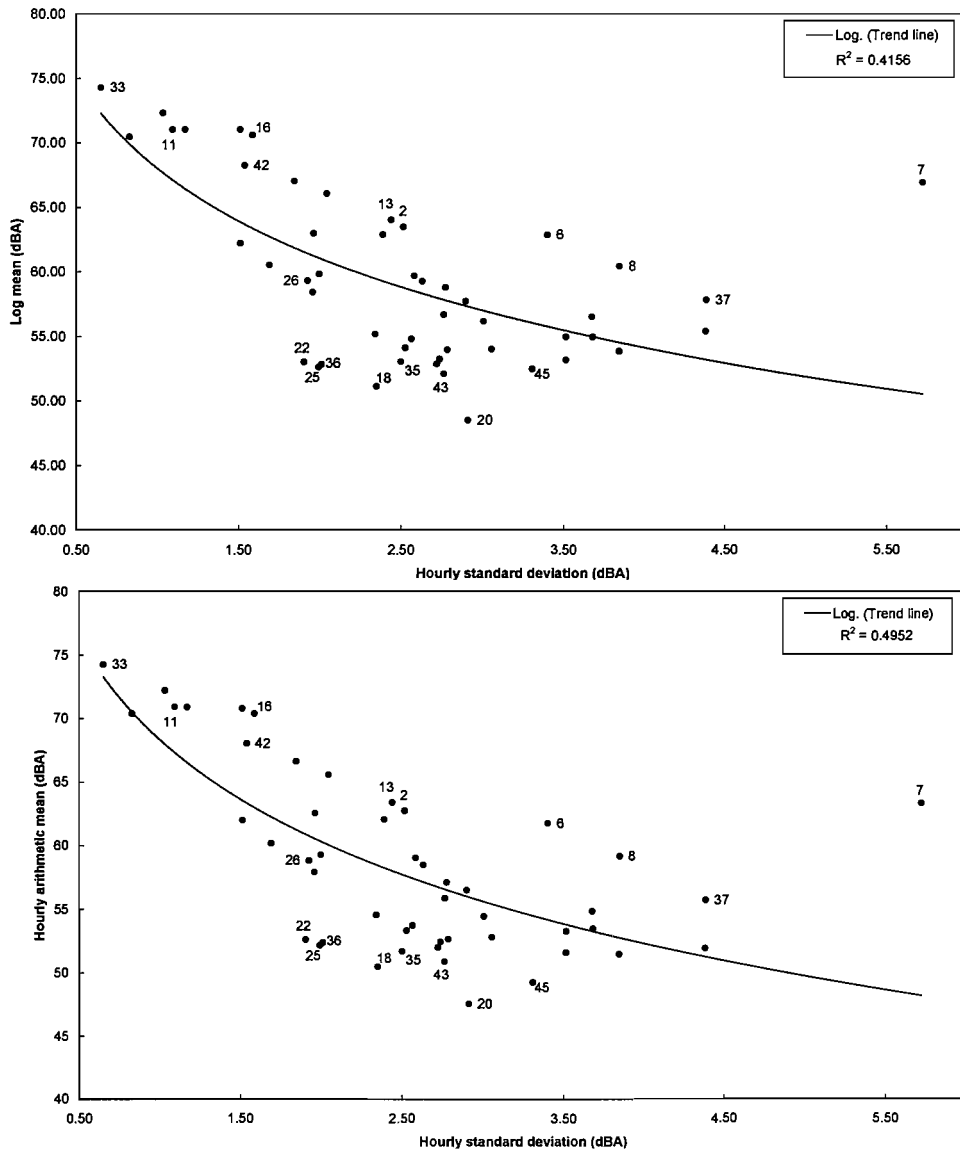
Figure 2.1 _Top:_ Long term average sound level over 2 weeks at weekdays (from 6am to 7pm) vs. standard deviation of $L_{Aeq,1h}$ values over the same period of time for each of the 50 sites. _Bottom:_ Same observations but with the $L_{Aeq,1h}$ arithmetic mean as y-axis

The use of the logarithmic mean requires no justification because it is the 'true' average 2 week 6am-7pm L_{Aeq} value. While the arithmetic mean was used, not only because this type of indicator has been selected for some existing standards and regulations, such as the calculation of road traffic noise applicable in England (CRTN), but also because this indicator might offer the theoretical possibility of a closer relationship to subjective response. Indeed, the presumption for annual (logarithmic) averages implicit in the (EU Directive) implies that short term peaks and dips in noise levels are only important for subjective response to the extent that they affect the annual average. However, most of the available evidence suggests that individual listeners tend to be more concerned about specific noisy events or noisy periods than the general level of continuous background noise. On the other hand, long term averaging is more convenient for regulatory and administrative purposes.

In view of this debate, it might still be appropriate to recommend alternative types of statistical averaging (such as the arithmetic average of hourly or even 1 min L_{Aeq}) if there was some demonstrable benefit such as more consistent statistical behaviour to be gained.

Figure 2.1 (top and bottom) shows a clear tendency for the standard deviation of the hourly values to increase as the overall average sound level decreases. There is no obvious difference between arithmetic and logarithmic averaging although the R^2 coefficient indicates a marginally stronger relationship for the arithmetic mean. There is only one measurement location with high standard deviation and high overall average sound level (location No. 7) and there are various location specific factors which can explain this outlier. This is a useful finding as it is consistent with the widely held assumption that conventional calculated values of road traffic noise mapping become increasingly less representative at lower sound levels or at increasing distances from either modelled or measured road traffic noise sources.

Figure 2.2 (top and bottom) shows the effect of looking at the 1 minute LAeq values instead of the 1 hour LAeq values as shown in Figure 2.1 (top and bottom). The overall pattern of the results is very similar. It should be noted that the marginally higher R^2 coefficients are more likely to be a consequence of the significantly in-

creased size of the database rather than any greater strength in the underlying relationships.
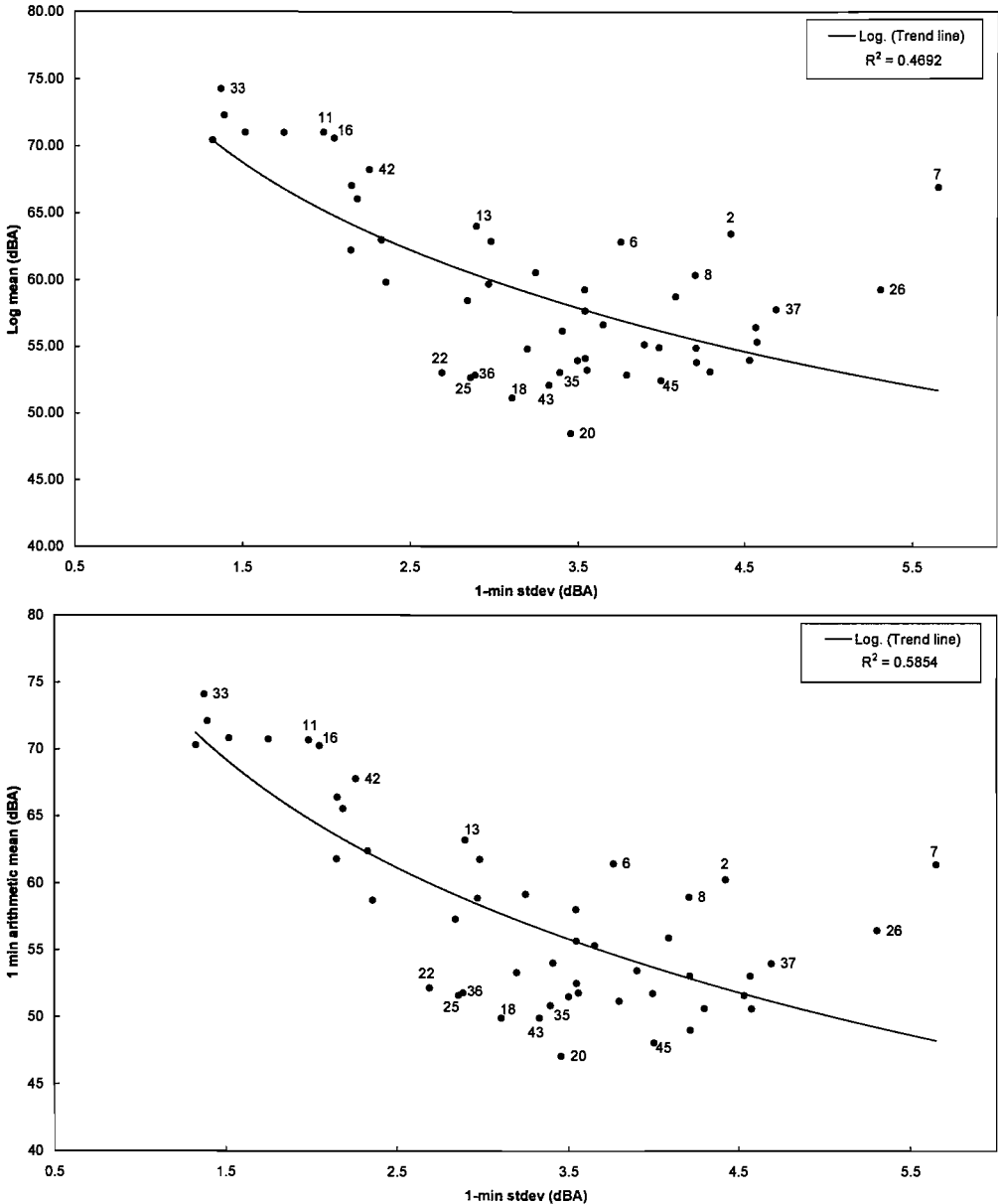
Figure 2.2 _Top_: _Long term average sound level over 2 weeks at weekdays (6am to 7pm) vs. standard deviation of_ $L_{Aeq,1min}$ _values over the same period of time for each of the 50 sites. Bottom: Same observations but with the arithmetic mean of_ $L_{Aeq,1min}$ _values as y-axis_

Figure 2.3 compares the trend lines for the logarithmic mean and the arithmetic means of the one hour and one minute values against the standard deviations of the hourly values. The three trend lines diverge at the lower overall average sound levels where the differences between the three methods of averaging increase as the standard deviations increase.

21
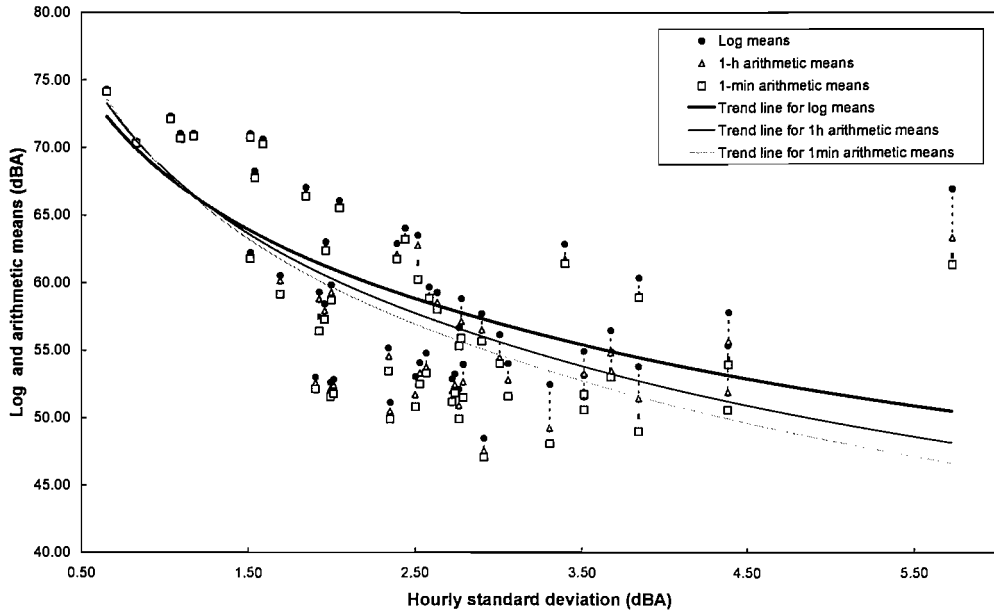
Figure 2.3 *Long term average sound levels (dBA) and arithmetic means of $L_{Aeq,1h}$ (dBA) and $L_{Aeq,1min}$ (dBA) vs. standard deviation of $L_{Aeq,1h}$ values over 2 weeks at weekdays (6am-7pm) for each of the 50 sites.*

The differences between the arithmetic means of the one hour values and the arithmetic means of the one minute values can be explained mathematically by the following reasoning: Considering the well-known principle by which any series of real positive numbers $a_1, a_2, ..., a_n$ satisfies:

$$\left(\frac{a_1 + a_2 + ... + a_n}{n} \right) \geq \sqrt[n]{a_1 \cdot a_2 \cdot ... \cdot a_n} \qquad (2.1)$$

Hence, applying (2.1) to the real positive values $10^{\frac{Leq_{1min,1}}{10}}$, $10^{\frac{Leq_{1min,2}}{10}}$, ..., $10^{\frac{Leq_{1min,60}}{10}}$, corresponding to the 60 $L_{Aeq1min}$ measurements covered in one hour:

$$\frac{1}{60} \cdot \sum_i^{60} 10^{\left(\frac{Leq_{1min,i}}{10}\right)} \geq \sqrt[60]{\prod_i^{60} 10^{\left(\frac{Leq_{1min,i}}{10}\right)}} \qquad (2.2)$$

Then working out both sides of the above expression:

$$10^{\frac{Leq_{1h}}{10}} \geq 10^{\frac{\overline{Leq_{1min}}}{10}} \qquad (2.3)$$

Figure 2.3 provides good evidence that for this type of environmental noise, the differences between logarithmic and arithmetic averaging (of either one hour or one minute values) are of no practical significance except at the lower overall average sound levels where the standard deviations are much greater.

22
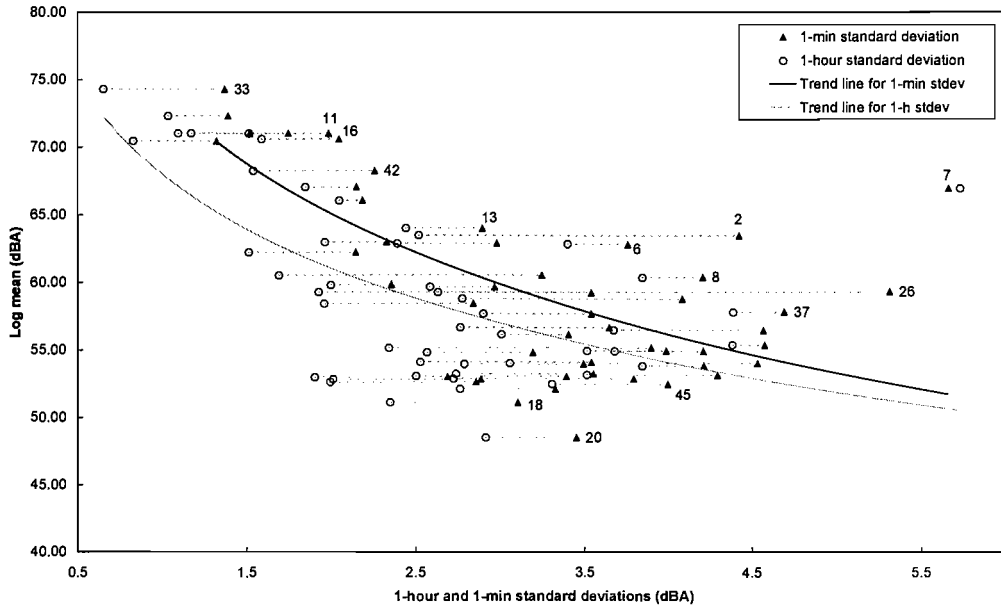
Figure 2.4 *Long term average sound levels (dBA) vs. both 1 hour and 1 min standard deviations for each of the 50 sites.*

Figure 2.4 shows the effect of comparing the standard deviations of the one hour and one minute values against the overall logarithmic means. As would be expected, the standard deviation of the one minute values always exceeds the standard deviation of the one hour values (except for receiver No. 7 under special environmental conditions explained further), but the figure shows that there is no tendency for the difference to increase at the lower sound levels with the higher standard deviations (measured by either method). There are some measurement locations with much greater differences between the two standard deviations than the norm and the particular properties of these locations are addressed in the next section below.

2.4.2. Detailed site characteristics affecting standard deviations

Figure 2.5 shows a wide range of differences between the 1 hour and 1 minute standard deviations (σ_{1h} and σ_{1min}) across the 50 measurement locations. In this section, we first describe the special characteristics of those locations with the highest differences between the 1 hour and 1 minute standard deviations (section A) and then go on to investigate other factors (meteorology in section B, and other noise sources in section C) which contribute to measurement variability in practical situations.
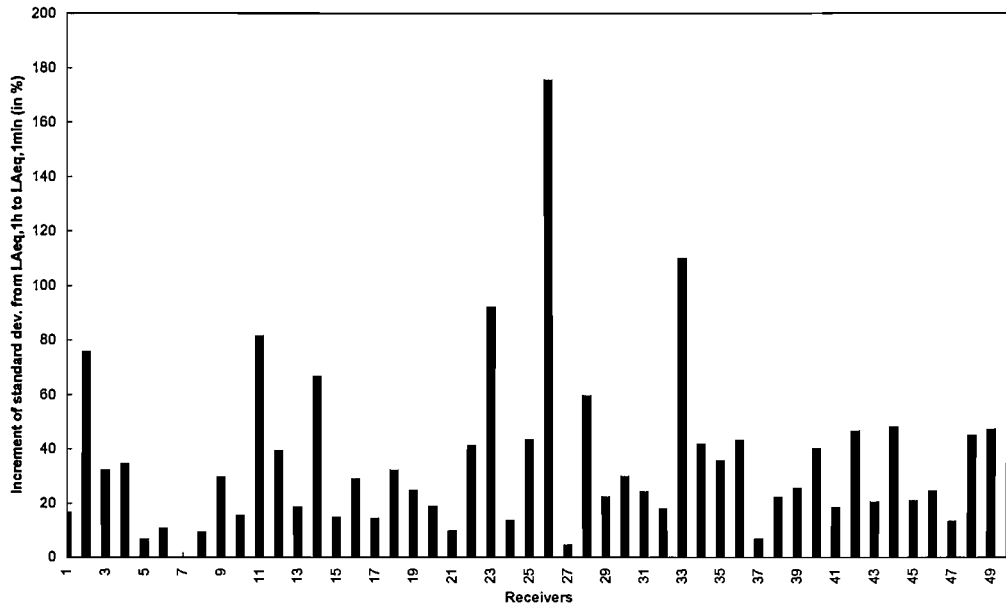
Figure 2.5 *Relative increments in percentage terms from $L_{Aeq,1h}$ to $L_{Aeq,1min}$ standard deviations for each of the 50 receivers.*

A) Differences between 1 hour and 1 minute standard deviations

The measurement location with the biggest difference between the 1h and 1min standard deviations is No. 26 (Figure 2.5). There are no obvious differences between this location and any of the other locations with otherwise similar geographical characteristics which could explain this finding. The noise monitor deployment engineers noted intermittent construction noise sources in the vicinity, but this cannot explain similarly anomalous results for this location at night, when it is extremely unlikely that any significant construction noise sources would be operating. Further investigation showed that while the 1h standard deviations are consistent with similar locations, the 1min standard deviations seem to be abnormally high. The 1min L_{Aeq} sequence recorded at this location shows continuous fluctuation over a 10 dB range throughout the measurement survey period. This is illustrated at Figure 2.6. Amongst the several possibilities considered to explain such behaviour the most plausible seems to be that there might have been some kind of instrument malfunction. There were no physical sources present in that area which might have been expected to have generated that particular type of noise event profile.

The next highest values of the difference between the 1 hour and 1 minute standard deviations are observed at locations Nos. 2, 11, 14, 23 and 33 (Figure 2.5). Considering first location No. 2, this site was positioned at approximately 30m from a

24

railway line carrying frequent train services. The time sequence data obtained at this site was compared against the corresponding data obtained at nearby locations Nos. 1 and 3. These two locations are in the same residential area but at slightly greater distances from the railway at 45m and 70m respectively. Location No. 1 is much closer to an existing motorway, while location No. 3 is in a quieter position because it is further away from both the railway line and the motorway and it is screened from the railway line by intervening buildings.
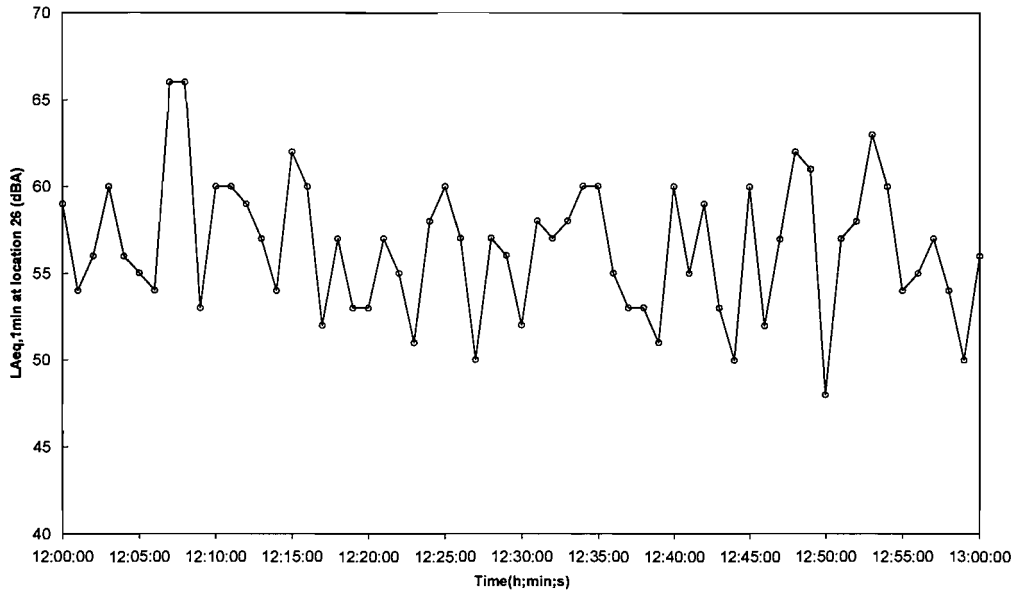
Figure 2.6 *Irregular variation of* $L_{Aeq,1m}$ *values at location 26.*
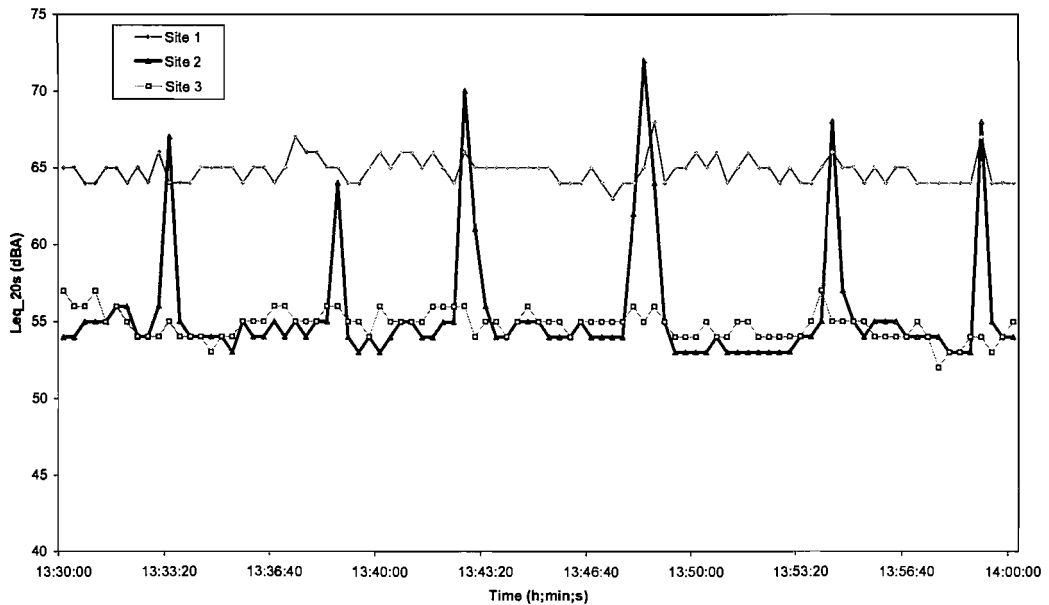
Figure 2.7 *Railway effects in* L_{Aeq20s} *measurements at locations 1, 2 and 3.*

25

Figure 2.7 shows a short sample of the simultaneous $L_{Aeq,20s}$ time histories observed at these three locations (Nos. 1, 2 and 3). The data for location No. 2 shows a clearly significant contribution from successive railway vehicle pass-bys at approximately 5 minute intervals which are not evident at locations Nos. 1 and 3. This appears to be the main reason for the larger difference between the 1 hour and 1 minute standard deviations observed at this location as compared to locations Nos. 1 and 3.

Locations Nos. 11, 14, 23 and 33, are all positioned at 30m or less from roads carrying mainly intermittent traffic with quieter periods observable between individual vehicle pass-bys, and with no intervening structures or topography capable of providing any significant acoustic screening. This suggests that the higher 1 minute standard deviations observed at these locations could be associated with relative proximity to roads carrying intermittent vehicle flows.
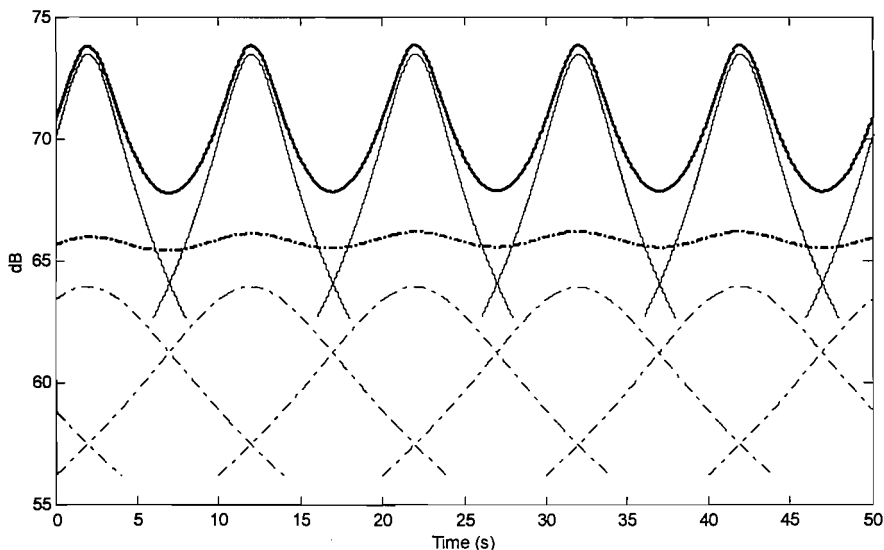
Figure 2.8 *Traffic effects with distance. Solid curves are SPL at 30m. distance from the road and dotted curves at 90m. Thicker lines are the overall contribution at the receivers whereas the faint lines are the independent noise contributions of each vehicle.*

Figure 2.8 shows how the calculated instantaneous time histories from 5 consecutive (and idealised) individual road vehicle pass-bys combine at two different distances (30m and 90m) over short time scales. It is clear that observation points which are close to the road are more likely to be able to pick out the separate rise and fall associated with each consecutive vehicle pass-by. Longer time averaging over 1 hour or more will 'smooth' out the effects of individual vehicle pass-bys

which might be observable on a 1 minute timescale. Similarly, heavier traffic flows would prevent the separate rise and fall associated with each consecutive vehicle pass-by from being observable at such locations.

B) Meteorology

Notwithstanding the above described tendency for the short time standard deviations to increase at decreasing distances from lightly trafficked roads, there is an opposing tendency for variability to increase at increasing distances because of the effects of different meteorological conditions on acoustic propagation (Bass, et al.). Differences in meteorological conditions become increasingly important at increasing distances because of the resulting differences in sound ray curvature associated with differences in the relative speed of sound at increasing heights above the ground.

There is an additional complication associated with suburban and rural noise measurement databases however. As receiver locations are moved further away from the dominant road traffic noise source in any particular direction, they are at the same time being moved closer to other road traffic noise sources in other directions. This means that the more distant measurement locations are likely to be both upwind and downwind from road traffic noise sources in different directions at the same time.

This effect can reduce overall variability from that which would otherwise be expected on the basis of differences in acoustic propagation that occur if there was only one noise source from a single direction. The majority of measurement locations for which the analysed data sits well below the trend line shown in any of the Figure 2.1 (top and bottom) and Figure 2.2 (top and bottom) (i.e. locations 18, 20, 22, 36 and 43) were situated in areas where this explanation applies. There was a reasonably wide range of different wind speed and direction conditions occurring over the 2 week measurement survey period for each of these sites, but the standard deviations were not as high as at other measurement locations with similarly low overall long term average sound levels. The most likely explanation for the low standard deviations is that, at those times when noise levels from one source would have been lower than average because of upwards sound ray curvature from one particular direction, another source from a different direction with downwards

sound ray curvature would have taken over as the dominant contributor to the over-all noise level at that measurement location.

Figure 2.1 (top and bottom) and Figure 2.2 (top and bottom) also show a number of measurement locations that demonstrate the opposite behaviour, with lower than average mean noise levels but higher than average standard deviations. Measurement locations Nos. 6, 7 and 8 were (by chance) positioned in areas that were subsequently found to be particularly sensitive to wind direction because of their relative height above the nearest significant main road traffic noise sources.
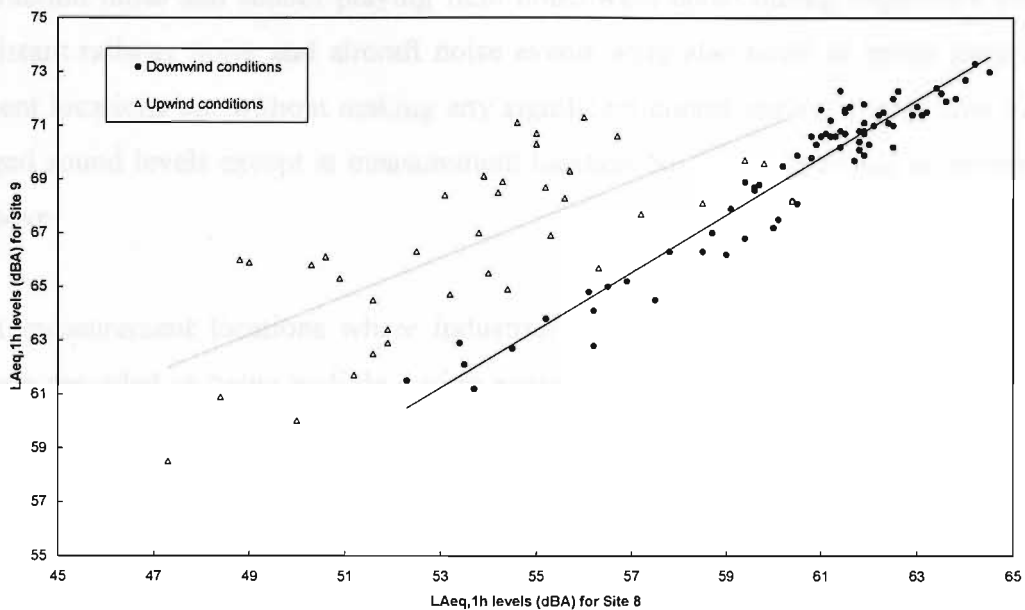
Figure 2.9 *Correlation between the $L_{Aeq,1h}$ levels for site 9 (close to the dominant source) and site 8 (far from source) under downwind and upwind conditions.*

Figure 2.9 shows the variation in $L_{Aeq,1h}$ noise levels at location No. 8 compared to simultaneously measured $L_{Aeq,1hr}$ noise levels at location No. 9. Location No. 9 was positioned significantly closer to the same main roads that affected location No. 8 but, and more importantly, at a much lower height relative to these main roads. By separating the hourly sound levels for upwind and downwind acoustical propagation conditions Figure 2.9 shows a much higher correlation between the two sites for downwind conditions than for upwind conditions. This finding is consistent with the theoretical finding that the effects of upward sound ray curvature tend to be much more significant at increasing distances away from the source than the effects

28

of downwards sound ray curvature at similar distances (Heimann, D., "Meteoro-logical aspects..."), (Alberola, J. et al.) and (McKenzie, A. et al.). Upwards sound ray curvature tends to cause proportionately more attenuation (as compared to the average) than the modest amplification that can occur under downwards sound ray curvature conditions.

C) Other noise sources

The most dominant noise source throughout most of the UK is usually road traffic, but there are other noise sources and many of these can be more significant than road traffic noise in many areas. Many different sources of industrial noise, construction noise and school playing field noise were noted during engineer's visits. Distant railway noise and aircraft noise events were also noted at many measurement locations but without making any significant contributions to long time averaged sound levels except at measurement location No. 2, as described in section A above.

At measurement locations where industrial noise and construction noise sources were recorded as being audible during engineer's visits, it should be noted that because the measurements were carried out on an unattended basis (except when setting up and subsequently taking down the equipment) it is not possible to identify at which other time periods these noise sources might have been present or even made significant contributions to overall ambient sound levels.

Closer inspection of the data in relation to what is known about the relative distances from each measurement location to each of the identified noise sources present does however suggest that neither industrial noise or construction noise would have been likely to have been particularly significant except at a small number of locations. For example, a continuous 'hum' like industrial background noise was noted at location No. 25. As a steady background noise this would have made no significant contribution to overall ambient noise levels during the day-time, but if it continued throughout each 24 hour period, then it could have set a noise 'floor' which overall ambient noise levels could not have dropped below even if the main road traffic noise sources in the vicinity had fallen completely silent. This hypothe-

sis is consistent with the otherwise lower than expected standard deviations observed at this location.
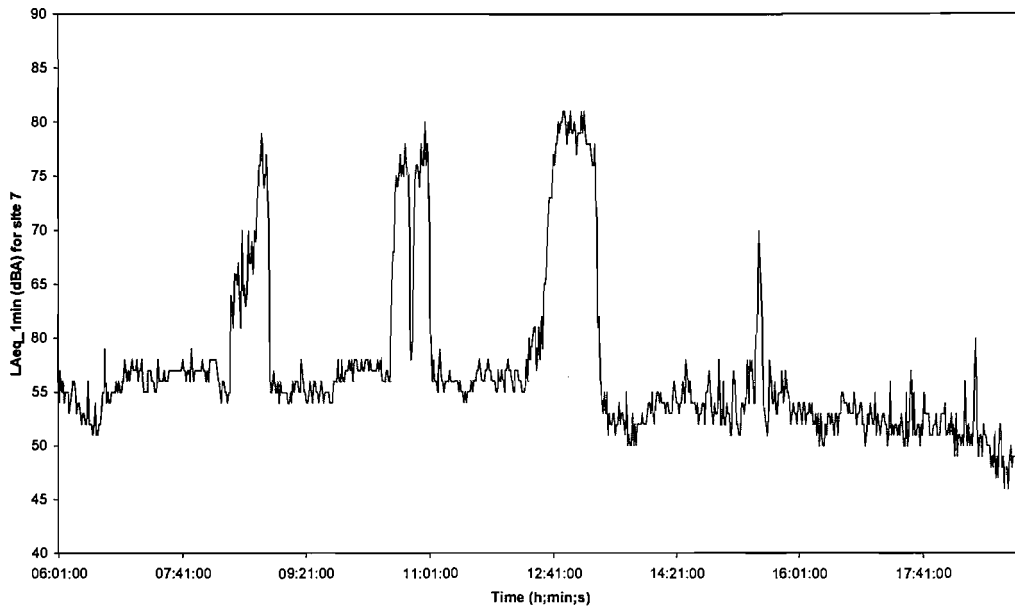
Figure 2.10 *Starting, break and lunch school times affecting $L_{Aeq,1min}$ measurements at site 7.*

Figure 2.10 shows a typical example of intermittent school playground noise as observed at location No. 7. The school playground noise can be clearly identified because it is only present at the relevant times which are entirely consistent with the school timetables. Similar contributions were also identified at locations Nos. 6 and 37.

2.4.3. Outlying data points

Based on the various findings reported above, we next investigated the possibility that the strength of the observed inverse relationship between standard deviations and mean noise levels might be improved by deleting or otherwise controlling for the observed effects of all non-road traffic noise sources or other factors such as unusual sensitivity to upwind conditions. There is no a priori reason why the contribution to standard deviation made by non-road traffic noise sources should follow any similar pattern to that made by road traffic noise sources.
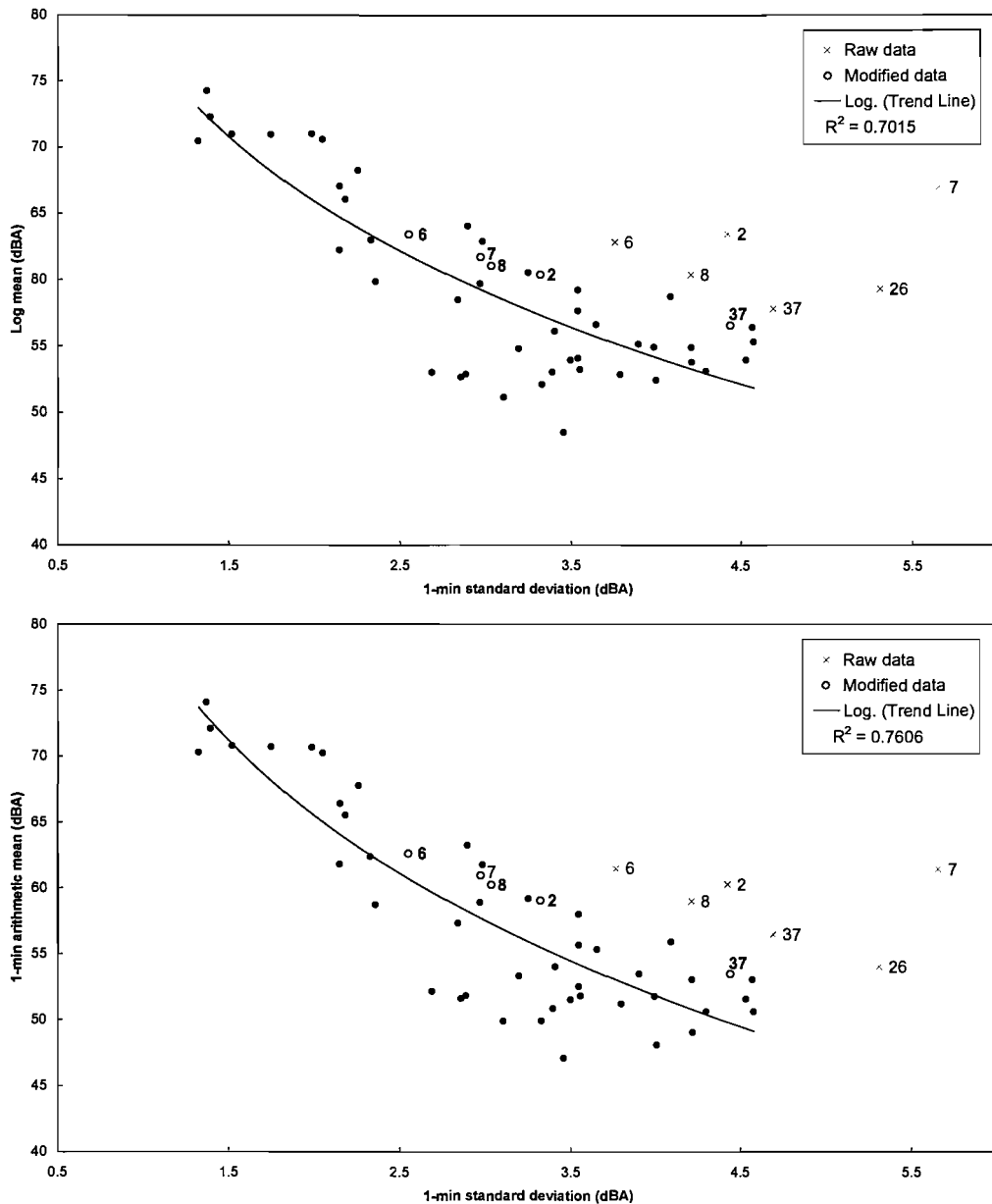
Figure 2.11 _Top_: _Logarithmic mean vs. standard deviation of_ $L_{Aeq,1min}$ _values with some modifications in 6 receivers._ _Bottom_: _Arithmetic mean of_ $L_{Aeq,1min}$ _values vs. standard deviation of_ $L_{Aeq,1min}$ _values with some modifications in 6 receivers._

Figure 2.11 (top and bottom) show the relationship between logarithmic mean and arithmetic mean noise levels against 1 minute standard deviations respectively and illustrate the resulting reduction in the overall dispersion of the data and the corresponding increases in the magnitude of the R^2 correlation coefficients when the following controls were applied:

-All data for location No 26 was removed from the analysis because of the suspected equipment malfunction as described in section A above.

31

-All data obtained under strong upwind conditions at locations Nos. 6, 7, and 8 was removed from the analysis, because of the unusual effects described in section B above.

-The specific contributions made by railway pass-by noise events at location No. 2 were removed from the analysis. Section A above refers. The 1 minute standard deviations for all three locations Nos. 1, 2 and 3 were calculated by combining the measured $L_{Aeq,20s}$ measurement sequences into the corresponding $L_{Aeq,1min}$ measurement sequences, missing out any $L_{Aeq,1min}$ period for which all three contributing $L_{Aeq,20s}$ data points had been separately attributed as railway pass-by events.

-The specific contributions made by school playground noise at locations Nos. 6, 7, and 37 were removed from the analysis (see Figure 2.10) by deleting those time periods during which school playground noise was observed to be present.

By applying the above controls, we note that the R^2 coefficients shown in Figure 2.11 (top: 0.7 and bottom: 0.76) are considerably higher than those presented in Figure 2.2 (top: 0.47 and bottom: 0.59). This reduction in the dispersion of the data between Figure 2.11 (top and bottom) and Figure 2.2 (top and bottom) suggests that there is an underlying strong inverse relationship between measured standard deviations and measured overall mean noise levels for measurement locations where the most dominant noise source is road traffic noise emanating from various roads both near and far, and that the apparent strength of this relationship can be at least partially concealed by the presence of non-road traffic noise sources and/or by other factors such as unusual sensitivity to upwind conditions associated with elevated measurement locations.

Since the accuracy and validity of calculated road traffic noise levels can only be determined from comparisons between calculated and measured values, then this analysis suggests that the representativeness of single calculated noise levels generated by road traffic calculation methods is likely to decrease at lower mean noise levels or wherever there are other non-road traffic noise sources present or other unusual factors affecting acoustical propagation.

There is no reason to doubt the statistical representativeness of the large 50 site measurement database for any generically similar suburban and rural districts anywhere in lowland Great Britain. However, since there were no measurements in either urban city areas or in very quiet rural areas in the database, then any extrapolation of the findings to any such areas might not be justified.

2.5. Conclusions

Preliminary analysis of a large and thus generically representative outdoor noise measurement database has revealed a strong inverse relationship between measured standard deviations and mean noise levels. There were no measurement locations with both high standard deviations and high mean noise levels, although the observed standard deviations did in fact cover a wide range at the lower mean noise levels.

More detailed analysis demonstrated marginally stronger inverse relationships between standard deviations and arithmetic means noise levels as compared to the more technically 'correct' logarithmic or 'true' mean noise levels. This observation is consistent with the demonstrated principle that the logarithmic mean noise levels are always higher than the arithmetic mean noise levels and that the arithmetic means of the $L_{Aeq,1hr}$ sequences are also always higher than the arithmetic means of the $L_{Aeq,1min}$ sequences. However, the observed differences between the standard deviations of the $L_{Aeq,1h}$ and $L_{Aeq,1min}$ sequences seem to be more important in practice than the observed differences between the different types of mean.

By using the differences between the standard deviations of the $L_{Aeq,1h}$ and $L_{Aeq,1min}$ sequences as an indicator, it was then possible to identify and then isolate those measurement locations and specific conditions within the database that did not conform to the general pattern of increasing standard deviation with decreasing mean noise level. These non-conforming situations included the following:

-Abnormally high standard deviation of LAeq,1min sequence suggesting equipment malfunction (location No. 26).

-Undue sensitivity to strong upwind conditions due to elevated position of measurement location (locations Nos. 6, 7 and 8).

-Significant contributions from non-road traffic noise sources such as railway pass-by events (location No. 2) and school playground noise (locations Nos. 6, 7 and 37).

When the potentially confounding effects of these non-conforming situations are removed from the analysis, the strength of the inverse relationship between the standard deviation and the mean noise level is in most cases significantly improved.

Subject to the caveat that the results should not be extrapolated to locations not generically represented in the overall measurement database, the general finding of relevance to the estimation of variability in noise measurements is that measured road traffic noise variation increases from typical standard deviations of one minute L_{Aeqs} of around 1.5 dB at overall average noise levels of around 70 L_{Aeq} and above to around 4.5 dB at lower average noise levels of around 50 L_{Aeq}. Any measured variability above the general trend is likely to be associated with significant non-road traffic noise sources, unusual propagation conditions, or otherwise unsuspected equipment malfunctions. It is anticipated that these ranges of observed variability may be of assistance when estimating the range of variation likely to be associated with environmental noise measurements. Furthermore, these results could be of value when, due to the limited time and resources, expert acousticians had to relied on a professional judgement to the estimation of variability associated with measured noise levels.

Chapter 3

Effects of Medium-Term Meteorology in Noise Level Variability

3.1. Introduction

The previous chapter reveals a strong inverse relationship between measured variability (standard deviations) and mean noise levels. Subsequent analysis suggests that this relationship might be driven by different environmental factors. Amongst them, the meteorology and the source-receiver distance seem to have a predominant influence on the trend. However, the 50 site database did not contain meteorological and noise source data to a sufficient level of detail to justify a quantitative explanation of the found relationships.

The research reported in this section was indeed undertaken to provide a quantitative explanation of the detected influence of meteorology and receiver distance on noise variability. The Joule database (Bass, et al.) was examined to determine the extent to which the variables included within current practical noise calculation methods (i.e. ISO 9613-2) would be capable of explaining observed variability and the extent to which medium-term meteorology effects might additionally need to be taken into account. This noise measurement database was collected over flat ground under controlled conditions under the European Joule III project framework.

For this investigation, the effects of upwards or downwards sound ray curvature were modelled using circular arcs arising from the assumption of linearity in sound speed profiles. The available noise measurement database did not contained meteorological data to a sufficient level of short-term detail to justify the use of more sophisticated models such as the Parabolic Equation or the Fast Field program. However, the analysis carried out in Chapter 4, based on a more detailed test (Salisbury Plain database) allows these potentially more exact theoretical models to be compared against actual field data over long ranges.

3.2. Literature review

The study of the measurement database presented here requires some knowledge about the processes involved in outdoor sound propagation. It has been found necessary to review the current theories that explain the specific phenomena occurring in the path of a sound wave when travelling from a point source to a receiver over flat terrain. In addition, this section reviews the fundamentals of ray-acoustic models as a basis to develop theoretical modelling to account for the experimental observations collected in the Joule database.

3.2.1. Physical phenomena

When travelling from source to receiver through the atmosphere over a defined surface, the sound wave loses acoustic energy by a number of processes. Some of the basic processes affecting sound wave propagation are present in any situation. These are:

-Geometrical spreading: Sound levels decrease with increasing distance from the source. There is no frequency dependence.

-Atmospheric absorption of sound: Sound energy is converted into heat as the sound wave propagates through the air. There is a strong dependence on frequency.

-Meteorological conditions: are twofold: short-term turbulence, which are produced by local variations in temperature and wind velocity, and overall sound speed verti-

cal gradients which make sound waves refract in the atmosphere. The present review will examine the medium-term meteorological effects, while the turbulent scattering will be studied in the next chapter.

Other phenomena occur only because of the presence of the ground and consequently are usually most significant near the ground. These phenomena and the features that cause them are:

-Reflection at the ground surface: The reflected sound path interferes with the direct sound field. In this process, both the source-receiver geometry and the acoustical properties of the ground surface are the most important factors.

-Terrain type: Surfaces have a finite and complex acoustic impedance that results in a reflection co-efficient which is a function of the angle of incidence. Depending on this reflection co-efficient the reflected wave can suffer a change in its phase.

-Shape of ground surface: Convex ground surfaces such as bounds or low hills can act as sound barriers and lead to an acoustical shadow that is penetrate by diffracted and scattered waves. Concave ground surfaces can result in multiple ray paths between the source and the receiver and hence increased sound levels. The present section will not go into greater detail on this subject as the experimental work is based on flat terrain situation exclusively.

For the study of noise variability arising in the Joule database, only some of the aforementioned factors are relevant: Geometrical spreading, Atmospheric absorption and Medium-term meteorological conditions. For this reason they are explained in more detail below. The rest of the factors (ground and short-term meteorological conditions) are adequately reviewed in Chapter 4.

3.2.1.1.Geometrical spreading

Assuming a point source in a loss-less medium with no reflections, see Figure 3.1, it is well known that the sound intensity is related to power and distance by:

$$I = p^2(r)/\rho_0 c_0 = W/4\pi r^2 \qquad (3.1)$$

Being: I = acoustic intensity (watts/m^2)

p(r) = sound pressure at radial distance r (N/m^2)

r = distance from the source in metres.

W = sound power level in watts.

$\rho_0 c_0$ = acoustic impedance of air (415 rayls)
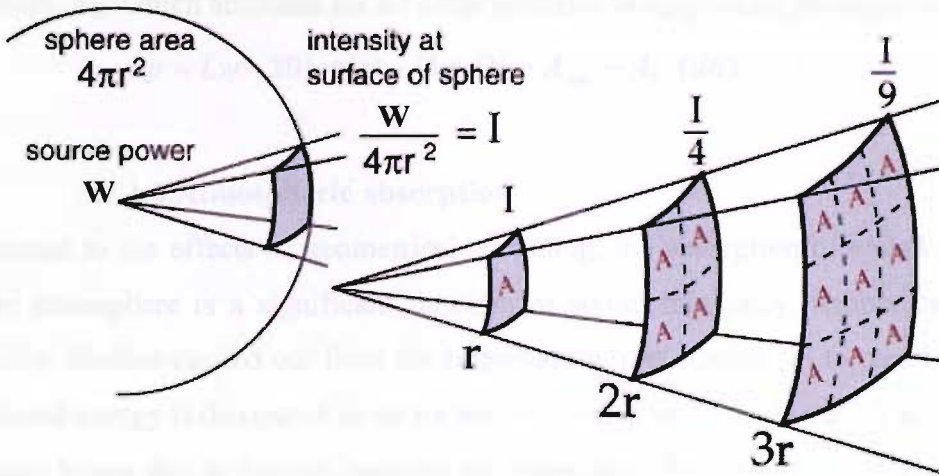
Figure 3.1 *The inverse-square law relating intensity to distance from a point source*

In terms of sound levels, this translates to:

$$Lp = Lw - 20\log(r) + 10\log\left(\frac{W_{ref}\rho_0 c_0}{P_{ref}^2 4\pi}\right)$$
(3.2)

The first two terms of the equation: Lp and Lw are respectively the sound pressure level (dB re $2 \cdot 10^{-5}$ N/m^2) and the sound power level (dB re 10^{-12} watts). Substituting the numerical value of the constants in the last term, the equation becomes:

$$Lp = Lw - 20\log(r) - 11 \ \ (dB)$$
(3.3)

If the source is directional, an additional term, the Directivity Index DI, is needed to account for the uneven distribution of the sound intensity as a function of direction. However, in the experimental work studied further this situation does not occur, and the DI factor takes a nil value. With this last consideration in mind, the general purpose propagation equation without reflection might be written as:

$$Lp = Lw - 20\log(r) - 11 + DI \ \ (dB)$$
(3.4)

By using equation (3.4) for calculating the sound pressure from an omni-directional point source, is easy to see that sound pressure level decreases by 6 dB per doubling of distance. This well-know 6dB relationship can be contemplated as certain both

for instantaneous or maximum levels and for every frequency in any spherical sound propagation. In case of cylindrical propagation (line source), the decrease rate would be, however, 3 dB.

Equation (3.4) is usually extended in most of the practical sound calculation methods by adding two terms: The absorption of sound in air, A_{atm} and the excess attenuation, A_E, which accounts for all other effects affecting sound propagation:

$$Lp = Lw - 20\log(r) - 11 + DI - A_{Atm} - A_E \quad (dB) \tag{3.5}$$

3.2.1.2. Atmospheric absorption

In contrast to the effects of geometrical spreading, the absorption of sound energy by the atmosphere is a significant function of sound frequency, temperature and humidity. Studies carried out from the beginning of last century up to date indicate that sound energy is dissipated in air by two major mechanisms (Piercy et al.):

-Viscous losses due to friction between air molecules which results in heat generation (also known as "classical absorption").

-Relaxational processes – sound energy is momentarily absorbed in the air molecules (mainly nitrogen and oxygen) and causes the molecules to vibrate and rotate. These molecules can then re-radiate sound at a later instant which can partially interfere with the incoming sound.
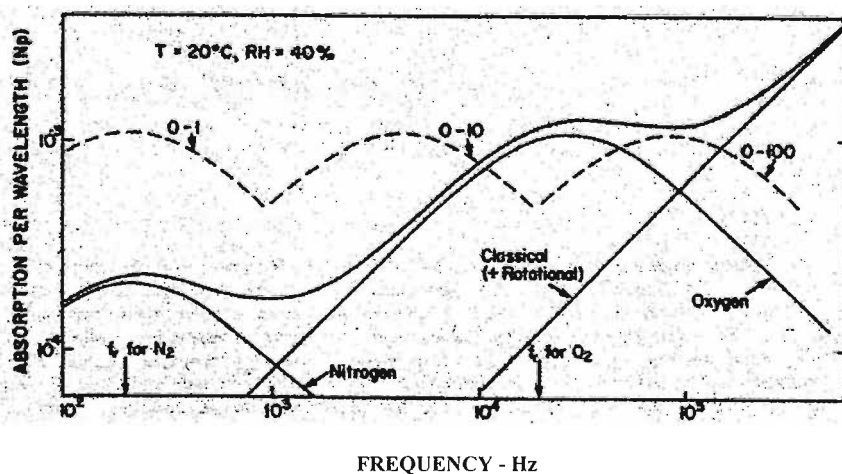
Figure 3.2 *Contributions of different processes (thin solid line) to the total molecular absorption (thick solid line), and an indication (dashed line) of how the absorption from the vibrational relaxation of oxygen varies with humidity. (Extracted from Piercy et al.)*

39

The classical absorption, which is a function of temperature, frequency and weakly of ambient pressure, is accepted as the dominant absorption mechanism for acoustic energy at high frequencies, as shown by Figure 3.2. In contrast, vibrational relaxation of oxygen and nitrogen are the main absorption mechanisms at low and mid frequencies. Figure 3.2 also shows an indication of how the absorption from the rotational relaxation of oxygen shifts up in frequency with relative humidity.

The variation of atmospheric absorption with frequency, temperature and relative humidity has been quantified by both (ANSI Standard S1-26:1995 and ISO 9613-1:1996) and has been described below. The following equations, extracted from the aforementioned standards, are included because they are used further in the chapter for deriving the mathematical expressions that theoretically explain part of the variation of sound pressure levels in terms of atmospheric absorption fluctuations.

The attenuation coefficient, A_{Atm} is a function of the absorption coefficient α (in dB/100m) and the distance, d':

$$A_{Atm} = \alpha d'/100 \quad (dB) \tag{3.6}$$

Whilst the absorption coefficient α is the parameter with a direct dependency on frequency f (Hz) and temperature T (Kelvin):

$$\alpha = 869 \cdot f^2 \left(1.84 \cdot 10^{-11} \cdot \left(\frac{T}{T_o}\right)^{\frac{1}{2}} + \left(\frac{T}{T_o}\right)^{\frac{-5}{2}} \left[0.01275 \frac{e^{-2239.1/T}}{F_O + \frac{f^2}{F_O}} + 0.1068 \frac{e^{-3352/T}}{F_N + \frac{f^2}{F_N}} \right] \right) \tag{3.7}$$

T_0 is 293.15 K and F_O and F_N are the respective vibrational relaxations of oxygen and nitrogen:

$$F_O(oxygen\ relaxation\ freq.) = 24 + 4.04 \cdot 10^4 H \frac{0.02 + H}{0.391 + H} \tag{3.8}$$

$$F_N(nitrogen\ relaxation\ freq.) = \left(\frac{T}{T_0}\right)^{\frac{-1}{2}} \left(9 + 280 He^{\left[-4.17\left(\left(\frac{T}{T_0}\right)^{\frac{-1}{3}} - 1\right)\right]} \right) \tag{3.9}$$

As we can see, F_O and F_N are functions of H, which is the molar concentration of water vapour (%) and that can be converted into relative humidity RH through the equations (3.10) and (3.11):

$$H = RH \cdot P_{sat}/P_e \qquad (3.10)$$

$$\log\left(\frac{P_{sat}}{P_{so}}\right) = 10.795\left(1-\frac{T_{01}}{T}\right) - 5.028\log\left(\frac{T}{T_{01}}\right) + 1.504\cdot10^{-4}\left[1-10^{-8.296\left[\left(\frac{T}{T_{01}}\right)-1\right]}\right] +$$

$$+ 0.428\cdot10^{-3}\left[-1+10^{4.769\left[1-\left(\frac{T_{01}}{T}\right)\right]}\right] - 2.219 \qquad (3.11)$$

T_{01} is the triple point isothermal temperature (=273.16 K), P_{so} is the reference atmospheric pressure (=101.325 kPa) and P_e the environmental pressure in Pa.

All these equations have been extensively studied, empirically quantified, and codified into international standards for calculation, which suggests that the molecular processes are reasonably well delineated. However, there are still disagreements between some standards. Figure 3.3 shows for example, a comparison between attenuation coefficients, A_{atm}, generated by three different models (ISO 9613-2, VDI 2714/2720 and Nordic Prediction Method). The comparison has been undertaken for 7 different distances (50, 100, 200, 300, 400, 500, 675m), under a temperature of 10°C and relative humidity of 70%.
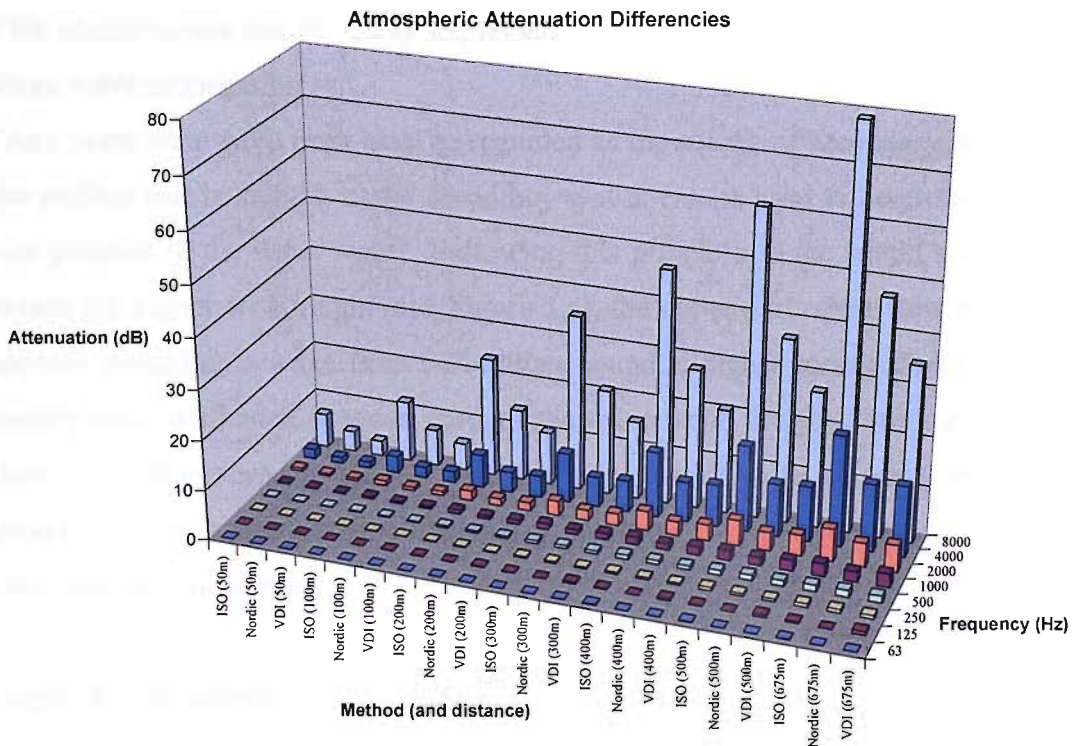
Figure 3.3 *Atmospheric sound attenuation comparison between ISO 9613-2, Nordic Prediction Method and VDI 2740.*

The figure shows small differences between methods at low-medium frequencies and short distances, but bigger disagreements at high frequencies (4-8 kHz) and long distances. The technical debate opened by these differences is out of the scope of this thesis, but considering these disagreements, it is necessary to specify that the atmospheric absorption model adopted onwards is that expressed through the equations (3.6) to (3.11) (extracted from the ANSI or ISO standards). ISO/ANSI Equations have been used here to the detriment of other models because they are the most widely accepted atmospheric absorption methods. It is advised that the use of other methods for undertaking the analysis that will be presented in this thesis might lead to different quantitative solutions.

3.2.1.3.Medium-term meteorological conditions

During most weather conditions both the temperature and wind vary with increased height above the ground. Because the velocity of sound relative to the ground is a function of both temperature and wind velocity, it also varies with height. In the presence of this vertical gradient of sound speed, the sound waves are refracted in the direction from higher sound speeds to lower sound speeds.

This phenomenon can be easily explained by considering the Huygens' Principle about wave propagation:

"Any point on a wave front may be regarded as the source of secondary waves and the surface that is tangent to the secondary waves can be used to determine the future position of the wave front". Following this principle, if the sound speed is increasingly higher with height (see Figure 3.4), the upper part of the new secondary sources located on a wave front will radiate sound at higher speeds than those secondary sources situated at lower parts of the wave front, thereby forming a tangent (new wave front) which will be bent downwards relative to its predecessor. Depending on the particular circumstances, there are two possible curving trends: Downwards or upwards.

<u>Downward refraction</u>

The downward propagation of acoustical paths usually occurs under a temperature inversion (stable atmospheric conditions) or under a downwind propagation. The resulting propagation of sound under any of these two atmospheric phenomena is

essentially very similar, but could differ if the shapes of the wind and temperature vertical profiles are different. Any resulting sound speed function with an increase ratio with height will generate a downward sound propagation, as shown by Figure 3.4, however depending on the obtained relationship between sound speed and height (i.e. linear, logarithmic...), the downward propagation will have specific properties:

-A linear sound speed variation with height will make sound rays travel from source to receiver along circular arcs characterised by the fact that their centres of curvature all lie on a horizontal line at a distance $1/\gamma_T$ from the surface (being γ_T the increase rate of the sound speed with height). For an analytical demonstration see (Rudnick, I.)

-In contrast to the linear case, logarithmic sound speed profiles do not generate a homogeneous sound path throughout the atmospheric boundary layer. Sound rays are almost circular arcs at high altitudes, where the logarithmic sound speed function is nearly linear, but they have a more difficult analytical definition at heights close to the ground where the logarithmic profile has a less linear behaviour.
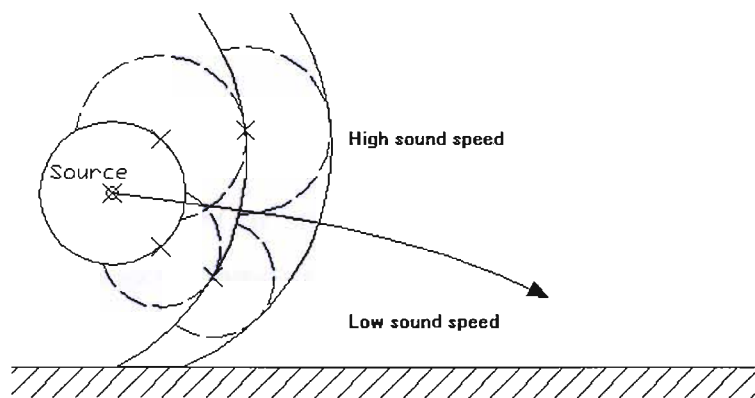
Figure 3.4 *Sound curvature under temperature inversion and/or downwind conditions*

Other less common profiles may be considered, like power or exponential relations, but understanding the above is easy to explain the effects of applying other functions. The main effect of downward sound propagation is the possible generation of more than only one reflected ray from source to receiver. Furthermore, a particular ray may be reflected several times. This increase of sound ray paths generally results in the amplification of the received overall noise levels, however the varying

43

lengths of the reflected rays and its several interactions with the ground can also cause destructive interference at some frequencies.

Upward refraction

When the sound speed decreases with height, the sound rays are bent upwards away from the ground, as depicted by Figure 3.5. For typical sound speed profiles, there is a limiting ray leaving the source which grazes the ground. Above this limiting ray the sound field is composed of direct and ground-reflected waves, whereas below the limiting ray there is an acoustical shadow in where sound waves do not theoretically exist.
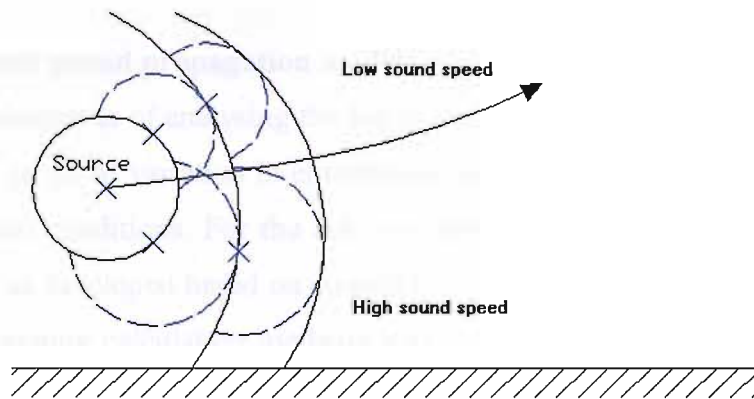
Figure 3.5 *Sound curvature under temperature lapse and/or upwind conditions*

A number of different contributions have studied in greater detail the process of sound penetration in shadow areas. (Embleton, T.W.D.), for example, explains that the most significant amount of energy penetrates into the shadow region via a creeping wave. This special wave travels near the ground inside the shadow region, as shown by Figure 3.6, and sheds energy upwards during propagation at a rate that depends on frequency and ground impedance. (Salomons, E.M.), in contrast, affirms that the penetration is due mainly to scattering effects and, in a weaker level, to diffractive propagation mechanisms. The scattering is a result of the turbulent inhomogeneities in the atmosphere and can be considered as small-scale refraction. Salomons considers that sound waves are scattered into the refractive shadow region by small random changes of the propagation direction, whereas the diffractive penetration mechanism is described as analogous to the diffraction of sound waves when facing an obstacle in its propagation.
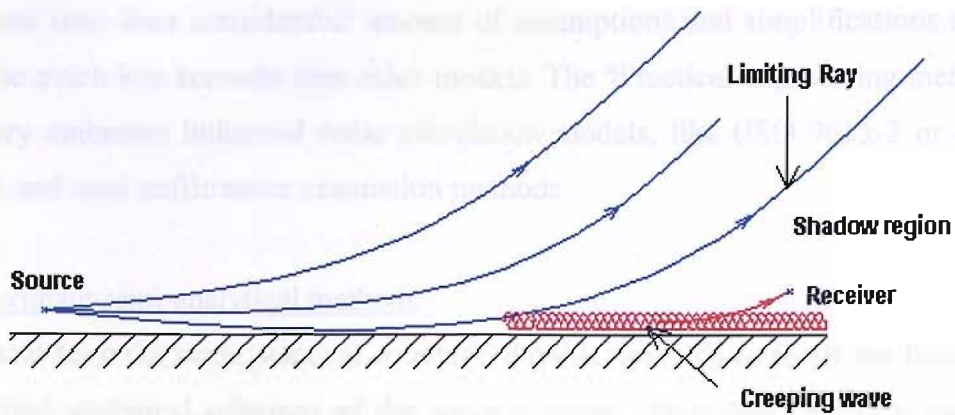
Figure 3.6 *Schematic diagram for propagation in a temperature lapse or upwind. Sound penetrates inside a shadow region via a creeping wave that sheds sound energy progressively during propagation. (Tutorial on sound propagation outdoors, Embleton, Fig.14)*

3.2.2. Outdoor sound propagation models

One of the objectives of analysing the Joule database was to find predictive tools to quantify the range of variation in environmental noise measurements under known meteorological conditions. For the achievement of this objective some theoretical modelling was developed based on current outdoor sound propagation models. The use of the existing calculation methods was essential as a starting point and as a way to ensure (to some extent) that the predicted ranges of variation were centred on the correct middle tendency.

Existing outdoor sound propagation models are quite diverse. The complexity of atmospheric conditions and the impracticability to measure all the relevant environmental parameters throughout the sound propagation path, require that several assumptions and simplifications in the models are adopted. This set of assumptions and approximations has led to the existence of a variety of sound propagation models, of which some are inter-related, others are hybrids and all are strictly limited in capability. Generally, all these models can be classified by the following three categories, in here sorted by increasing complexity and accuracy:

Practical engineering methods

The technique adopted by these models involves the calculation of noise levels by adding the separate contributions that each sound attenuation factor has on noise propagation. The common factor in all these models is that they are mainly based

45

on empirical results. In general, they are very simple and very easy-to-use, but at the same time their considerable amount of assumptions and simplifications make them be much less accurate than other models. The "Practical-engineering method" category embraces industrial noise calculation models, like (ISO 9613-2 or Concawe), and road traffic noise calculation methods.

Approximate semi-analytical methods

They still keep the same practical structure, but this time, the methods are based on simplified analytical solutions of the wave equation rather than empirical results. While the practical engineering methods only take into account averaged meteorological effects, these methods allow a better tracking of the influence of specific meteorological conditions on noise levels, such as upwind or downwind situations. Simple ray tracing models are the most popular methods within this category.

Numerical methods

This group includes methods like: the Fast Field Program (FFP), the Parabolic Equation (PE) and other models based on the direct solution of the wave equation. In general, all these methods allow the calculation of sound propagation over non-complex level terrain with any user-specified atmospheric conditions. They are extremely useful for analysing the propagation under specific meteorological conditions. The problem is that they yield results for only those specific conditions and give little indication of statistical mean values of sound levels. The user must provide substantially more information. This information can be difficult to generate, such as complete profiles of wind and temperature. These models are reviewed in detail and applied in Chapter 4.

In the following chapter, a practical engineering model (ISO 9613-2) is used as a starting point for predicting the central tendency of the noise data collected in the Joule database. Subsequent theoretical modelling aimed to predict overall variability associated with the different effects of all the separate mechanisms considered by ISO 9613-2 arising under different meteorological conditions. These separate effects, even when aggregated together, were not enough to represent the entire range of sound level variability observed (as is described further in section 3.4.1). It was therefore decided to investigate the additional effects of refraction by consider-

ing a combined model. This model was developed by using the ray tracing theory when the coefficient of increase in sound velocity with height was positive and by extending the existing curved ground analogy with the use of diffraction theory in the negative case.

The ray-acoustic theory used in the analysis of the Joule database is essentially an application of (Embleton, T. F. W. et al.) method. For this reason it is useful to review here the theoretical basis of the method and its advantages and limitations towards the calculation of noise levels.

3.2.2.1. Ray-Acoustics

A) Origin and basis

As in many other outdoor sound propagation models, the starting point of basic ray-acoustics methods is the Helmholtz equation for the complex sound pressure p, analytically used for calculating the sound field in an environment remote from any acoustic sources:

$$\nabla^2 p + \frac{\omega^2}{c^2} p = \nabla^2 p + k^2 p = 0 \tag{3.12}$$

following a common notation, c=c(x,y,z) denotes the speed of sound, ∇^2 the Laplacian operation and k=k(x,y,z) the wavenumber.

Except for the very simplest boundary conditions and uniform media, it is not possible to obtain a complete analytic solution for equation (3.12) (White, P. R.), thereby one is forced to use numerical methods or make simplifying assumptions to solve the equation. Indeed, the way used for the resolution of this equation determines in the end a variety of outdoor sound propagation models: Using numerical methods, for example, one can obtain the PE or FFP models (see Chapter 4), while using simplifications, the basic ray-acoustic method can be derived (see below).

Hence, to solve the above equation, we first express the complex sound pressure amplitude of a harmonic sound field in polar form:

$$p(x, y, z) = A(x, y, z)e^{ik_0\varphi(x,y,z)} \tag{3.13}$$

47

The first component of this polar notation, A(x, y, z), denotes the modulus of p(x, y, z), φ(x, y, z) stands for the argument (phase), and k_0 designates a reference wavenumber. Substitution of (3.13) into the Helmholtz equation (3.12) yields:

$$\nabla^2 A e^{ik_0\varphi} + 2ik_0\nabla A\nabla\varphi e^{ik_0\varphi} + iAk_0\nabla^2\varphi e^{ik_0\varphi} - Ak_0^2\nabla\varphi\nabla\varphi e^{ik_0\varphi} + k^2 A e^{ik_0\varphi} = 0$$

Cancelling common terms and equating real and imaginary parts, the following equations are obtained:

$$\text{Real:} \qquad \nabla^2 A - Ak_0^2\nabla\varphi\nabla\varphi + k^2 A = 0 \qquad (3.14)$$

and

$$\text{Imaginary:} \qquad 2\nabla A \cdot \nabla\varphi + A\nabla^2\varphi = 0 \qquad (3.15)$$

If we simplify by making the assumption that, at least locally, the wavefront propagates as a plane wave:

$$\frac{\nabla^2 A}{A} \ll k^2 \qquad (3.16)$$

The first term in equation (3.14) may be neglected to yield:

$$\nabla\varphi \cdot \nabla\varphi = \left(\frac{k}{k_0}\right)^2 = n^2 \qquad (3.17)$$

Here n denotes the "refractive index" and is defined as:

$$n = \frac{k}{k_0} = \frac{c_0}{c} \qquad (3.18)$$

Equation (3.17) is termed the Eikonal equation and its companion, equation (3.15), is called the transport equation. The Eikonal equation fully relies on the assumption adopted in equation (3.16). This assumption imposes several restrictions on the physics, which in turn limit the applicability of ray theory. These conditions are:

- The amplitude must not vary significantly over a wavelength; i.e. the theory would be invalid when diffraction takes place about a solid object, because in the shadow of the object the pressure field has regions which exhibit large spatial variations.

- The speed of sound must not vary significantly over a wavelength; This implies that the above theory may not be valid with abrupt changes in the sound speed.

Considering these assumptions, the main objective now is to be able to plot the ray paths. As these are by definition perpendicular to the wavefront and the wavefront is defined by φ, an expression for the variation of the vector $\nabla\varphi$ with position along the ray may be essential. This can be obtained in derivative form by working out an expression for:

$$\frac{d}{ds}(\nabla\varphi) \tag{3.19}$$

As shown by Figure 3.7, s is the measure of the distance along the ray, that is, the path length.

From equation (3.18) we see that the length of the vector $\nabla\varphi$ is n while the direction of $\nabla\varphi$ is normal to the surface of constant phase (wave-front). If we define a unit vector e which is perpendicular to the wave-front (see Figure 3.7), then by construction:

$$\nabla\varphi = ne \tag{3.20}$$
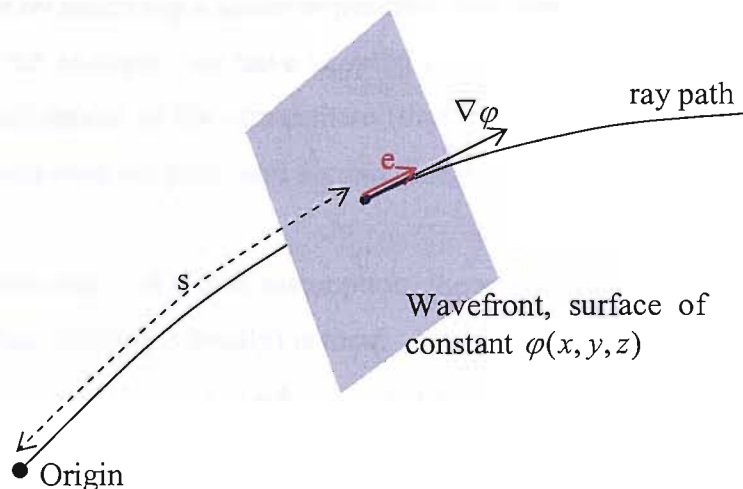
Figure 3.7 *Schematic 3D view of the wavefront geometry*

The procedure to differentiate the last equation with respect to s is as follows:

$$\frac{d}{ds}(\nabla\varphi) = (e\cdot\nabla)\nabla\varphi = \frac{(\nabla\varphi\cdot\nabla)\nabla\varphi}{n} \tag{3.21}$$

The first step in the differentiation may be explained by considering that s advances in a direction perpendicular to the wave-front. This means that the differentiation

49

with respect to s is equivalent to applying the grad operator and then projecting the answer onto the e direction.

By using the property applicable to an arbitrary scalar field E:

$$(\nabla E \cdot \nabla)\nabla E = \frac{\nabla(\nabla E \cdot \nabla E)}{2} = \frac{\nabla(\nabla E)^2}{2}$$

It is easy to convey to the result:

$$\frac{d}{ds}(\nabla \varphi) = \frac{\nabla(\nabla \varphi)^2}{2n} = \frac{\nabla n^2}{2n} = \frac{2n\nabla n}{2n} = \nabla n \qquad (3.22)$$

We note here that the Eikonal equation has been used again (second equality). Equation (3.22) describes how variation in the sound speed (appearing here as the refractive index n) translates into changes in the direction of propagation of a wavefront.

B) Assumptions

The above equations set the general basis of the theory, but they might be still simplified further by accepting a series of possible assumptions. In the work reported in this chapter, for example, we have adopted two assumptions: First, a two dimensional stratified model of the atmosphere (that is, a constant sound vertical profile along the source-receiver path) and second, linear sound speed profiles.

-Under the premises of the first assumption, the preceding results simplify considerably; the phase function (locally) is then:

$$\varphi(x,z) = -\frac{k_x x + k_z z}{k_0} = -\frac{k \cos\phi x + k \sin\phi z}{k_0} \qquad (3.23)$$

So that

$$\nabla \varphi = -n \cos\phi i - n \sin\phi k \qquad (3.24)$$

Given that we are adopting the assumption of a stratified atmosphere, then n = n(z), in which case:

$$\nabla n = 0i + \frac{dn}{dz}k \qquad (3.25)$$

Using now the result of equation (3.22), the two previous equations can be related as follows:

$$\frac{d}{ds}(n\cos\phi)i + \frac{d}{ds}(n\sin\phi)k = 0i - \frac{dn}{dz}k \qquad (3.26)$$

Equating and integrating the i components gives:

$$\frac{c_0\cos\phi}{c} = constant \rightarrow \frac{\cos\phi}{c} = constant \qquad (3.27)$$

This is simply Snell's law. Indeed we can regard equation (3.22) as a generalisation of Snell's law into three dimensions; it describes the rate at which the normal to the wave-front departs from the ray path (see Figure 3.7)

-Regarding the second assumption, with linear sound speed profiles the radius of curvature for any ray adopts a form that allows an analytical resolution of the ray equation. The radius of curvature R_c is defined as:

$$R_c = |ds/d\phi| \qquad (3.28)$$

By equation (3.27) (Snell's law), the sound speed equals a constant K($=c_0/\cos\phi_0$) multiplied by the cosine of the angle ø. Differentiating this equality respect to z yields:

$$\frac{dc}{dz} = K\frac{d(\cos\phi)}{dz} = -K\frac{\sin\phi \cdot d\phi}{dz} \qquad (3.29)$$

As ds sinø = dz, then:

$$\frac{1}{R_c} = \left|\frac{d\phi}{ds}\right| = \frac{\cos\phi_0}{c_0}\left|\frac{dc}{dz}\right| \qquad (3.30)$$

If we assume a linear sound speed profile so that

$$c = c_0(1 \pm \gamma_T \cdot z) \qquad (3.31)$$

Equation (3.30) states that the inverse of the radius of curvature of a ray is a constant and therefore the ray path is circular. Furthermore, the centres of curvature of all such paths lie on a horizontal line at a distance $\pm 1/\gamma_T$ below (+) or above (-) the surface (Rudnick, I). Under these conditions, (Embleton, T. F. W., et al.) was able to deduce analytically a direct expression for calculating the path travelled by any ray. His method is briefly explained below.

C) Embleton's method

Based on the assumptions described above, (Embleton et al.) developed a theory with which it was possible to evaluate the effects of reflection at a ground of

known, finite impedance and also to evaluate the net sound intensity of waves at the receiver. The method works for linear sound speed profiles with positive slope (downwind conditions or temperature inversion). Under these conditions, we have just demonstrated that ray paths are circular concave arcs with centres of curvature lying all on a horizontal line at a distance $1/\gamma_T$ below the surface. Making use of this geometrical property, (Embleton et al) constructed an analytical equation that described all possible ray paths from source to receiver. For the general case of finite height for source and receiver hs and hr, there were a total of four reflected ray paths for each number of reflections per ray, n, greater than one (in Figure 3.8 is shown the case of n = 1, where the ray group consists of 3 ray paths instead of 4). Furthermore, there were also a total of four ray paths with a similar height H_n at zenith (in Figure 3.9 is depicted the first 4-ray group with maximum height H_1).
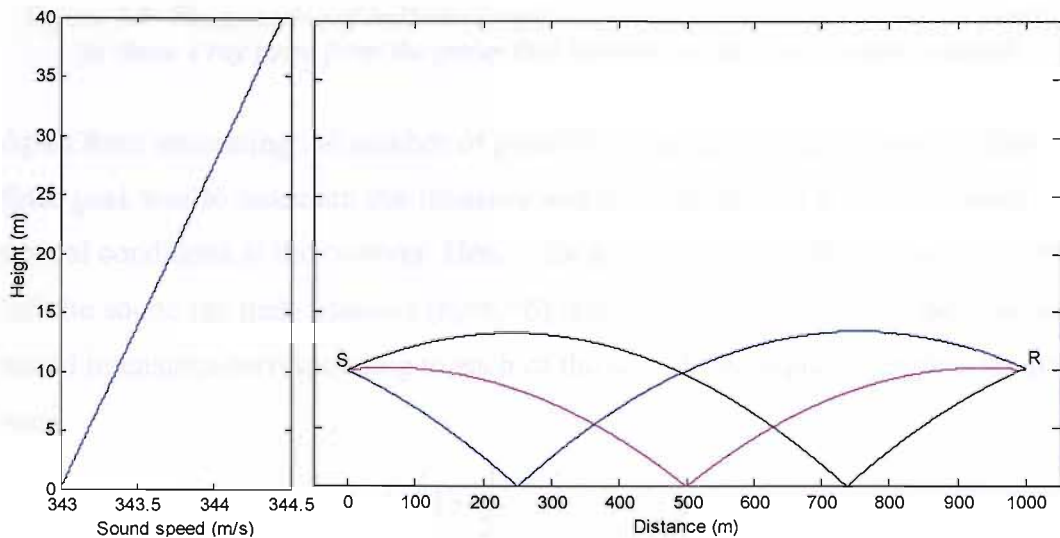
Figure 3.8 *The grouping of individual rays according to Embleton's theory. In particular, these 3 ray paths form the group of rays that reaches the receiver with only one reflection (n=1). With n≥2, the group of rays is formed by 4 rays instead of 3.*

This height is determinant in the theory to find out how many ray paths over the standard two (directed and first reflected) exist in a specific situation. The procedure is described by the equation:

$$H_n = \frac{\gamma_T d_x^2}{8n^2} > \min(h_s, h_r) \qquad for \qquad n = 1,2,3... \qquad (3.32)$$

having used the notation d_x to designate the horizontal distance from source to receiver. Equation (3.32) basically states that if the height reached by a predicted ray, H, is smaller than whatever height is minimum of the source and receiver, then the

ray cannot exist. Therefore it defines an upper limit to the number of possible reflections, since the zenith height is a function of n.
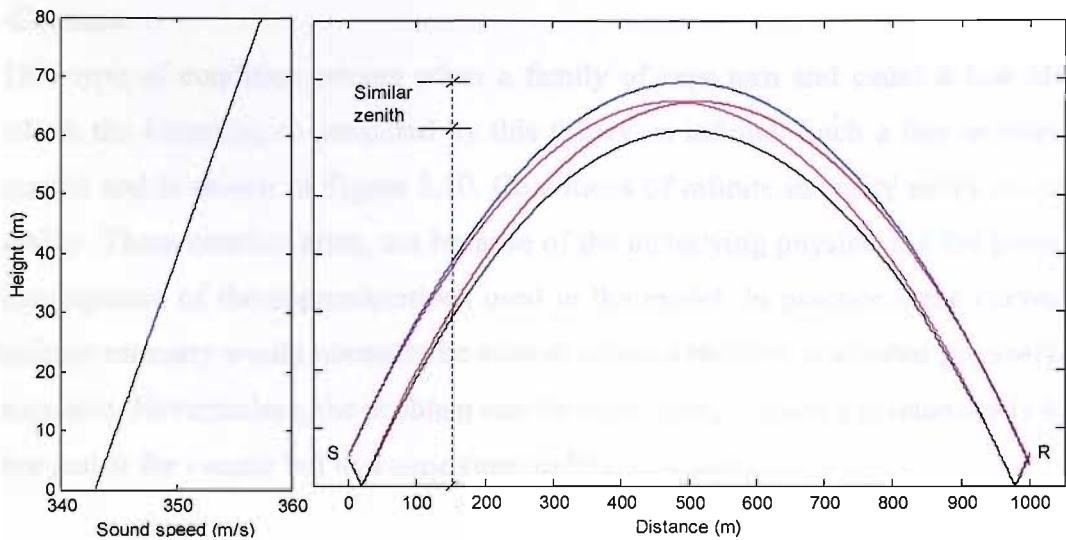
Figure 3.9 *The grouping of individual rays according to Embleton's theory. In particular these 4 ray paths form the group that reaches the maximum height at zenith.*

Apart from estimating the number of possible ray paths and reflections, Embleton's final goal was to calculate the intensity and exceeds of sound pressure level over neutral conditions at the receiver. Hence, for a reflecting hard ground surface and an infinite sound ray path situation ($h_s=h_r=0$), Embleton determined that the sum of all sound intensities corresponding to each of the sets of four equally zenithal ray paths was:

$$I_1 + I_2 + I_3 + ... = I_1 \cdot \left(1 + \frac{1}{2^2} + \frac{1}{3^2} + ...\right) = \frac{\pi^2}{6} I_1 = 1.64 I_1 \qquad (3.33)$$

This suggests that the maximum correction to be added in an inversion/downwind situation over a neutral one is approximately 10log (1.64) = 2.2 dB. A lower value is obtained with soft ground by assuming a reflection coefficient less than unity for the intermediate reflections at the surface, however in the case studied in this chapter (range of maximum and minimum sound pressure levels), the interest focuses on the maximum correction.

D) Ray anomalies

Perhaps, the most serious disadvantage of ray-based models is that wave effects such as diffraction and caustics cannot be handled satisfactorily by ray tracing,

which limits its usefulness for investigating atmospheric sound propagation especially at low frequencies. The main problems arising in ray-acoustics are twofold:

-Caustics:

This type of condition occurs when a family of rays turn and cause a line along which the intensity, as predicted by this theory, is infinite. Such a line is called a caustic and is shown in Figure 3.10. Conditions of infinite intensity never occur in reality. These caustics arise, not because of the underlying physics, but are purely a consequence of the approximations used in the model. In practice these curves of infinite intensity would normally be missed unless a receiver is situated precisely on a caustic. Nevertheless, the problem can be significant, because the intensity is high not just at the caustic but in a zone surrounding the caustic.
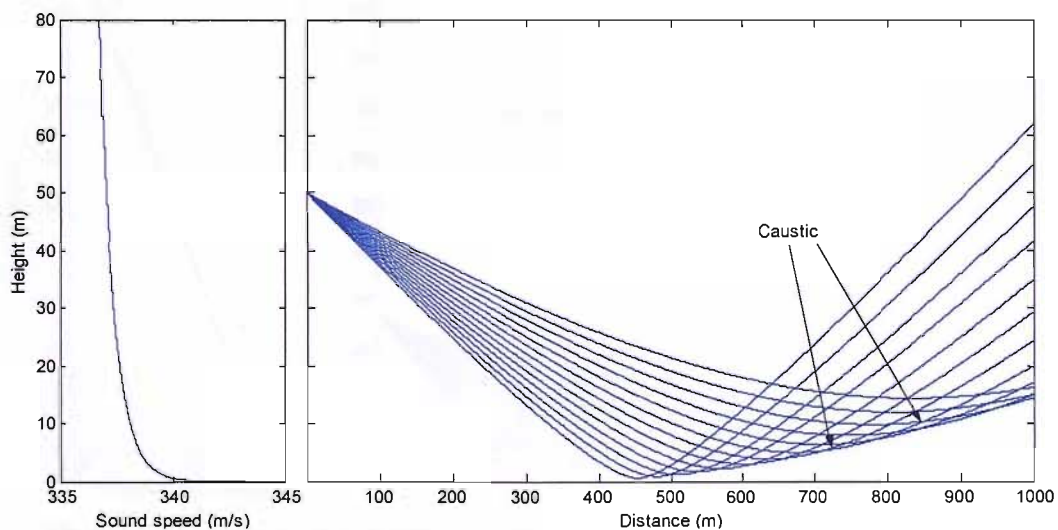
Figure 3.10 *Sound-speed profile and ray trace for an upwind logarithmic profile with a source at 50m high. It can be noted the caustic formed by the rays after the turning point*

It is possible to add corrections to ray theory in order to avoid caustics, but then the method becomes somewhat complicated and at that point, it is perhaps more efficient to adopt a numerical method. A further and more detailed analysis of these corrections is not within the scope of this thesis, but detailed information can be found in (Jensen F. B., et al.) reference.

-Shadow areas

The other common flaw of ray-based models is the occurrence of shadow zones where no rays pass and therefore the pressure field is identically zero. To illustrate

this point, we consider a simpler upwind sound-speed profile in which the sound speed decreases linearly with height. The sound speed profile and resulting ray trace are shown in Figure 3.11 for a source height of 27.65m. As it can be noted, in the range of 0 to about 500m the pressure field is composed of contributions from a direct ray (blue solid lines) and a surface-reflected ray (discontinuous black lines). Beyond about 600m we can see clearly from the ray trace that we are entering a shadow region where there are no rays. The ray (black solid line) that forms the border between the shadow zone and the two-ray region is called the limiting ray. Since no rays get into this shadow area, the sound pressure field predicted by the ray theory becomes -∞ dB, while in reality some sound energy enters the shadow region via diffraction and scattering of the sound waves.
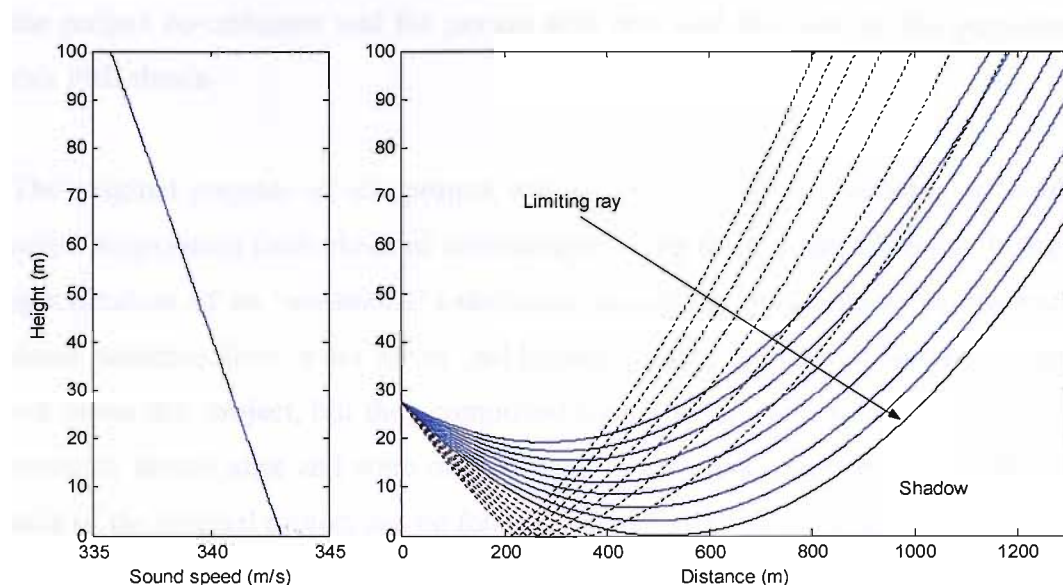
Figure 3.11 *Sound-speed profile and ray trace for an upwind linear profile with a source at 27.65m high. The blue solid lines are direct ray paths, the black solid line is the limiting ray and the discontinuous lines are reflected rays.*

Further studies (Jensen, F. B., et al.) show that it is possible to cope with shadow regions by considering complex take-off angles. Indeed, with complex ray angles one finds that complex eigenrays exist in what we had previously considered a shadow zone. These complex rays can be used to complete the ray theory result and provide a useful prediction into the shadow area. However, in practical applications, these complex rays are almost never used. The reason arises from the fact that they introduce an increased complexity in identifying eigenrays. The approach followed herein is different and more practical: Embleton's ray theory is used for positive

sound speed profiles, while for negative slopes, the curved ground analogy and diffraction theories are used instead.

3.3. The Joule database

The measurement exercise was carried out over flat terrain in the Fenlands area on the eastern coast of England during the first two weeks of August 1996. The propagation test was part of a group project partially funded by the European Commission in the framework of the Non-Nuclear Energy Programme. The project team consisted of three different parties: Renewable Energy Systems Ltd, Hoare Lea and Acoustica a/s, of which Dr. JH. Bass, Dr. AJ Bullmore and E. Sloth were respectively representative and directly responsible of the project. Dr. AJ Bullmore was the project co-ordinator and the person who provided the data for the purposes of this PhD thesis.

The original purpose of the project was to further the understanding of outdoor noise propagation from elevated noise sources, with the ultimate objective being the specification of an 'optimised' calculation procedure applicable to environmental noise radiation from wind farms. Additional measurement exercises were carried out under this project, but they comprised sound propagation tests over rolling and complex terrain sites and were not analysed in the work reported here. Further details of the original project can be found in the ref. (Bass, J. H. et al.).

Continuing the description of the measurement field characteristics, the site was several kilometres from the nearest residence and was similarly remote from other sound sources such as main roads, railways or industries. As Figure 3.12 shows, a series of 7 data logging sound level meters were deployed along a line extending out to 675m away from an approximately omnidirectional source erected at 29m height above the ground and having a sound power output level of approximately 111dB(A) of pink noise. The monitoring points were located at 51, 101, 202, 300, 400, 523, and 676m horizontal distances from the point source and at a height of 1.2 m above the ground. In order to study the sound level variability resulting from a wide range of meteorological conditions, the acoustical propagation test was undertaken over a 2 week monitoring period.

Figure 3.12 *Aerial picture of the test site. Receiver locations are shown in black and white with its respective reference numbers and the source is pointed with a red cross.*

A meteorological monitoring station was deployed in a central location relative to the distribution of the sound measurement locations and was set-up to record 1 minute met data continuously throughout the measurement exercise. The met station comprised a 30m mast holding 2 anemometers at 11.6 and 27.6m, 2 temperature sensors at 1.75 and 27.6m and humidity, pressure and rainfall gauges, all at ground level.

Amongst the large range of results reached by the analysis of these empirical data (Bass, J. H. et al.) found a significant and increasing relationship between the standard deviation of the recorded $L_{Aeq,1min}$ values for each of the 7 receivers and their respective distances to the source. Figure 3.13 shows this increasing relationship for the sub-set of the overall database used for the analysis reported in this work. Only those data for which simultaneous measurements were available at all 7 receiver positions were selected for the analysis reported in this thesis. The original report (Bass, et al.) shows a linear relationship when the entire dataset was included in the analysis.
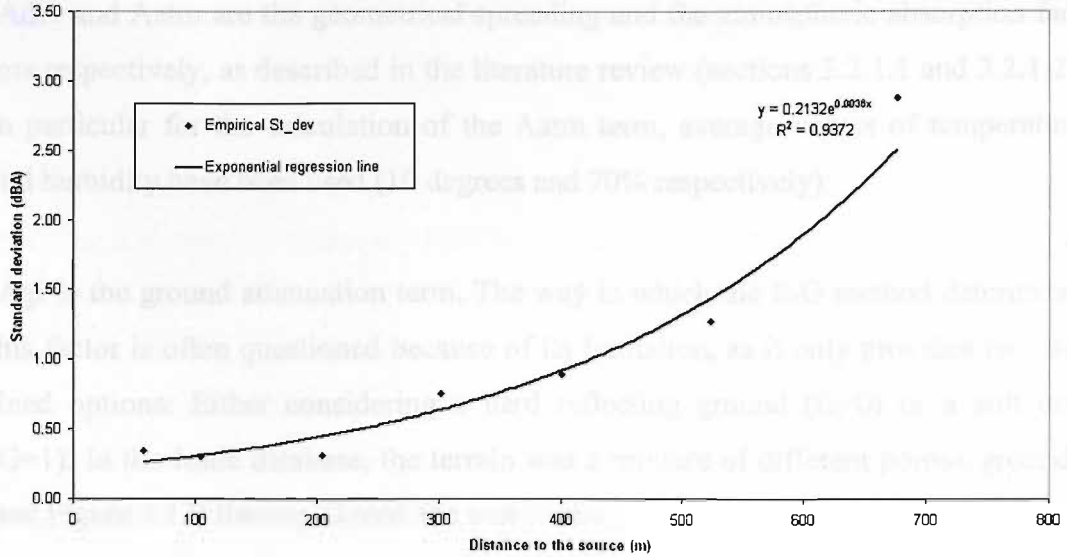
Figure 3.13 *Standard deviation of recorded $L_{Aeq,1min}$ values against source-receiver distances, using a sub-set of (Bass, et al.) measurement database*

3.4. Results

3.4.1. Comparison against ISO 9613-2

Starting from the methods set out in (ISO 9613-2), it was first investigated if ISO predictions were any closer to the averaged measured levels of the 7 receivers. This was undertaken by calculating the different terms that appear on the ISO basic formula for predicting sound pressure levels. This formula states that the sound level at the receiver, Lft, for each nominal midband frequency of the octave band, equals the sum of the following factors:

$$Lft(i) = Lw - Adiv - Agr - Aatm \qquad (3.34)$$

ISO 9613 combines this equation with the following expression for calculating the equivalent continuous A-weighted sound pressure level:

$$L_T = 10\log\left[\sum_{j=1}^{8} 10^{0.1(Lft(j))}\right] \qquad (3.35)$$

-In (3.34), Lw represents the sound power level of the source (see Table 3.1).

Table 3.1 *Sound power level in octave frequency bands (dBA).*

63Hz	125Hz	250Hz	500Hz	1kHz	2kHz	4kHz	8kHz	DBA
71.1	92.2	106.8	104.2	106.4	100.8	99.6	71.2	111.5

-Adiv and Aatm are the geometrical spreading and the atmospheric absorption factors respectively, as described in the literature review (sections 3.2.1.1 and 3.2.1.2). In particular for the calculation of the Aatm term, average values of temperature and humidity have been used (10 degrees and 70% respectively)

-Agr is the ground attenuation term. The way in which the ISO method determines this factor is often questioned because of its limitation, as it only provides two defined options: Either considering a hard reflecting ground (G=0) or a soft one (G=1). In the Joule database, the terrain was a mixture of different porous grounds (see Figure 3.12) thereby G took the unity value.

The ISO method clearly states that is only applicable for 'meteorological conditions favourable to propagation from sources of known condition'. This arises from the ISO approach to find a generic worse case scenario to environmental noise impact rather than the exact solution to any sound propagation situation. Despite this approach, it is true that the model includes a factor, C_{met} to account for any other wind condition unfavourable to sound propagation. However, the calculation of C_{met} is not clearly defined by the standard; The ISO method just provides an estimation of the maximum or minimum value that C_{met} can reach in practice, but no information about how to quantify it exactly. For this reason C_{met} has not been considered in equation (3.34) and neglected from this study.

The predictions of the ISO method have been compared against average sound measured levels in Figure 3.14. Despite the "worse case" approach of the ISO method, the two trends show a sensible match. The maximum deviations between the two lines occur at short distances from the source, but never exceed 2 dB. Amongst the possible reasons why the predicted and measurement trends agree, the following two have been considered:

-Since the ISO method only applies to downwind conditions to sound propagation, the first idea was to investigate whether the actual met conditions during the measurement exercise were predominantly under favorable meteorological conditions. A revision of the met data shows that negative sound speed gradients (unfavorable conditions) were present at a percentage of 35% over the test duration. The met

conditions applicable to the ISO method were the most dominant (65%), which gives the most likely explanation of the agreement shown by Figure 3.14.

-One other possible justification is that upwind conditions might not contribute much to the average measured levels over a long or mid term average period. (Heimann, D. and Salomons E.) show that instantaneous sound levels vary due to different meteorological conditions by up to 1 dB (20 m), 9 dB (200 m), and 21 dB (1000 m range) for one year over an absorbing ground. Noise levels recorded under unfavorable met conditions can then be well below downwind sound levels contributing very little to the average noise value.
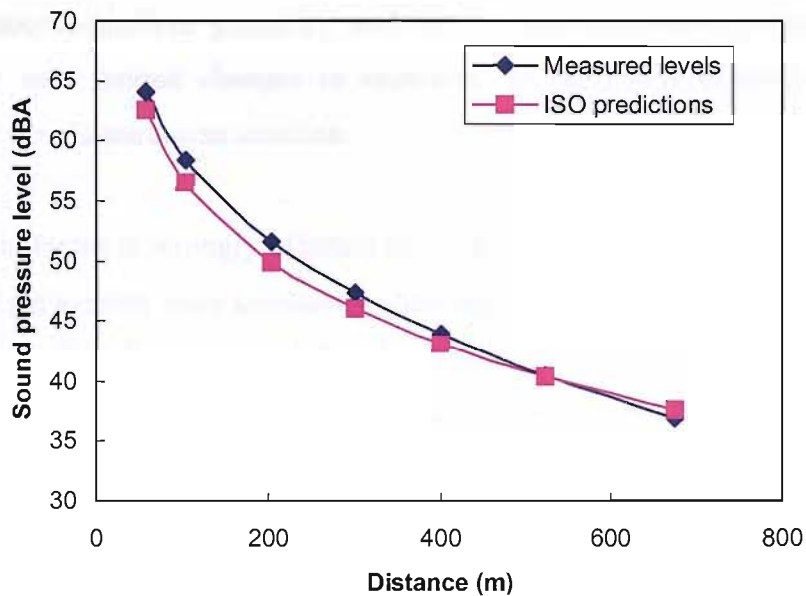
Figure 3.14 *Differences between average sound measured levels & ISO9613 predictions*

Whether one of the two above reasons is applicable or a combination of the two, the fact is that the ISO method seems to work properly for this particular exercise. The small differences between the two results ensure that further predictions and analysis of noise level variability using the ISO method as a starting point are to be suitably fixed on a correct central value.

After validating ISO predictions against measured central values, the variability of all separate mechanisms considered by the ISO method was examined to explain theoretically the observed relationship of Figure 3.13. By considering all separate terms of equation (3.34), it was investigated how much of the standard deviation of

each of these features contributed to the overall sound level variability shown in Figure 3.13:

-**Lw.** Although the loudspeaker system was programmed to produce a constant sound power level throughout the experiment, some limited fluctuation in sound power output is unavoidable. (Bass et al.), anticipating this possibility, tested the sound generating system under both reverberant and anechoic conditions, and calculated by reproducibility a standard deviation in the output level of 0.36 dB.

-**Adiv, Agr.** Both factors are negligible for a sound variability analysis. Adiv only varies with distance (which is constant for each receiver) and Agr depends on the unaltered source-receiver geometry and the surface characteristics which, apart from some very limited changes in vegetation growth, were otherwise constant throughout the measurement exercise.

-**Aatm.** This factor is strongly affected by both temperature and humidity fluctuations. Both parameters were constantly changing throughout the sound propagation test and it was therefore expected that Aatm would contribute to the overall sound level variability. A clear demonstration of the not inconsiderable magnitude of the Aatm variation is given by (Larsson C), who undertook a very comprehensive study in Sweden based on hourly values of temperature and relative humidity over 30 years. The duration of our experiment is in contrast limited to 2 weeks, but the 1-min values of temperature and relative humidity are still sufficiently dispersed to have some effect on the overall noise level variability. For calculating the combined contribution of the different meteorological factors involved, the statistical propagating error theory (Young, H.D.) was used. This theory states that when a quantity, Q, is to be calculated from several observed quantities a, b, c... by a relation Q = f (a, b, c...), its variance is related to the variances of the independent parameters a, b, c... by:

$$\sigma_Q^2 = \left(\frac{\partial Q}{\partial a}\right)^2 \cdot \sigma_a^2 + \left(\frac{\partial Q}{\partial b}\right)^2 \cdot \sigma_b^2 + \left(\frac{\partial Q}{\partial c}\right)^2 \cdot \sigma_c^2 + ... \qquad (3.36)$$

Applying this equation to equations (3.35) and (3.34), considering only the contribution of Aatm to the overall sound level variability, a function was obtained that

described the standard deviation of Aatm in terms of the overall dB(A) sound pressure levels. Applying again equation (3.36) over the theoretical expression (see ANSI or section 3.2.1.2) that relates the Aatm with the two assumed independent variables temperature, T, and molar concentration of water vapour, H (linked to humidity), we obtained:

$$\sigma_{L_T} = d' \cdot \left[\frac{1}{100} \sqrt{\sum_{i=1}^{8} \left\{ \left(\frac{10^{0.1 L_{ft}(i)}}{10^{0.1 L_T}} \right)^2 \cdot \left(\left(\frac{\partial \alpha}{\partial T} \right)^2 \cdot \sigma_T^2 + \left(\frac{\partial \alpha}{\partial H} \right)^2 \cdot \sigma_h^2 \right)_i \right\}} \right]$$

(3.37)

In equation (3.37), L_T and Lft(j) are the values that the ISO 9613 predicts by using averaged environmental conditions (and that have already been validated against measured levels), d' is the horizontal source-receiver distance and α is the absorption coefficient (in dB/100m). Substituting the variables by their respective numerical values observed experimentally, equation (3.37) can be approximately expressed by the relation $\sigma_{L_T} = 0.0007 \cdot d'$. This relation shows that the contribution of Aatm to the overall sound level standard deviation is proportional to the distance.
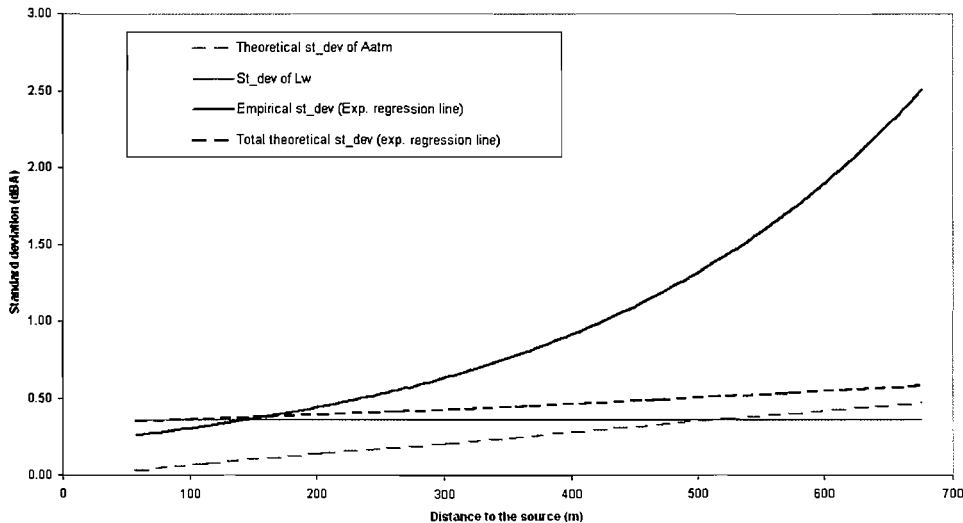
Figure 3.15 *Differences between empirical variability and theoretical sound level standard deviation based on Lw and Aatm*

By plotting the sound variability contributions of the sound source power output (Lw) and the atmospheric absorption changes (Figure 3.15), we note that the resulting combined standard deviation from both contributions is well below the empirical variability observed in the measurement exercise at distances exceeding 200-300m. This difference suggests that additional variables to those considered by the ISO 9613 method must also contribute to the observed fluctuations in sound levels.

62

3.4.2. Meteorological variability

In order to account for the additional sound level variability not explained by the variables included in ISO 9613-2, a further investigation of the additional effects of sound ray curvature dependant on meteorological conditions was carried out. The sound speed profile for each measured minute throughout the experiment was first calculated. In the estimation of this profile both temperature and wind gradients were assumed linear.

-Under the assumption of a temperature, T, linearly dependant on height, T(z) could be written as $T(z) = T_0 + dT/dz \cdot z$, where T_0 is the temperature at 0m (in Kelvin). Knowing that the sound speed varies with temperature according to:

$$c = c_0 \sqrt{\frac{T}{T_0}} \tag{3.38}$$

and applying Taylor approximation at $z_0 = 0m$, the sound speed gradient was finally expressed by:

$$c(z) = c_0 \cdot \left(1 + \frac{dT}{dz} \frac{1}{2T_0} \cdot z \right) \approx c_0 \cdot \left(1 + k_T \cdot z \right) \tag{3.39}$$

-Regarding the mathematical expression of the linear wind gradient, a Taylor approximation at z_0=0m was not entirely appropriate here, since the tangent at 0m height of a theoretical log wind profile stands more for the abscise axis than for the actual overall wind-front. Hence, the linear wind profile was directly calculated by using the two wind speed measurements at both 11.6 and 27.6m anemometers. With these measurements was possible to extrapolate the overall wind-front gradient dv/dz, and express the wind speed v(z) by:

$$v(z) = \left(v_{h1} - \frac{dv}{dz} h_1 \right) + \frac{dv}{dz} z = \alpha + \frac{dv}{dz} z \tag{3.40}$$

the term v_{h1} accounts for the wind speed measured at h_1=11.6m.

The total linear sound speed profile was then obtained combining equations (3.39) and (3.40):

$$c(z) = c_0 \cdot (1 + \gamma \cdot z) + v(z) = (c_0 + \alpha) \cdot \left[1 + \left(\frac{c_0\gamma + dv/dz}{c_0 + \alpha} \right) z \right] = k_0(1 + \gamma_T \cdot z) \quad (3.41)$$

Calculating the numerical values taken by γ_T for each of the measured minutes, we could differentiate those time periods with positive sound speed gradients (downwardly curving effects) from those with negative values of γ_T (upwardly curving effects). Depending on the sign of this parameter, we used either Embleton's ray-acoustic theory (+ γ_T) or a curved ground analogy combined with diffraction theories (-γ_T) to explain the meteorology variability in noise levels.

A) Downwardly curving effects (+ γ_T)

The maximum positive gradient, γ_T, obtained for the whole measured period was 0.0006 m^{-1}. With this value it was determined the maximum number of reflections (n) and the excess of the sound pressure level over neutral conditions at each receiver according to Embleton's method described in page 51. The results are shown in the following table (for the microphone reference see Figure 3.12):

Table 3.2 *Sound level increment predictions for the downward refraction effects of the flat ground acoustical test.*

Ref.	Distance (m)	$H_1 = d^2\gamma/8$	$H_n = H_1/n^2$ if $< h_s = 29.37$	n	Increment (dB)
M11	51	0.20	0.20 < 29.37 =>	1	0
M1	100.8	0.76	0.76 < 29.37 =>	1	0
M12	202.4	3.07	3.07 < 29.37 =>	1	0
M9	300.3	6.76	6.76 < 29.37 =>	1	0
M13	400.1	12.01	12.01 < 29.37 =>	1	0
M7	523.1	20.52	20.52 < 29.37 =>	1	0
M15	675.8	34.25	34.25/4 < 29.37 =>	2	$10\log(1+1/2^2) = 0.97$

B) Upwardly curving effects (-γ_T)

In this case, Embleton's theory is not applicable for calculating the negative excess of sound pressure level over neutral conditions. Sound rays still travel from source to receiver along circular arcs, since the assumption of linearity in both temperature and wind gradients is still valid. However, this time, the arcs are convex upwards and the centres of curvature of such convex arcs all lie on a horizontal line at a dis-

tance $1/\gamma_T$ above the surface. When tracing the sound convex rays from the source with centre in the horizontal line $1/\gamma_T$ above the surface, we note (see Figure 3.16) the appearance of a shadow area which makes inappropriate the application of basic ray-acoustic models (as discussed in page 54).
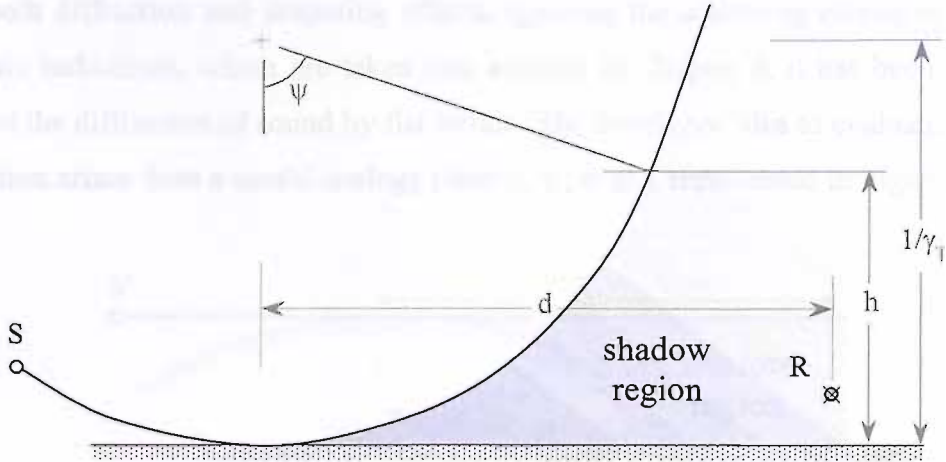
Figure 3.16 *Schematic 2D view of the limiting ray geometry under lapse or/and upwind conditions.*

The ray from which no further rays can be drawn is called the limiting ray, shown in Figure 3.16, and is geometrically defined as the one that leaving S is tangent to the surface. The relative situation of this ray with regard to the receiver indicates whether the receiver R is inside or outside the shadow region. Mathematically, the geometrical criteria can be written as follows:

$$If \quad \frac{1}{\gamma_T} - \sqrt{\frac{1}{\gamma_T^2} - \left(d_x - \sqrt{\frac{2h_s}{\gamma_T} - h_s^2}\right)^2} \geq h_r \ or \notin \Re \Rightarrow R \ is \ in \ shadow \qquad (3.42)$$

the horizontal distance between the source and the receiver is here expressed by d_x.

Substituting the most negative value of γ_T registered during the measurements (which is -0.0006 m^{-1}) into the above criterion (3.42), only three out of the seven receivers were inside shadow areas: M13, M7 and M15 (the three furthest measurement locations). The other four receivers were permanently reachable by at least two ray paths: the direct and the one reflected. The non-shadowed situation is not more different than the typical situation of source-receiver over flat surface in neutral meteorological conditions, thereby no additional correction should be considered for these 4 receivers.

65

Instead, for shadowed locations, some corrections are required over the neutral case. The calculation of these corrections may be poorly performed by Embleton's method as the lack of sound rays intersecting the receivers would provide a $-\infty$ dB level; when in reality, shadow areas do receive some sound pressure, partially due to both diffraction and scattering effects. Ignoring the scattering effects of atmospheric turbulence, which are taken into account in Chapter 4, it has been investigated the diffraction of sound by flat terrain. The developed idea to evaluate the diffraction arises from a useful analogy (Berry, A., et al.), represented in Figure 3.17.
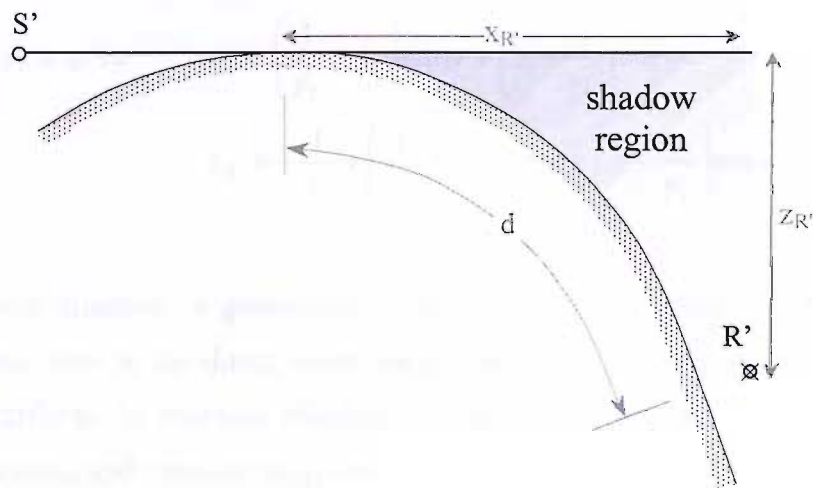
Figure 3.17 *Curved ground analogy. The scenario is analogous in terms of received sound pressure in R to the situation depicted in Figure 3.16.*

Upwardly curving sound paths travelling through a refracting atmosphere over flat ground can be equally seen as straight paths over a downwardly curved ground in neutral meteorological conditions. It is important to highlight that, at certain height, h (i.e. 100-150m; see Figure 3.16), sound rays become straight, since the wind speed at those altitudes and thereafter has a negligible variation. This characteristic must be bore in mind to avoid the unrealistic situation in which sound rays (or similarly the imaginary surface ground of Figure 3.17) keep on curving up to reach its origin.

When using the above analogy, source and receivers require to be relocated over the so-generated convex ground. To this end, their new locations have been assumed to

be: same distance away from the tangent point, but projected along the circular surface, and as elevated from the ground as in the initial scenario.
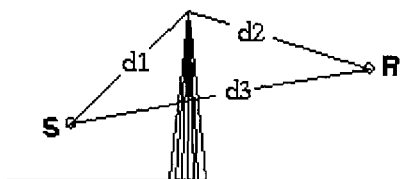
Analytically, setting a reference origin in the tangent point between the limiting ray and the ground surface, the shifting criteria for the new co-ordinates can be written as:

$$If \; d \cdot \gamma_T \leq \psi \Rightarrow \quad x_{R'} = \left(\frac{1}{\gamma_T} + h_r \right) \sin(d \cdot \gamma_T)$$

$$z_{R'} = -\frac{1}{\gamma_T} + \left(\frac{1}{\gamma_T} + h_r \right) \cos(d \cdot \gamma_T)$$

$$If \; d \cdot \gamma_T \geq \psi \Rightarrow \quad x_{R'} = \left(\frac{1}{\gamma_T} + h_r \right) \sin\psi + \left(d - \frac{\psi}{\gamma_T} \right) \cos\psi$$

$$z_{R'} = -\frac{1}{\gamma_T} + \left(\frac{1}{\gamma_T} + h_r \right) \cos\psi - \left(d - \frac{\psi}{\gamma_T} \right) \sin\psi$$

(3.43)

Once the new situation is geometrically defined, one can noted that the curved ground stands now in the direct sound path, leaving the receivers in a shadow region. Contrarily to the previous situation, the general diffraction theory can be applied in this case, and consequently, sound pressure levels can then be calculated by standard methods. In the present investigation, it has been adopted the procedures of the ISO 9613-2, which are mainly based on (Maekawa)'s theory. In general terms, the ISO 9613 states that the screening attenuation can be calculated by the equation:

$$D_z = 10 \lg \left[3 + \left(\frac{20}{\lambda} \right) z_{eq} \right]$$

(3.44)

being λ the wavelength of sound at the nominal midband frequency of the octave band, in metres; and z_{eq} the equivalent distance:

$$z_{eq} = d_1 + d_2 - d_3$$

(3.45)

Expressing the distances shown in the above figure in terms of our particular diffraction exercise, we come up with:

$$d_1 = \sqrt{\left(\frac{1}{\gamma_T} + h_s\right)^2 - \frac{1}{\gamma_T^2}}; \quad d_2 = \sqrt{x_{R'}^2 + z_{R'}^2}; \quad d_3 = \sqrt{(d_1 + x_{R'})^2 + z_{R'}^2} \qquad (3.46)$$

Applying the curved ground analogy, and using jointly equations (3.46), (3.45) and (3.44) for the receivers M13, M7 and M15, the maximum sound attenuation generated by the upwardly curving effect can then be easily calculated (see Table 3.3)

Table 3.3 *Sound level corrections for the upward refraction effects of the flat ground acoustical test.*

M11	M1	M12	M9	M13	M7	M15
No shadow	No shadow	No shadow	No shadow	-3.06 dB	-7.30 dB	-11.78 dB

C) Overall corrections

Having calculated the maximum (Table 3.2) and minimum (Table 3.3) sound level corrections from both downwards and upwards ray curvature, the overall standard deviation for atmospheric refraction effects was estimated by assuming that its statistical distribution satisfied:

$$largest \;\; value - smallest \;\; value \approx (mean + 3\sigma) - (mean - 3\sigma) \approx 6\sigma \qquad (3.47)$$

This '6 times standard deviation' rule is commonly applied in well-behaved statistical distributions with properties that are not extremely far from standardised distributions (i.e. Gaussian, Gamma, Chi Square, Student's t, etc...). The calculated corrections presented in Table 3.2 and Table 3.3 suggest that our particular distribution is slightly skewed towards the negative values of the sound speed gradient and therefore, that our sample might not be normally distributed about the mean. However, there are not reasons to believe that other skewed standardised distributions (such as the Chi-Square or the Gamma) could not be adjusted for our sample. Only distributions with very extreme statistical properties (i.e. multi-modal peaks), which are far from being our case, might compromise the approximation expressed by equation (3.47).

By using then the assumption stated in (3.47), we obtained a sound level standard deviation from the atmospheric refraction effects of 0.51, 1.22 and 2.13 dB respectively for the three furthest microphone sites.

Figure 3.18 shows the separate contributions to overall standard deviations from variability at source, variability in atmospheric attenuation, and variability in atmospheric refraction, all compared with the overall observed standard deviations of Figure 3.13. By combining the separate modelled effects, the figure shows much better agreement between the overall experimental (solid black) and the overall theoretical (dashed black) sound variability regression lines.
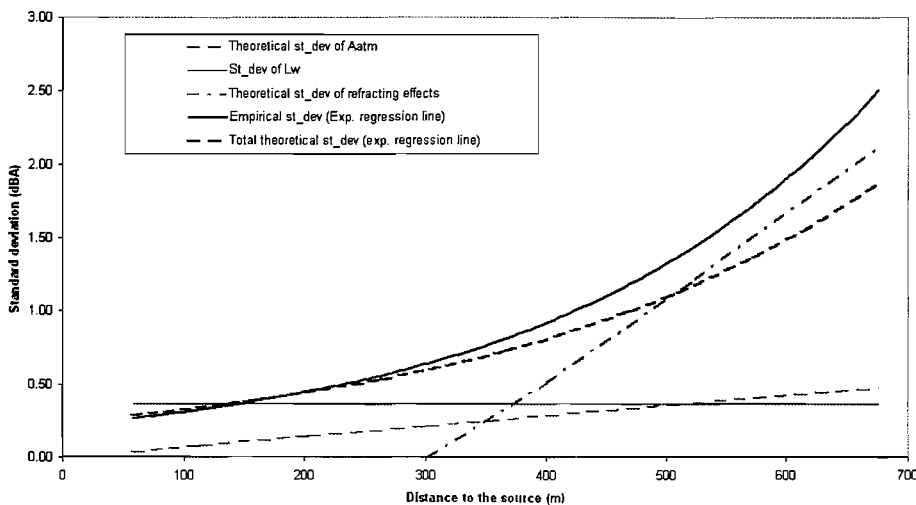
Figure 3.18 *Differences between experimental results and theoretical prediction of sound level variability.*

The procedure described in A-C sections above is an approximate method for the estimation of the noise level standard deviation. There are more detailed methods (for example, the residue series, Montecarlo analysis, etc...) which could calculate the noise level variability computing all meteorological data recorded during the acoustical experiment. However, the aim pursued here was to develop a practical method to estimate the noise variability contribution from atmospheric refraction effects based on limited meteorological information. In fact, a common problem in practical environmental acoustics is that meteorological data is rarely available in a sufficient level of detail to derive the statistics on met variation. The method described above is less demanding and good enough for our purposes as shown by Figure 3.18, thereby the application of more detailed methods is not required.

3.5. Conclusions

Out to a distance of 300m from the source, our analysis suggests that just those variables considered by ISO 9613-2 are sufficient to represent the overall sound level variability observed in the Joule III measurement database. Within the 300m distance, small changes in measured source sound power output and predicted changes in atmospheric absorption rates were the most important controlling factors.

Beyond 300m, however, just those mechanisms included within ISO 9613-2 were not enough on their own to explain the observed variability in measured sound levels. Instead as the source to receiver separation distance increases, the atmospheric refraction effects not included in the ISO standard seem to become the increasingly dominant factor.

For predicting the range of noise variation arising under these refraction effects, an hybrid theoretical model was developed. The ray-tracing model of (Embleton, T. W. F) explained the excess of sound pressure level with positive sound speed gradients, while an extended curved ground analogy accounted for the negative sound level corrections in shadow areas. The application of both theories resulted in the expression of the atmospheric refraction effects in terms of noise level variability. These predictions combined with the theoretical variability modelled considering only ISO variables were in good agreement with the overall variation observed in the data.

Subject to the particular conditions of the Joule database (i.e. the flat ground propagation and the relatively high noise source), the general finding of relevance of this analysis is the identification and quantification of the different noise variability contributions associated with the main environmental factors controlling the outdoor sound propagation. Furthermore, the predicted influence of medium-term meteorology and source-receiver distance on noise level variation fully agrees with the qualitative explanation given in the previous chapter.

Chapter 4

Effects of Short-Term Meteorology in Noise Level Variability

4.1. Introduction

Chapter 3 covered the effects of medium-term meteorology on noise level variability by investigating a flat ground sound propagation test (Joule database) over 2 weeks. One of the results of this investigation showed that the atmospheric effects (specially the wind shear effects) were the predominant cause of noise level variability at long and medium distances. The Joule database covered wind speed records on a time scale of minutes, hours and days, but did not contain wind information in a sufficient level of short-term detail to analyse the effects of faster atmospheric variations.

In reality, the wind profiles also change on a time scale of seconds, as illustrated by the (Van de Hoven) spectrum of Figure 4.1. This figure shows the amount of variation in the wind speed associated with a particular time scale. By looking at the figure, one can notice three major peaks: The largest, occurring over a few days (100 hours) and the smallest, at 10 hours, arise respectively from the pressure system pass-byes (synoptic variations) and the daily atmospheric variability. While the second most significant peak, occurring in a time-scale of seconds, is originated by the

mechanical and convective turbulence of the atmosphere. Influence of both synoptic and diurnal variations on noise levels were investigated in Chapter 3 through the analysis of the Joule database, however the turbulence effects were excluded as the Joule records were insufficiently time-scale detailed to track these fast variations.
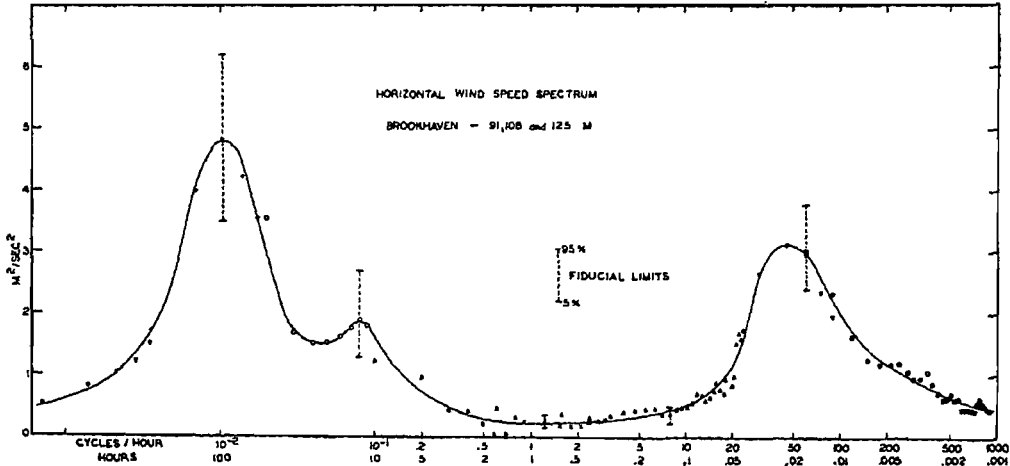
Figure 4.1 *The Van de Hoven Spectrum showing the amount of variation in wind speed on a particular time-scale*

There is a clear borderline between the short-term wind variations (turbulence) and both the daily and synoptic variations. In the case of short-term variability, turbulence take place on time scales of seconds, resulting in a rate of variation which is much quicker than the fluctuating rate of the bulk of the wind flow. Daily and synoptic variations are instead dominated by the variability of average wind profiles, averaged over a period that could range between ten minutes and two hours (which corresponds to the spectral gap in Figure 4.1, just beyond the time-scale affected by turbulence). The average wind profiles are smooth functions of height and represent the bulk of the wind flow, while the instantaneous profiles are driven by atmospheric turbulence and are sharper and irregular.

In the same way that turbulence and daily-synoptic variations occur on different time-scales, they also size differently in the space domain. The physical base of atmospheric turbulence is the eddy (which denotes the loops given by the particles when they are part of a turbulent flow), while the physical base of the synoptic variability corresponds to the pressure system pass-bys, on the understanding that a pressure system pass-by is also an eddy but in a very large-scale (indeed, when one

observes a satellite picture of the Earth, the weather systems actually appear as eddies). Compared to the dimension of our field experiment, the size of the pressure systems is so large that the same average wind profile can be assumed between the source and the receivers when calculating the sound level in a particular instant of the slow movement of the pressure system. Hence, the sound wave propagation can be considered in this case as being range independent (and can then be modelled by range-independent methods, like the FFP). In contrast, the turbulent eddies are usually much smaller than the source-receiver distance and consequently, if one wants to calculate the sound pressure levels, different wind profiles should be assumed along the propagation path. In this case the propagation is range dependent (and the PE method becomes the most suitable way of modelling).

The objective of this chapter is to focus on the influence of atmospheric turbulence on measured noise levels. To assist in this analysis, a PE model was developed so that the complex sound speed profiles generated by the atmospheric turbulence could be taken into account.

4.2. Literature review

This section reviews three main subjects:

-First, the current knowledge on how to model the atmospheric-acoustic environment in detail, specially the sound speed vertical profiles. In Chapter 3, these profiles were approximated as linearly dependant on height, but in here, other more exact approximations are used.

-Second, the ground interaction. The use of a sound propagation model based on the direct solution of the wave equation requires the mathematical description of the boundaries of our propagation area. While the top boundary corresponds to the free field condition and is easily characterised acoustically, the bottom one refers to the ground and has a more complex acoustical definition, as demonstrated by the variety of theories available for its mathematical description.

-Third, the fundamentals of the PE model. It is important to understand the basis of this numerical method as is the starting point for developing a turbulence model to account for the experimental observations collected in the Salisbury Plain database.

4.2.1. The atmospheric-acoustic environment

Repeated measurements of outdoor sound levels often vary over a wide range, from a few decibels up to 15-20 dB or even more. Most of the causes of this variation arise from the complex nature of the atmospheric-acoustic environment.

The atmosphere is an acoustic waveguide without top acoustical boundaries, but limited below by a broad range of shapes and terrain types. Despite of its extension, the region acoustically relevant to environmental noise lies below a height of about 1-2 km over the ground. This region is known as the planetary boundary layer and is characterised by the fact that all the friction phenomena between the atmosphere and the ground take place within. The planetary boundary layer is in turn divided in two: the surface layer, which extends to 100 m high over the ground and the Ekman layer. The former one is, for most of the outdoor noise propagation cases, the actual acoustical waveguide.

The variation of sound speed at different heights within this waveguide plays an important role and essentially determines the characteristics of the sound propagation within it. In the atmosphere, sound speed is related to density, moving properties of the medium and compressibility; however the key variables to account for sound speed are temperature and wind as all the other basic properties can be computed from them.

Unfortunately, these two controlling parameters do not have a constant homogeneous behaviour in the atmospheric surface layer. The wind and temperature fields are highly sensitive to terrain variability and to the heterogeneity of the atmosphere which results in the impracticability to have precise information of these fields by using current measurement techniques. Nevertheless, there are several atmospheric models which can provide a "best guess" based on few observations. These models generally agree when predicting vertical temperature profiles: They accept a constant temperature slope with height along the Eknam layer (see Figure 4.2-left) and

a number of different behaviours within the surface layer depending on the stability in the atmosphere. Stability can be categorised in the well-known Pasquill classes that depend on observations of wind speed and cloud cover (see Table 4.1). They are usually referred to as classes A (extremely unstable) through F (very stable) or as numbers, where m is usually the symbol that represents the numerical value given to each class.

Table 4.1 *Pasquill stability classes*

Class	Category	Description	m
A	Extremely unstable	Weather conditions are very unpredictable. Wind speed average 1 m/s but is gusty. The temperature rapidly decreases with altitude. It is common on a hot sunny day.	0.09
B	Moderately unstable	Weather conditions are still unpredictable, but less so than "A". Wind speeds average 2 m/s, and is not gusty. The temperature still decreases, but not as rapidly, with altitude. This condition is common on a sunny warn day.	0.2
C	Neutral	Weather conditions are more predictable. Wind speeds average 5 m/s, with no expected gustiness. The temperature still decreases with altitude, but the change is less pronounced. This condition is common on an overcast day or night (heavy overcast)	0.22
D	Slightly stable	Weather conditions turn more predictable than with "D". Wind speeds average 3 m/s. The temperature does not change with altitude. This condition generally occurs at night, and is considered an average night (partly cloudy)	0.28
E	Moderately stable	Weather conditions become very predictable. Wind speeds average 2 m/s. Temperature increase with altitude. This condition generally occurs at clear-sky nights with light winds.	0.37
F	Very stable	This condition is very predictable, but rarely occurs. No winds blow and the temperature increases rapidly with altitude.	0.41

Hence, for example, at the first half of clear-sky nights in the absence of relatively high winds (stable conditions), there is often a radiation cooling of the ground which produces cooler air near the surface, leading to a temperature inversion. During the day, when solar radiation heats the earth's surface (unstable conditions), there is an opposite effect, warmer air remains near the ground decreasing gradually with height. The variation of temperature for the atmospheric surface layer is generally estimated for more practical purposes by assuming a decreasing or increasing linear relationship with height. This relationship was mathematically derived in last chapter on page 63 through equations (3.38) and (3.39).

For vertical wind profiles, modelling theories show more disagreement. They all agree that the wind speed increases smoothly with height up to the end of the sur-

face layer and then negligibly thereafter. However, the rate of increase is modelled in different ways:

-Usually a fixed relation is assumed between the wind speed v_h at height h and the wind speed v_{ref} at a reference height h_{ref}, which is the widely used logarithmic wind profile with surface roughness z_L, see Table 4.2, as the only parameter. See for example (Rudnick, I.) or the international recommendations for wind turbine noise emission measurements (IEC 61400-11). For height h the wind speed v_h is calculated as follows:

$$v_h = v_{ref} \log\left(\frac{h}{z_L}\right) \Big/ \log\left(\frac{h_{ref}}{z_L}\right) \qquad (4.1)$$

Table 4.2 *Typical values of surface roughness length z_L for various types of terrain.*

Type of terrain	z_L (m)
Mud flats, ice	10^{-5} to 3×10^{-5}
Sand	2×10^{-4} to 10^{-3}
Mown grass	0.001 to 0.01
Low grass	0.01 to 0.04
High grass	0.04 to 0.1

-Other authors, such as (Bradley, S. G.), suggest that wind profiles can have such an enormous complexity that a linear approximation is probably not significantly worse than a logarithmic one in many cases. Adopting wind speed linearity with height, the velocity of wind can be mathematically expressed following the same derivation as in page 63, equation (3.40).

-The most sophisticated theory explains the variation of wind speed with height by a logarithmic law which, in stability dependent form, is given by (Holtslag, AAM):

$$v_h = v_{ref} \left[\log\left(\frac{h}{z_L}\right) - \Psi_m\right] \Big/ \left[\log\left(\frac{h_{ref}}{z_L}\right) - \Psi_m\right] \qquad (4.2)$$

$\psi_m = \psi_m(h/L)$ is a rather elaborate function of height h and Monin-Obukhov length L. L is a stability measure and is positive for a stable and negative for an unstable atmosphere; while for a neutral atmosphere L is a large number, either positive or negative. For calculations of sound propagation in the atmosphere, (Kühner, D.)

proposes a simpler equation than (4.2), but also based on the atmospheric stability dependency:

$$v_h = v_{ref} \left(h/h_{ref} \right)^m \tag{4.3}$$

In this case m is a number that stands for stability (see Table 4.1).

According to this last equation, the central picture of Figure 4.2 shows an overview of the wind vertical profiles for the different classes of stability in the atmospheric boundary layer. The figure also plots, in its right side, an estimation of the amount of turbulence for each different stability category. For stable conditions, when air masses move very smoothly, following an almost isothermical process, is expected to have very few turbulences. However, when air moves adiabatically (neutral) or superadiabatically (unstable), the kinetic energy exchange increases generating a more turbulent atmospheric environment. The atmospheric turbulence causes that the instantaneous profiles of the temperature and the wind velocity are not as smooth functions of height as they are shown in Figure 4.2. The turbulent fluctuations of the temperature and the wind velocity generally occur on a time scale of seconds (as discussed in Figure 4.1) and have a considerable effect on atmospheric sound propagation, as analysed experimentally further in the chapter.
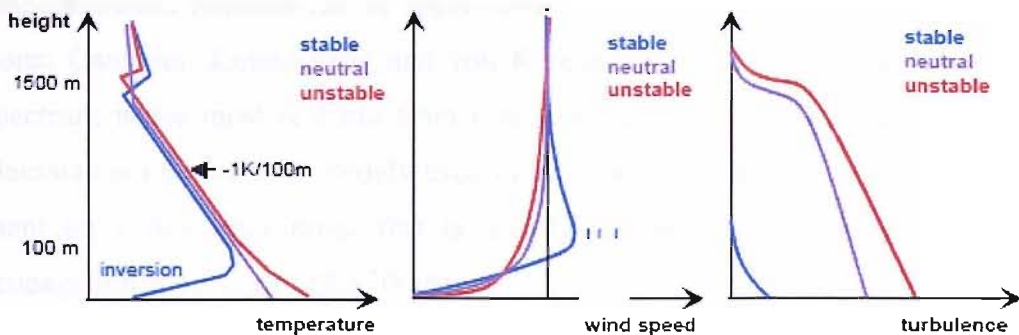
Figure 4.2 *Vertical profiles of temperature (left), wind speed (centre), and turbulent kinetic energy (right) for stable, neutral and unstable stratification. 'Inversion' means a layer with positive vertical temperature gradient. (Extracted from Heimann, D.)*

Turbulence arises from time-varying atmospheric temperature and velocity inhomogeneities that naturally occur due to mechanical and convective atmospheric processes, but that can also be induced in areas with a high heat-transfer activity (such a petrochemical plant). Paths of air particles in a turbulent atmosphere often contains loops. The loops corresponds to swirls in the fluid, which are called eddies.

The eddy sizes that occur in a turbulent flow depend on a characteristic dimension of the flow. In a pipe, for example, eddies larger than the pipe diameter cannot occur. In the atmosphere, a characteristic dimension is the height above the ground surface. With increasing height, larger eddies occur. At the same time, the largest eddies break down into smaller eddies, which break down into even smaller eddies, and so on. Consequently there is a broad distribution of eddy sizes in the atmosphere. This distribution corresponds to a broad distribution of characteristic periods of turbulent fluctuations. Small eddies correspond to rapid fluctuations and large eddies correspond to slow variations.

Turbulence has most effect on sound propagation when wavelengths are of the same or smaller size than the size of the eddies. Hence, high and mid frequencies are more prone to be affected by turbulence than lower frequencies.

In sum, the turbulence effect on the sound propagation is to produce three-dimensional, short-term changes in wave speed that cause diffraction of the sound and consequently fluctuations in the signal received. The mathematical function describing the turbulence is generally built considering a spatial autocorrelation function between points positioned in the x-y plane. (Salomons, E. M.) explains that this autocorrelation function can be approximated by three different statistical distributions: Gaussian, Kolmogorov and von Kármán. Amongst them, the von Kármán spectrum is the most realistic from a meteorological point of view, however the Gaussian is one the most widely used in acoustics as it also reaches a good agreement for a frequency range that is usually relevant for most of outdoor sound propagation experiments (20-2000Hz).

4.2.2. Ground interaction

Several special factors are important when sound waves travel more-or-less horizontally near the ground. This is usually the case for ground-to-ground propagation where sound waves propagate over ground surface conditions ranging from hard concrete to dense jungle.
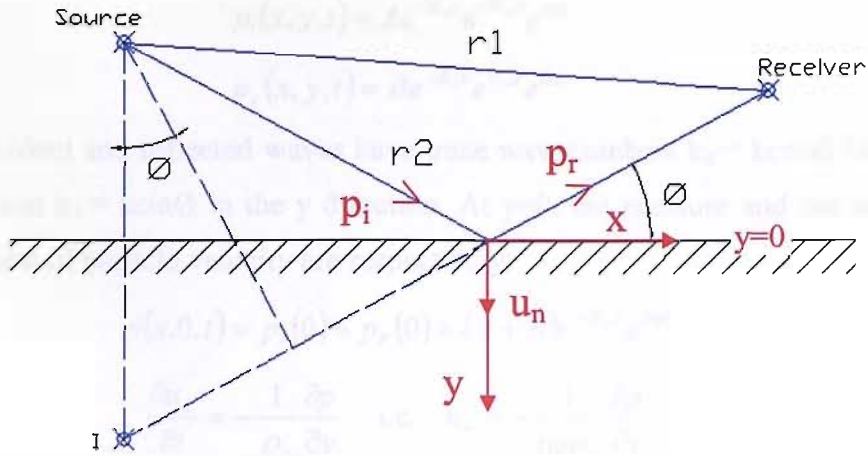
Figure 4.3 *Schematic representation of the direct and reflected sound fields when both source and receiver are near a ground surface*

The basic problem can be visualised from Figure 4.3. When the sound source and receiver locations are above flat open ground the sound from the source will reach the receiver via two paths: the direct field from source to receiver, and the reflected field. The difference in path lengths between direct and reflected sound fields could be, depending on the geometrical configuration and on the frequency, of the order of a wavelength, which may result in a constructive addition or a destructive interference between the two sound fields at the receiver location. The acoustical properties of the ground are also very important in calculating the structure and nature of the sound field that is due to the combination of the direct and ground-reflected sound fields. The simplest way to implement ground surface properties in the models is via the plane-wave reflection coefficient, R:

$$P_t = P_d + R \cdot P_{sr} \tag{4.4}$$

The different symbols of this equation stand for: P_t, the total pressure at the receiver; P_d, the direct contribution and P_{sr}, the specularly reflected contribution.

Assuming local reaction, which means that wave motion parallel to the surface within the medium is strongly attenuated, and considering a plane wave incident on the plane boundary at y = 0 at an angle Ø, see red indications of Figure 4.3, it can be calculated the plane-wave reflection coefficient. This can be done by determining the normal impedance of the ground, which by definition is pressure over normal particle velocity:

The analytical forms of both incident and reflected pressure waves are respectively:

$$p_i(x,y,t) = A e^{-ik_x x} e^{-ik_y y} e^{i\omega t} \tag{4.5}$$

$$p_r(x,y,t) = B e^{-ik_x x} e^{ik_y y} e^{i\omega t} \tag{4.6}$$

Both incident and reflected waves have trace wavenumbers $k_x = k\cos\varnothing$ in the x direction and $k_y = k\sin\varnothing$ in the y direction. At y=0, the pressure and the normal (y) component of particle velocity are respectively:

$$p(x,0,t) = p_i(0) + p_r(0) = (A+B)e^{-ik_x x} e^{i\omega t} \tag{4.7}$$

$$\frac{\partial u_n}{\partial t} = -\frac{1}{\rho_0}\frac{\partial p}{\partial y} \quad \text{i.e.} \quad u_n = -\frac{1}{i\omega\rho_0}\frac{\partial p}{\partial y} \tag{4.8}$$

$$\Rightarrow u_n(0) = -\frac{1}{i\omega\rho_0}\left(-ik_y A + ik_y B\right)e^{-ik_x x} e^{i\omega t}$$

Working out this last expression and dividing the calculated pressure over the normal particle velocity, we can obtain the normal acoustic impedance Z:

$$Z = \frac{p(0)}{u_n(0)} = \frac{(A+B)\rho_0 c_0}{(A-B)\sin\phi} \tag{4.9}$$

Writing $\rho_0 c_0$ as Z_0 the acoustical impedance of air, and B/A as the reflection coefficient R, then:

$$R = \frac{\sin\phi - {Z_0}/{Z}}{\sin\phi + {Z_0}/{Z}} \tag{4.10}$$

This reflection coefficient varies with angle unless one of the following extreme cases occurs. These cases are:

-Either $Z_0/Z = \infty$ which implies that the ground is infinitely soft and R$\rightarrow$ -1,

-Or $Z_0/Z = 0$ which implies that the ground is infinitely hard and R$\rightarrow$ +1.

In short, equation (4.4) accounting for the interaction between sound plane waves and flat open ground is only representative for the two extreme above cases. In practice, sound waves in outdoor sound propagation are more nearly spherical, as though from a point source, than plane, and flat ground surfaces are rather rough than perfectly smooth. In such conditions, varying reflected paths with different angle of incidence, and subsequently different acoustical properties, can reach the receiver location (Embleton, T. F. W; Attenborough, K.), leading to a more complex situation than that modelled by equation (4.4).

Most of the contributions approaching the modelling of this more realistic sound-ground interaction have been based on the analogous and earlier study of radio-wave propagation near to the Earth's surface. The total pressure is calculated here by a more complete expression than equation (4.4), known as the Weyl-Van der Pol solution (Embleton, TFW, et al):

$$\frac{P_t}{\rho_0 c_0} = \frac{e^{ikr_1}}{r_1} + R\frac{e^{ikr_2}}{r_2} + (1-R)F\frac{e^{ikr_2}}{r_2} \tag{4.11}$$

As shown by Figure 4.3, r_1 and r_2 are the incident and reflected ray paths, while F is the complex amplitude function that allows for the curvature of the incident sound field and the possible existence of irregularities at the ground surface. Mathematically, F is related to the complex error function of a parameter w, referred to in this context as the numerical distance by:

$$w = (ikr_2/2)\cdot\left(\sin\phi + \frac{Z_0}{Z}\right)^2 \tag{4.12}$$

The first term of the right hand side of equation (4.11) represents the direct sound field in both phase and amplitude. The second term represents the reflected field at the ground surface assuming the plane-wave reflection coefficient at the angle of specular reflection. The third term is the corrected reflected field to account for the angle of reflection which systematically varies with position along the ground surface for non-plane incident waves. Literature justifies the inclusion of this third term by the following reasoning:

-When both source and receiver are relatively close to the ground and a significant distance apart, the direct and reflected fields (ray paths r_1 and r_2) become nearly equal and the angle of incidence tends towards zero. As a consequence, the direct and reflected fields then tend to cancel out each other as R → -1, and any sound reaching the receiver is explained, theoretically at least, by the third term in equation (4.11).

The Weyl-Van der Pol solution, expressed by equation (4.11), provides, as discussed above, a theoretical explanation of the ground effect on outdoor sound propagation. However, the application of numerical methods for modelling the

sound propagation requires in first place the mathematical description of the normal specific impedance of the ground. In this respect, significant contributions have been made for describing theoretically the complex impedance of the ground. One of the first contributions dates back from 1977, when (Chessel, C. I.) used a theory developed by (Delany and Bazley) for fibrous materials to show that Z could be explained using a single parameter, which to a rough approximation was the flow resistivity of the ground. The flow resistivity, σ_f accounts for the viscous resistance to a steady flow of air when passing through a layer of porous material with mean flow velocity u' and is defined mathematically as:

$$\frac{\partial p}{\partial x} = -\sigma_f \cdot u'$$
(4.13)

$\partial p/\partial x$ stands for the static pressure gradient generated by the resistance to flow.

The semi-empirical formula for calculating Z based on the flow resistivity of the ground has been widely used and is expressed as follows:

$$Z/Z_0 = 1 + 0.0571 \cdot C^{-0.754} + i \cdot 0.087 \cdot C^{-0.732}$$
(4.14)

being $C = \omega \rho_0 / 2\pi\sigma_f$, and $0.01 < C < 1$ implying a lower and higher limiting frequency for any given flow resistivity.

Later (Attenborough, K.) showed that better agreement was obtained using five parameters each of which was a clearly relevant property of the ground material; these are its porosity, flow resistivity, tortuosity, steady-flow shape factor and dynamic shape factor. Of these, the flow resistivity and porosity are the most important. Furthermore, the two can be combined into a single term that may be described as an "effective flow resistivity". Indeed, (Attenborough, K. J. Sound Vib) derived an expression for the normalised surface impedance from the five-parameter model, based only on the effective flow resistivity, σ_e (in Pa-s/m^2), that is widely used and accepted at low frequencies and for more practical purposes:

$$Z/Z_0 = 0.218(\sigma_e/f)^{0.5}(1+i)$$
(4.15)

the frequency is expressed here by f.

Given that the study of Salisbury Plain database has been focused on mid-low frequencies, equation (4.15) was found to be the most suitable for the theoretical modelling of the terrain adopted within the PE model.

4.2.3. PE model

Amongst the current numerical methods for explaining outdoor sound propagation, three of them could be considered as the most popular and widely-used: ray-based models, Fast Field Programs (FFP) and Parabolic Equation (PE) algorithms. For the purpose of studying the effect of short-term meteorology variation on noise levels, the PE method is the only one capable to adopt a range-dependent turbulence model within its algorithm, and therefore the one used for the investigation reported in next sections.

Despite the suitability of the PE method for this investigation, PE algorithms have a mayor disadvantage: They only give accurate results in a region limited by a maximum elevation angle. The value of this angle oscillates from 10° to 70° or higher (Jensen FB, et al, or Salomons EM), depending on the angle approximation used in the derivation of the parabolic equation. However, a maximum elevation angle of 10° is sufficient for many ground-to-ground propagation configurations.

The parabolic equation method was first introduced into underwater acoustics in the early 1970s by (Hardin and Tappert), who devised an efficient numerical solution scheme based on fast Fourier transforms. Since then, the PE method has been widely used in underwater acoustics, becoming the most popular numerical method for solving range-dependent propagation problems in the ocean. Despite this success, it was not until 1989, when (Gilbert and White) presented a PE method for atmospheric acoustics. Thereafter, some important contributions were made in this field, however PE solution schemes are not yet so numerous for atmospheric acoustics as for underwater acoustics.

Reviewing the solution techniques developed for atmospheric acoustics, one can find two main groups (Salomons, E. M.): The Crack-Nicholson PE (CNPE) method and the Green's Function PE (GFPE) method. Both PE methods are two-dimensional methods, based on the axisymmetric approximation. This approach involves neglecting the variation of the sound field with azimuthal angle around the vertical axis through the source, which in practical terms is a good approximation as

wind and temperature variations with azimuthal angle are usually considerably smaller than wind and temperature variations with height.

The first PE method suited for atmospheric acoustics by (Gilbert and White) was a CNPE method. Other versions of the CNPE method are described by (Chen et al. or Delrieux et al.), but their principle is essentially the same: a finite-difference solution of a wide-angle parabolic equation. In contrast, the GFPE method, described in (Gilbert and Di or Sack and West) is less accurate than the CNPE method in situations with wide-angle propagation and large sound speed gradients; however for most applications and particularly for the small-angle propagation tests described in this chapter, the GFPE method is sufficiently accurate. The advantage of the GFPE over the CNPE method is that can take considerably larger extrapolation steps (i.e. range steps), resulting in a more efficient and faster computation.

The method developed here is an adaptation into atmospheric acoustics of the Fourier split-step PE solution commonly used in underwater acoustics. The FSSPE method is similar to the GFPE method, as they both reduce to the same equation for a system without a ground surface, however the algorithm implementation is slightly different when the ground surface is present:

-In the GFPE, the inclusion of a finite-impedance ground surface adds into the main PE marching equation two more terms accounting for the ground reflection and surface wave, which, due to their mathematical complexity tend to slow the computational time down.

-In the FSSPE, we make use of the periodicity of the Fourier transforms to double the computational domain by covering the height interval $-z_{max} < z < z_{max}$ and adding an image source to account for the ground reflection (details explained in section C below).

In sum, the two-dimensional PE method developed in this thesis has the same advantages and disadvantages as the GFPE method over the CNPE technique, but presents some implementation improvements as compared to the GFPE algorithm. Its mathematical derivation and its computational implementation are discussed in the following subsections.

A) Mathematical derivation

The basic PE mathematical derivation begins with two-dimensional (range and height) Helmholtz equation in cylindrical co-ordinates which is:

$$\phi_{rr} + \frac{1}{r}\phi_r + \phi_{zz} + k^2(r,z)\phi = 0 \qquad (4.16)$$

In this case the subscripts indicate derivatives, $\Phi(r, z)$ is the wave field, $k(r, z) = \omega / c(r, z)$ is the wavenumber, $\omega = 2\pi$ times the source frequency, and $c(r, z)$ is the sound speed.

Substituting $\Phi(r, z) = u(r, z) v(r)$ into equation (4.16) gives:

$$\left[v_{rr} + \frac{1}{r}v_r \right]u + \left[u_{rr} + \left(\frac{1}{r} + \frac{2}{v}v_r \right)u_r + u_{zz} + k_0^2 n^2 u \right]v = 0 \qquad (4.17)$$

k_0 is the reference wavenumber which is related to the wavenumber $k(r, z)$ by $k(r, z) = k_0 n(r, z)$, $n(r, z)$ is the index of refraction and is defined equal to c_0 (the reference sound speed) / $c(r, z)$ where the $c(r, z)$ is the sound speed. Using k_0 as a separation constant and setting the first [ ] of equation (4.17) equal to $-k_0^2 v$ and the second [ ] of equation (4.17) equal to $-k_0^2 u$, equation (4.17) is separated into two equations in which $u(r, z)$ and $v(r)$ are still coupled:

-One equation is:

$$v_{rr} + \frac{1}{r}v_r + k_0^2 v = 0 \qquad (4.18)$$

-And the other is:

$$u_{rr} + \left(\frac{1}{r} + \frac{2}{v}v_r \right)u_r + u_{zz} + k_0^2\left(n^2(r,z) - 1 \right)u = 0 \qquad (4.19)$$

The first equation can be regarded as a second-order ordinary differential equation in the range variable r. It has a solution involving two exponentials; one indicates the outgoing wave involving the zeroth-order Hankel function of the first kind, $H_0^{(1)}(k_0 r)$ and the other indicates the incoming wave involving the zeroth-order Hankel function of the second kind, $H_0^{(2)}(k_0 r)$. Neglecting the incoming portion, and applying the far-field condition, $k_0 r > 1$, for $H_0^{(1)}(k_0 r)$, the solution of $v(r)$ can be written as:

$$v(r) \approx \sqrt{\frac{2}{\pi k_0 r}} \cdot e^{i\left(k_0 r - \left(\frac{\pi}{4}\right)\right)} \tag{4.20}$$

Expression (4.20) is applied for v(r) to simplify the coefficient of u_r in equation (4.19), which gives:

$$u_{rr} + 2ik_0 u_r + u_{zz} + k_0^2 \left(n^2(r,z) - 1\right)u = 0 \tag{4.21}$$

For easy understanding, (Lee, D. et al.) includes a factorisation approach to transform equation (4.21) by the help of the following equation:

$$\left(\frac{\partial}{\partial r} + ik_0 - ik_0\sqrt{1+X}\right) \cdot \left(\frac{\partial}{\partial r} + ik_0 + ik_0\sqrt{1+X}\right)u =$$
$$= -ik_0\left(\frac{\partial}{\partial r}\sqrt{1+X} - \sqrt{1+X}\frac{\partial}{\partial r}\right)u \tag{4.22}$$

where:

$$X = \left(n^2(r,z) - 1\right) + \frac{1}{k_0^2}\frac{\partial^2}{\partial z^2} \tag{4.23}$$

If δ/δz and δ/δr commute, then, the right-hand side of equation (4.22) becomes zero. In this case, a representative outgoing wave equation can be identified by:

$$\left(\frac{\partial}{\partial r} + ik_0 - ik_0\sqrt{1+X}\right)u = 0 \tag{4.24}$$

This last equation plays an important role for deriving the narrow or wide-angle PE. Depending on how the square-root of (1+X) is approximated it will appear the formulation for the narrow or wide-angle PE. As the objective is to get the narrow-angle expression, it has been taken the approximation $(1+X)^{1/2} \approx (1+ (1/2)X)$. However, other approximations are discussed in (Salomons, E. M.) or in (Lee, D., et al.).

Upon rearrangement, the adopted approximation gives the explicit equation:

$$2ik_0\frac{\partial u}{\partial r} + \frac{\partial^2 u}{\partial z^2} + k_0^2\left(n^2(r,z) - 1\right)u = 0 \tag{4.25}$$

Which is the standard parabolic equation introduced into underwater acoustics by Hardin and Tappert. This equation is generally solved by any of the following two methods: the finite-difference / finite-element technique (i.e. CNPE) or a Fourier

transformation scheme (i.e. GFPE). In the thesis, the Fourier transform solution has been adopted (derived below), but with some differences as compared to the typical GFPE method. Further information about the mathematical derivation of other solution techniques can be found in (Salomons, E. M.).

B) The Split-Step Fourier Algorithm

To solve numerically equation (4.25) through the Split-step Fourier transform technique it is required the introduction of the complex Fourier transform pair:

$$u(r,z) = \frac{1}{2\pi} \int_{-\infty}^{\infty} u(r,k_z) e^{ik_z z} dk_z \tag{4.26}$$

$$u(r,k_z) = \int_{-\infty}^{\infty} u(r,z) e^{-ik_z z} dz \tag{4.27}$$

being k_z the vertical wavenumber.

Under the assumption that both u(r,z) and $\partial u/\partial z$ are well-behaved functions and approach zero as z→±∞, we can easily transform the standard parabolic equation (4.25) into:

$$2ik_0 \frac{\partial u}{\partial r} - k_z^2 u + k_0^2 (n^2 - 1) u = 0 \tag{4.28}$$

By rearranging terms:

$$\frac{\partial u}{\partial r} + \frac{k_0^2 (n^2 - 1) - k_z^2}{2ik_0} u = 0 \tag{4.29}$$

This is a linear, first-order differential equation with the solution:

$$u(r,k_z) = u(r_0,k_z) e^{-\frac{k_0^2 (n^2 - 1) - k_z^2}{2ik_0}(r - r_0)} \tag{4.30}$$

If we now transform back the expression to the z-domain, introducing the symbol F for denoting the Fourier transform from the z-domain to the k_z-domain and F^{-1} as the inverse transform, we can then write the field solution in the following compact form:

$$u(r + \Delta r, z) = e^{\frac{ik_0}{2}[n^2(r,z) - 1]\Delta r} \cdot F^{-1}\left\{ e^{-\frac{i\Delta r}{2k_0} k_z^2} \cdot F\{u(r,z)\} \right\} \tag{4.31}$$

Equation (4.31) represents the core of the split-step marching algorithm proposed by Hardin and Tappert for solving the standard parabolic equation. Note that this

87

algorithm basically requires a Fourier transformation of a starting field (i.e. the standard Gaussian source), followed by a multiplication by a phase factor, then an inverse Fourier transform, and finally a multiplication by another phase factor containing the environmental information [through $n^2(z)$].

C) Algorithm implementation

The PE code used in this thesis was mainly written following the equation (4.31). The starting field for initialising the PE model was selected as being a Gaussian source. Placed at $r = 0$ and expressed by:

$$u(0,z) = \sqrt{k_0} e^{-\frac{k_0^2}{2}(z-z_s)^2}$$
(4.32)

The computation was limited to a finite solution domain in height ($0 < z < z_{max}$), which covered the physical domain as well as the "sponge" layer required to avoid spurious reflections off the top end boundary. The z_{max} was chosen as the sum of an interface height of 100m plus a "sponge" layer of 10 times the wavelength (following recommendations of Salomons).

The environmental information was entered via the squared index of refraction $n^2(r, z)$, which also included the attenuation in the sponge layer by adding an imaginary part to the index according to:

$$n^2 = (c_0/c)^2 [1 + i\alpha/27.29]$$
(4.33)

β stands for the attenuation coefficient in dB/λ (the value for this parameter is 0.00868λ following recommendations of Jensen et al.).

Having defined the initial field and the index of refraction, the next step was to implement the marching FFT algorithm given in (4.31). This marching scheme is generally implemented using a discrete FST (fast sine transform), but it was finally preferred a more standard transform, the FFT, as this code is more efficiently implemented in Matlab than the FST. The use of the standard FFT obliged to double the computational domain covering a height interval $-z_{max} < z < z_{max}$. At the same time, it was necessary to include in the initial field the surface boundary condition by adding an image source multiplied by the coefficient $(Z-1)/(Z+1)$, as follows:

$$u(0,z) = u(0, z-z_s) + ((Z-1)/(Z+1)) \cdot u(0, z+z_s)$$
(4.34)

as in previous equations, Z represents the normalised ground impedance. This value was computed from the empirical equation (4.15) developed by (Attenborough, K.).

We note here that the image field must be multiplied by the ground coefficient before advancing the solution another range step. This has been done by simply folding the real and imaginary parts of $u(r_0,z)$ around the ground surface and multiplying the result by the known $(Z-1)/(Z+1)$.

The last issue to conclude the algorithm implementation involves which FFT size and which range step size to use. Insofar as it is possible, it has been followed the recommendations of (Jesen et al.), who suggests a FFT size bigger than $8z_{max}/\lambda$ and a range step size, Δr, somewhat larger than the vertical step size, Δz.

C) PE Testing

Once the PE code was fully operational, it was tested against increasingly more difficult problems with known solutions:

a) The simplest documented underwater PE problem was the one discussed in the NORDA PE Workshop held in April '81 with the input parameters (see Figure 4.4 for details):

source frequency = 250 Hz   attenuation in the water = 0

source depth = 99.5 m   attenuation at the bottom = 0.5 dB/λ

receiver depth = 99.5 m   maximum range = 10km
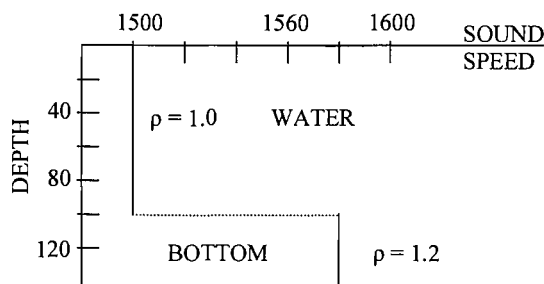
Figure 4.4 *Sound speed profile & density variation for the underwater Pekeris problem.*

The results provided by the PE code (Figure 4.5, left) agree with those showed in pages 532-533 of Lee review (Figure 4.5, right):
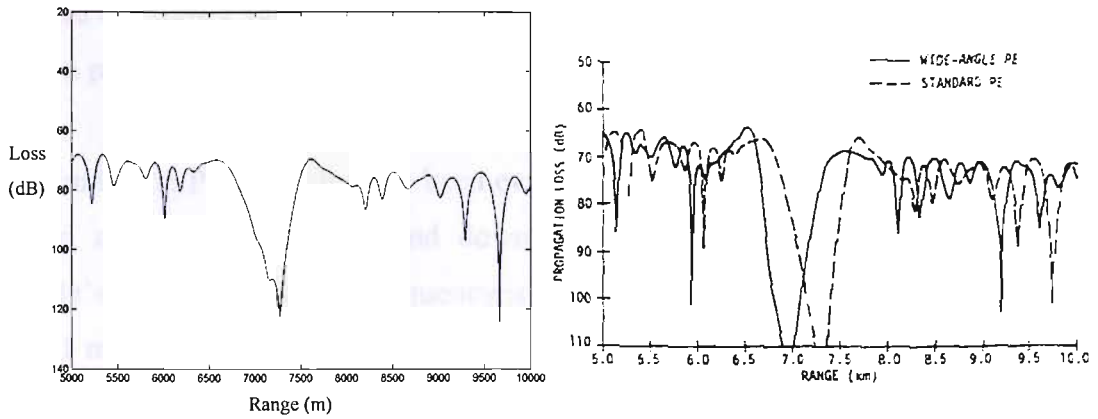
Figure 4.5 *Left: Transmission loss as a function of range for the Pekeris problem calculated by the Split Step PE code. Right: Figure extracted from (Lee, D et al.)*

b) To test the resolution capability of the PE algorithm with variable sound speed gradients, the sound propagation problem defined by Bucker was solved. This problem is described in Figure 4.6:
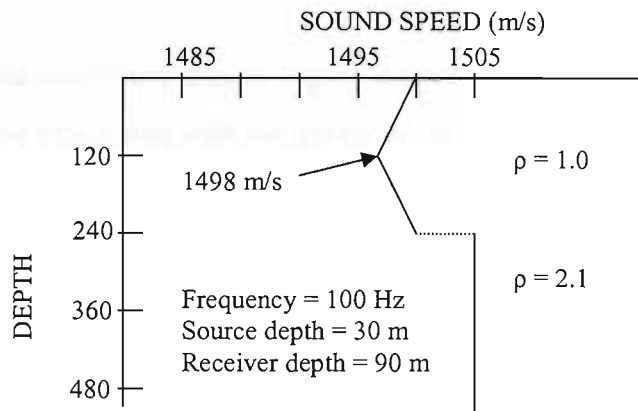
Figure 4.6 *Sound speed profile and density variation for the Bucker problem.*
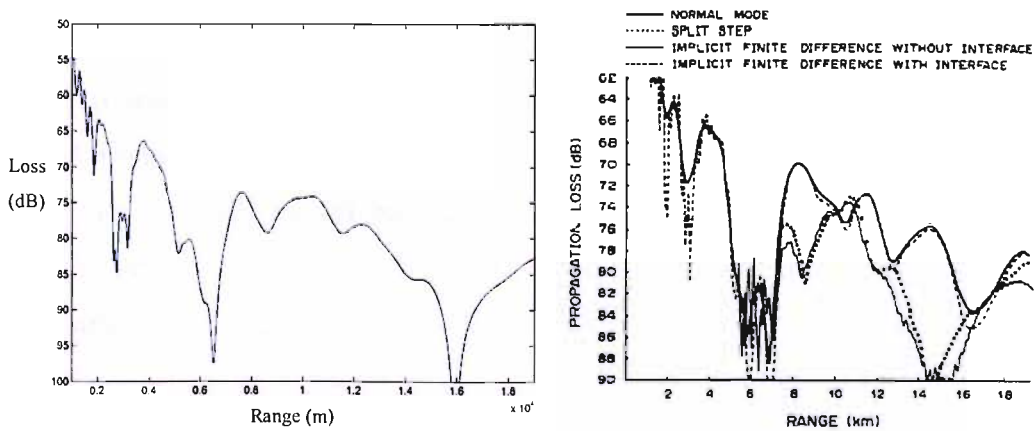
Figure 4.7 *Left: Transmission loss as a function of range for the Bucker problem calculated by the Split Step PE code. Right: Figure extracted from (Lee, D et al.)*

90

Figure 4.7 shows again successful results when is compared against the known solution presented in (Lee, D, et al.).

c) Finally the PE algorithm has been evaluated in a refracting atmosphere and compared against both upwind and downwind problems presented in (Gilbert and White's paper). The source frequency is 40 Hz with source and receiver heights of 2 and 1 m respectively. The ground impedance in ρc units is $31.4 + i38.5$. The sound speed is linear initially, and is capped by a homogeneous half-space above, according to:

$$c(z) = \begin{vmatrix} c_0 + gz, & for & z \leq h \\ c_0 + gh, & for & z > h \end{vmatrix} \tag{4.35}$$

the sound-speed gradient is represented here by g, z is height, c_0 is 330 m/s, and h is 100m. For the upward refraction case $g = -0.12$ s^{-1}, whereas for the downward problem $g = 0.12$ s^{-1}.

Considering all the conditions above, Figure 4.8 shows the results obtained by Gilbert et al. and those calculated with the developed PE algorithm. It can be noted that the Split-Step solution not only agrees with the finite element solution given by Gilbert, but also clears up the numerical inaccuracies existing in Gilbert's upwind figure beyond 2.5 Km. For the downward refraction case the results are very similar until around 2.5 Km, but then, the differences become more palpable, suggesting that the same numerical inaccuracies encountered for the upward refraction conditions could be behind this deviation.

All these examples provide an initial good stand for using the developed PE algorithm to understand how the different and variable environmental factors in outdoor sound propagation result in sound level variability at the receiver locations. In addition, the last example (c) has demonstrated that the Split-Step Fourier solution scheme developed in this thesis shows better results when dealing with numerical inaccuracies as compared to the CNPE method used by (Gilbert and White) for atmospheric sound propagation.
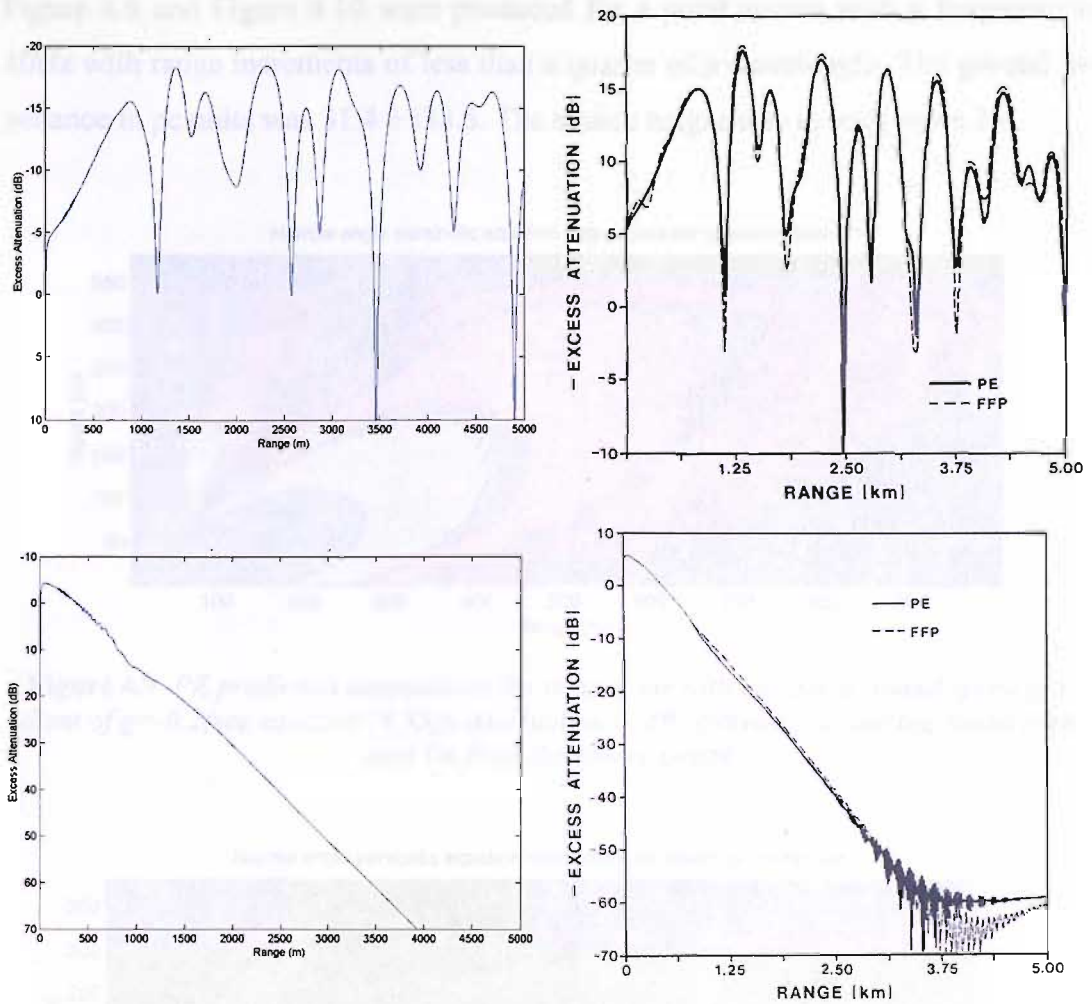
Figure 4.8 *Top-left: Split-Step Fourier PE results for downward refraction conditions. Top-Right: The same downward refraction case resolved by Gilbert, using the FD/FE solution. The bottom figures referred to the upward refraction conditions.*

D) Examples of PE predictions and practical issues

The PE method described in this chapter has been implemented as a Matlab algorithm. The PE predictions have been plotted in a 2D coloured form for allowing a better understanding of how the different environmental factors affect the sound as propagates from source to receiver. The 2D coloured presenting form also reveals some practical issues and limitations of the PE method than would not be detected otherwise. The following examples review these and other issues by covering a series of different environmental assumptions that highlight the capabilities and the practical limitations of the PE method.

Figure 4.9 and Figure 4.10 were produced for a point source with a frequency of 40Hz with range increments of less than a quarter of a wavelength. The ground impedance in ρc units was $31.4 + i38.5$. The source height was in both cases 2m.

Narrow angle parabolic equation calculations for upward refraction
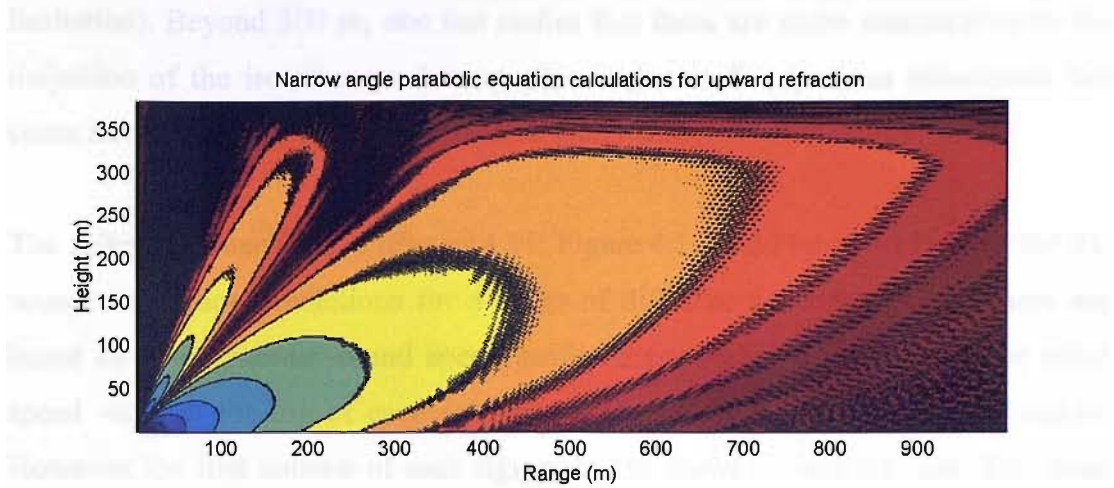
Figure 4.9 *PE prediction attenuations for moving air with a negative sound speed gradient of g=-0.2(see equation (4.35)). Attenuation in dB referred to a starting sound pressure 1m from the source centre.*

Narrow angle parabolic equation calculations for downward refraction
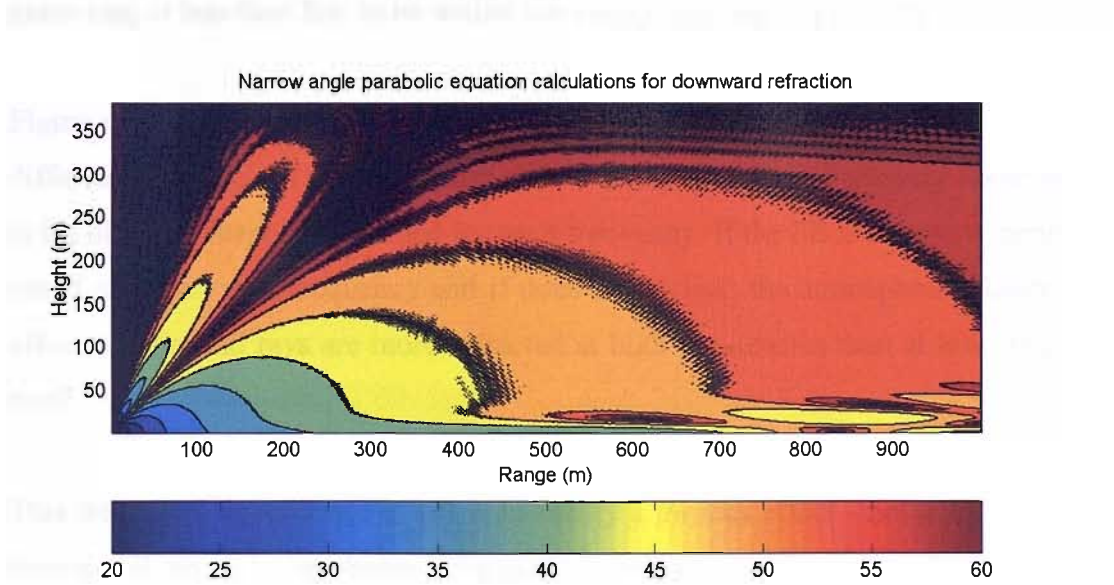
Figure 4.10 *PE prediction attenuations for moving air with a positive sound speed gradient of g=0.2 (see equation (4.35)). Attenuation in dB referred to a starting sound pressure 1m from the source centre.*

Figure 4.10 shows the strong enhancement effects close to the ground due to an increase of downward refracted energy. It can also be noted the existence of some areas in where cancellation effects between direct and reflected sound paths take place. Figure 4.9 shows the corresponding case with a constant negative sound speed gradient of 0.2; in this case the upward refraction produces shadow conditions at points close to the ground for distances greater than 300m. Both figures pre-

sent untrue results for starting angles of more than 25°, which reveals one of the limitations of the PE method: Its validity range is of ±20° about the horizontal line (see (Jensen, B. F et al) or (McDaniel, S. T) for a theoretical derivation of this angle limitation). Beyond 300 m, one can realise that there are some inaccuracies in the definition of the iso-attenuated areas; this is due to the spurious reflections that come from the top boundaries of the area under study.

The following three figures (Figure 4.11, Figure 4.12 and Figure 4.13) show the PE sound attenuation predictions for a range of different situations. All of them are based on a logarithmic sound speed profile extrapolated assuming that the wind speed value at the top of each subfigure corresponds to the value at 3m height. However, the first column of each figure always shows the still air case. The three figures depict a short range situation (25m), which is unusual for PE applications (as they are commonly used for long and mid ranges); Note that the height of the noise map is less than 8m. to be within the valid range angles (i.e. ±20°).

Figure 4.11 shows the sound attenuation over a perfectly reflective surface for three different frequencies (100 Hz, 1 kHz and 10 kHz). The first interesting observation is the different response obtained for each frequency. If the PE is assuming constant speed of sound with frequency and if does not include the atmospheric absorption effect, why sound rays are more refracted at high frequencies than at low frequencies?

This frequency dependence effect is in reality a physics effect - not a PE effect. It does not show up in ray theory because ray methods are based on an "infinite" frequency approximation and therefore paths are independent of frequency.

Physically, ray paths are not as fundamental as wavefronts. The Eikonal equation (derived in Chapter 3 and expressed by (3.17)) is for wavefronts and one solves for rays as a mathematical construct perpendicular to the wavefronts. A wavefront is a surface of constant phase, if we consider long and short wavelengths it is easy to see that at high frequencies fronts are closer together in space, whereas at low frequencies the intra-space becomes larger. Thereby if due to wind or temperature gradients, the sound speed profile varies in space, as the wavefront goes through the

sound-speed field, it is curved accordingly with respect to space position. High frequency wavefronts will be affected more per unit distance than at lower frequencies and therefore the high frequency wavefronts curve more than the low frequency ones.

Another effect of the same physical nature is that the more horizontal a ray is, the "more it sees" a vertical sound speed profile. Hence, a ray going straight up continues to go more or less straight rather than one more horizontal which curves much more. This is simply Snell's law. The combination of the two effects is that higher frequency and more horizontal rays are most affected by vertical sound speed profiles.

Figure 4.12 has been produced under the same conditions of Figure 4.11, except that the range marching step has been increased up to 1m., which is more than a quarter of a wavelength for both 1kHz and 10kHz frequencies. This leads to the unstable solutions obtained at medium and high frequencies when the propagation medium is not still. In theory a range step of less than a quarter of a wavelength is enough to avoid these inaccuracies, but sometimes it could be even smaller. The only way to ensure numerically accurate PE results is through a convergence test, in where the range step is systematically reduced until a stable solution is obtained.

Finally Figure 4.13 shows the same case as in previous figures, but under a soft ground. The plots indicate that for medium and high frequencies there is a sound transmission loss of more than 30 dB beyond 10m. for whatever moving medium condition. Although the effect can be suspicious at glance, in practice these predictions agree with noise measurements taken under the same conditions. For a more detailed comparison one can use the sound level measured by (Embleton, T. F. W., et al.) over grass at a horizontal distance of 50ft (around 15.2m) – see FIG. 5 of his paper titled "Outdoor Sound Propagation Over Ground of Finite Impedance".

All these examples show that the PE model is a useful tool for a wide range of environmental situations and that can be used for the particular conditions of the Salisbury Plain database as long as the PE limitations are understood and observed.
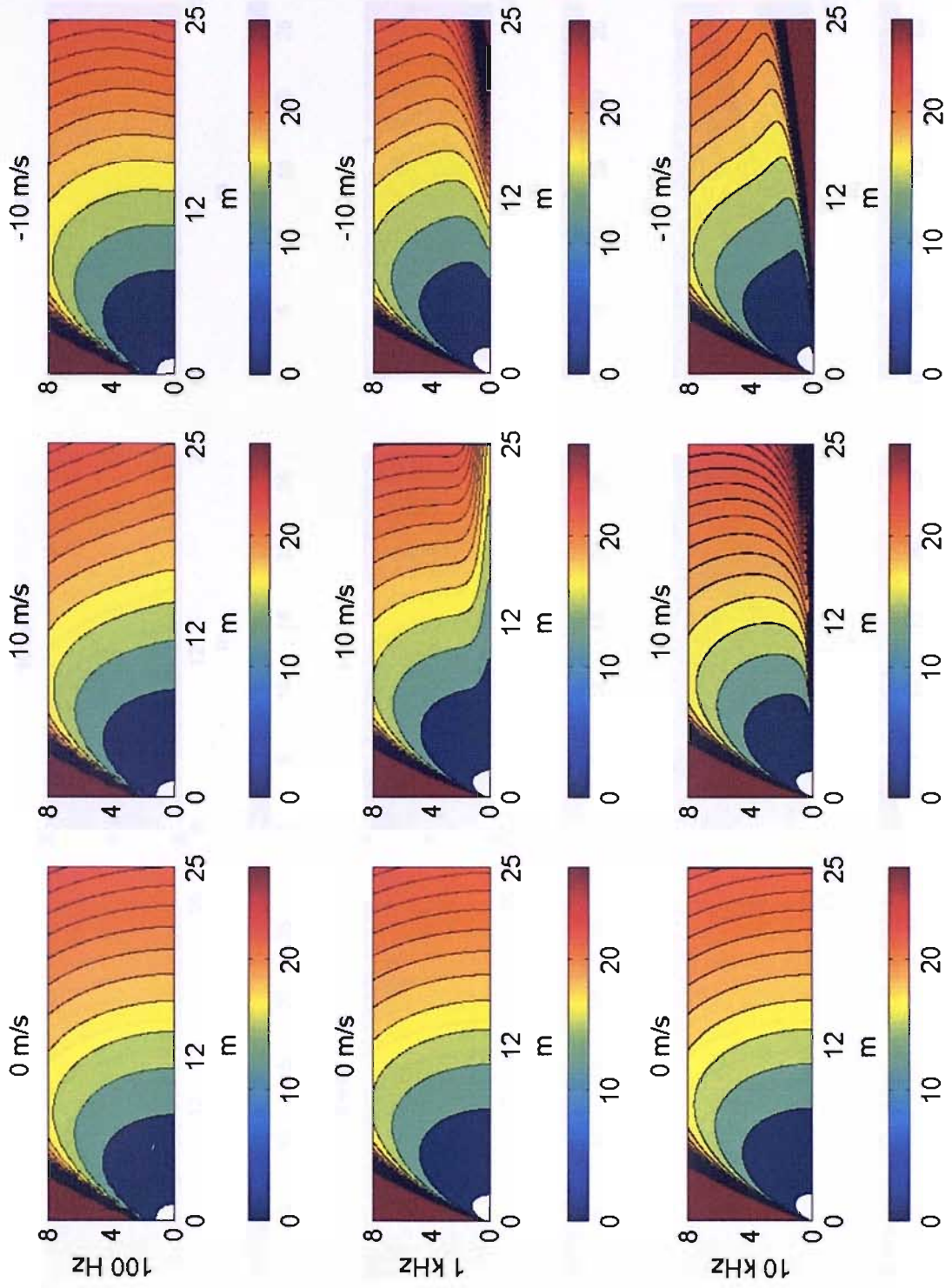
Figure 4.11 *PE attenuation in dB referred to a starting sound pressure 1m from the source centre. The figures have been produced assuming a logarithmic sound speed profile extrapolated considering that the wind speed value at the top of each figure was at 3m. The PE range step is less than a quarter of a wavelength, the ground is a perfectly reflective surface and the source is at 0m height.*
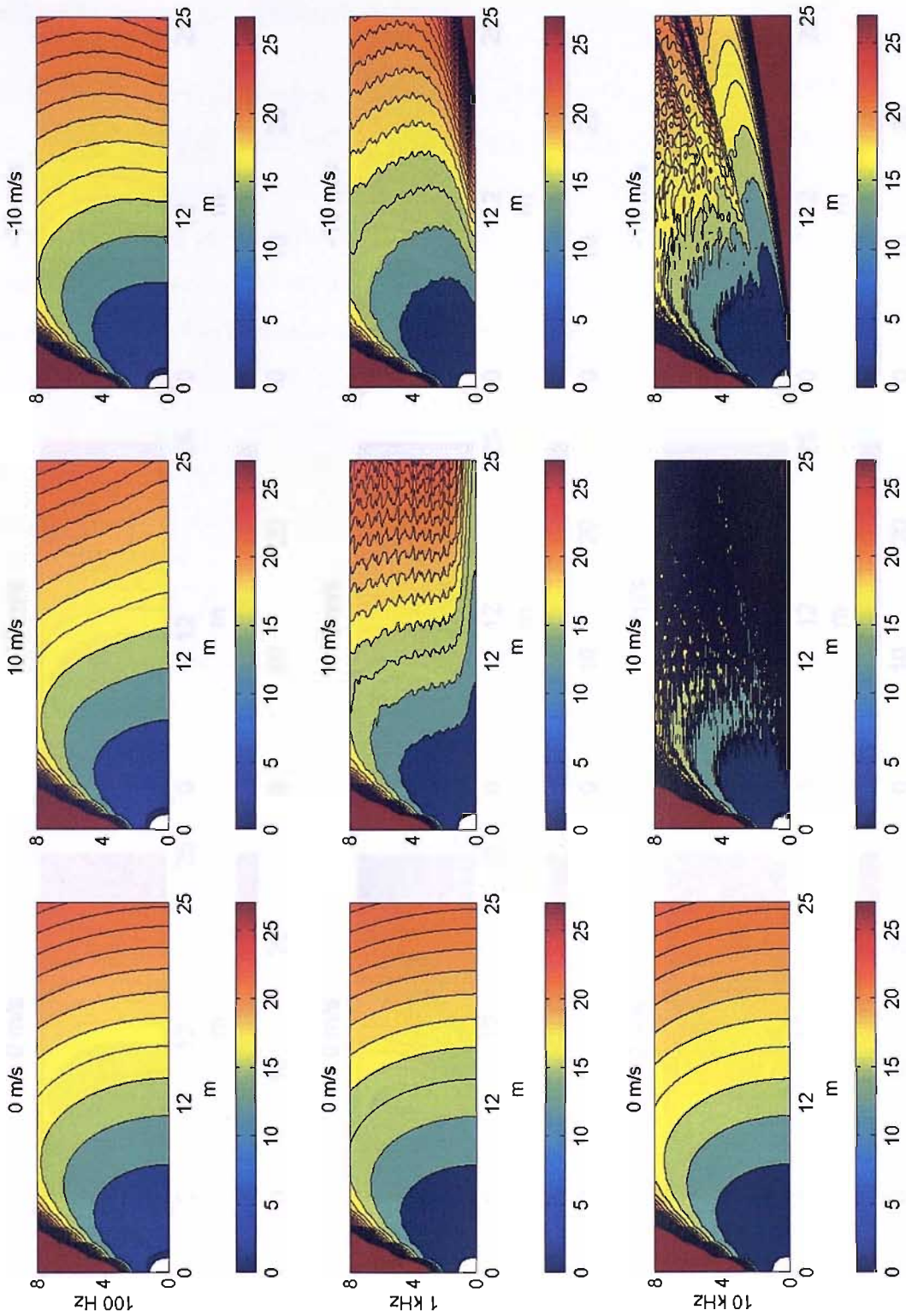
Figure 4.12 *PE attenuation in dB referred to a starting sound pressure 1m from the source centre. The figures have been produced assuming a logarithmic sound speed profile extrapolated considering that the wind speed value at the top of each figure was at 3m. The PE range step is 1m (in some cases higher than a quarter of a wavelength), the ground is a perfectly reflective surface and the source is at 0m height.*
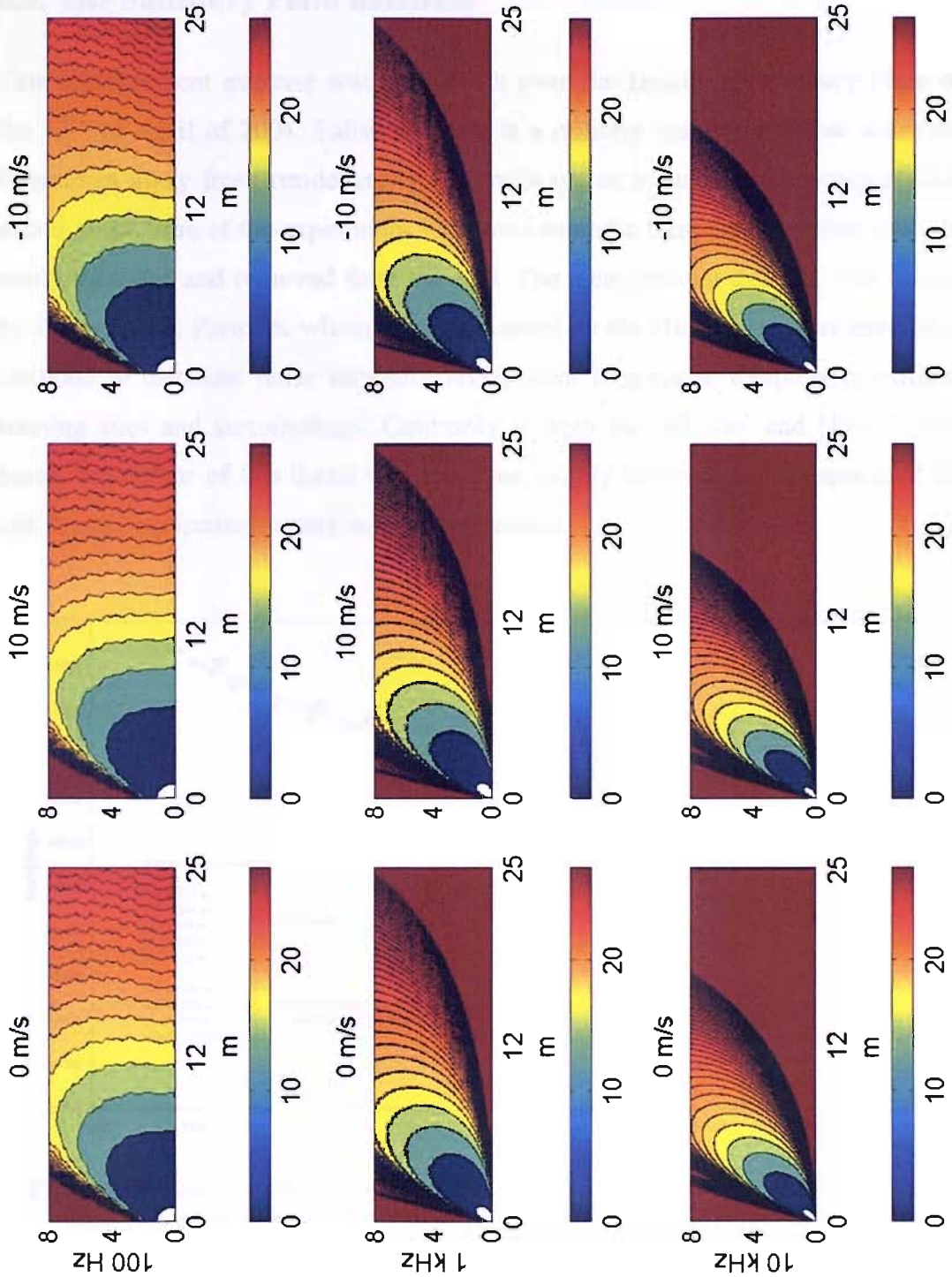
Figure 4.13 *PE attenuation in dB referred to a starting sound pressure 1m from the source centre. The figures have been produced assuming a logarithmic sound speed profile extrapolated considering that the wind speed value at the top of each figure was at 3m. The PE range step is less than a quarter of a wavelength, the ground impedance is based on a flow resistivity of 200000 MKS units (typical of a grassland surface) and the source is at 0m height.*

4.3. The Salisbury Plain database

This measurement exercise was carried out over flat terrain in Salisbury Plain on the 22nd of April of 2004. Salisbury Plain is a military training site that is several kilometres away from residences, roads, railways or industries. The only audible sound at the time of the experiment was some sporadic weapon firing that could be easily localised and removed from the data. The measurement exercise was funded by Hoare Lea & Partners, whom were contracted by the MoD to improve prediction methods to calculate noise exposure levels from long-range weapons in military training sites and surroundings. Contrarily to both the '50 site' and 'Joule' databases, the author of this thesis was this time, highly involved in all aspects of the test design, equipment setting and data collection.
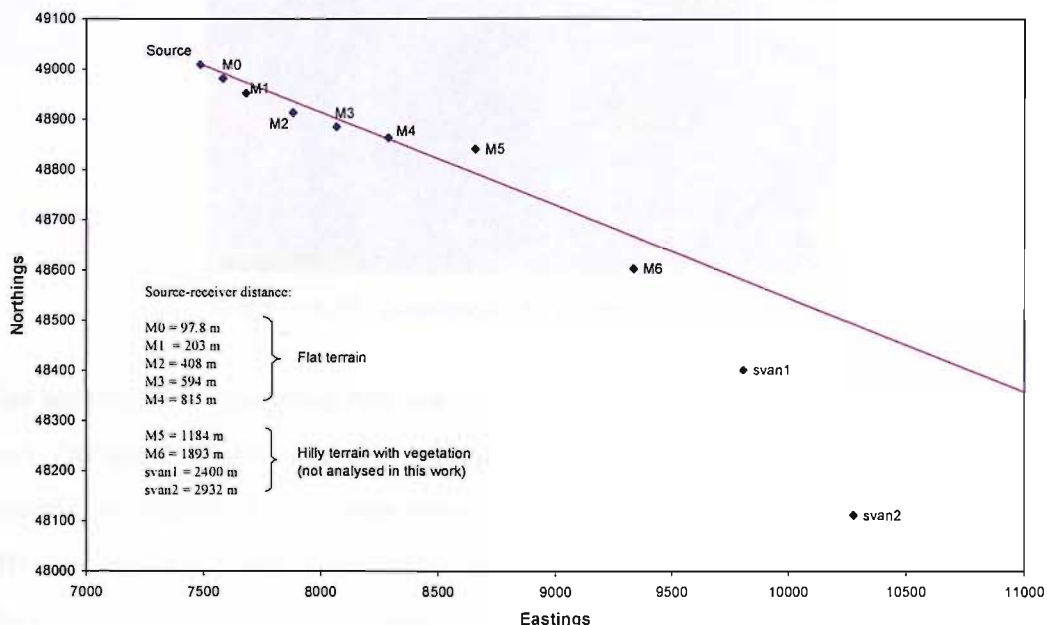
Figure 4.14 *Source and receiver distribution for the Salisbury Plain experiment. Last four microphones (M5, M6, svan1 and svan2) were not considered in this work*

A series of 9 data logging sound level meters were deployed approximately along a line extending out to 3km away from the source, as shown in Figure 4.14. The source system comprises four mid/top boxes and four sub-bass bins (about 6kw RMS power) complete with Amprack, digital controller and signal generator. The loudspeakers are IVYSOUND Celestion CX rig with 90 horizontal x 40 vertical degree dispersion (depicted in Figure 4.15). The source system was able to reach easily a sound level of around 130 dB at 20m distance, thereby the signal to noise

ratio at the furthest receivers was still acceptable. The monitoring points were located at a height of 1.4 m above the ground, while the source was situated at 0.6 m. Only the first five receivers were used for this analysis, the other four positions had an obstructed line of sight and were not considered here, as the main goal of the study was to focus on the turbulence influence on flat ground sound propagation.

Figure 4.15 *Loudspeaker system at Salisbury Plain*

The acoustical propagation test was undertaken over an eight-hour monitoring period. During this time, a source signal comprising a range of different noise types was played 4 times. These noise types are as follows:

-30 s. of pure tones at 63, 125, 250, 500, 1k and 2k Hz with 10 s intervals of silence.

-30 s. of filtered pink noise at the following 1/3 Octave bands: 40, 50, 63, 80, 100, 125, 160, 200, 250, 315, 400, 500, 630, 800, 1k, 1.25k, 1.6k, 2k, 2.5k, 3.125k Hz, with 10 s silence intervals between each frequency.

-Broad band pink noise for 2.5 min. This noise type was played twice in each run.

The following interval data were collected at each measurement location: L_{Aeq}, L_{A10}, L_{A90}, L_{Amax} and L_{Amin} for each consecutive 1s interval throughout the survey period. Audible files were also recorded for 20s each time that any of the microphones was triggered by an instantaneous level of more than 80 dB. The sound level meters were type 1 microphones and protected by double skin foam windshields.

Two meteorological monitoring stations were deployed in two different locations: The first one is shown in Figure 4.16 and is relatively close to the source (around 100m), whereas the other is situated between receiver M4 and M5 (at around 1 km away from the source). Both of them were set-up to record 15 s met data continuously throughout the measurement exercise. The source met station comprised a 12m mast holding 2 anemometers at 10 and 2m, 2 temperature sensors at 10 and 2m and humidity, pressure and rainfall gauges, all at 2m height. The receiver met station comprised the same measurement system, but only at 10m above ground.

Figure 4.16 *Panoramic view of Salisbury Plain experimental site. The track at the left runs parallel to the source-receiver line path. At the right is shown the source met mast.*

Figure 4.16 also shows the condition of the sky at the time of the exercise. It can be seen that the sky was partially covered, however, as the day progressed there were increasingly more sunny spells. This description is very important to estimate the stability of the atmosphere, which in turn is essential for calculating the shape of the vertical wind profiles. By looking at the Pasquill stability classes of Table 4.1, it can be noted that the observed atmospheric conditions match the neutral stability category with factor $m = 0.22$. Knowing the value of m, the vertical wind speed profile can be easily extrapolated by using the equation (4.3). This equation provides the value of the wind speed at any height as a function of m and the measured wind speed at a certain height. Figure 4.17 shows indeed the result of this equation at a height of 11.2 m, by using as a reference the wind speed measurements taken at 2m height and by assuming different values of m (0.09; extremely unstable, 0.22; neutral, 0.41; very stable). The figure clearly shows that the neutral stability assumption provides the best-fit between the predicted and measured data. The left column represents the typical sound speed profile under the three different assumptions of atmospheric stability with the same wind speed value at 2m height.
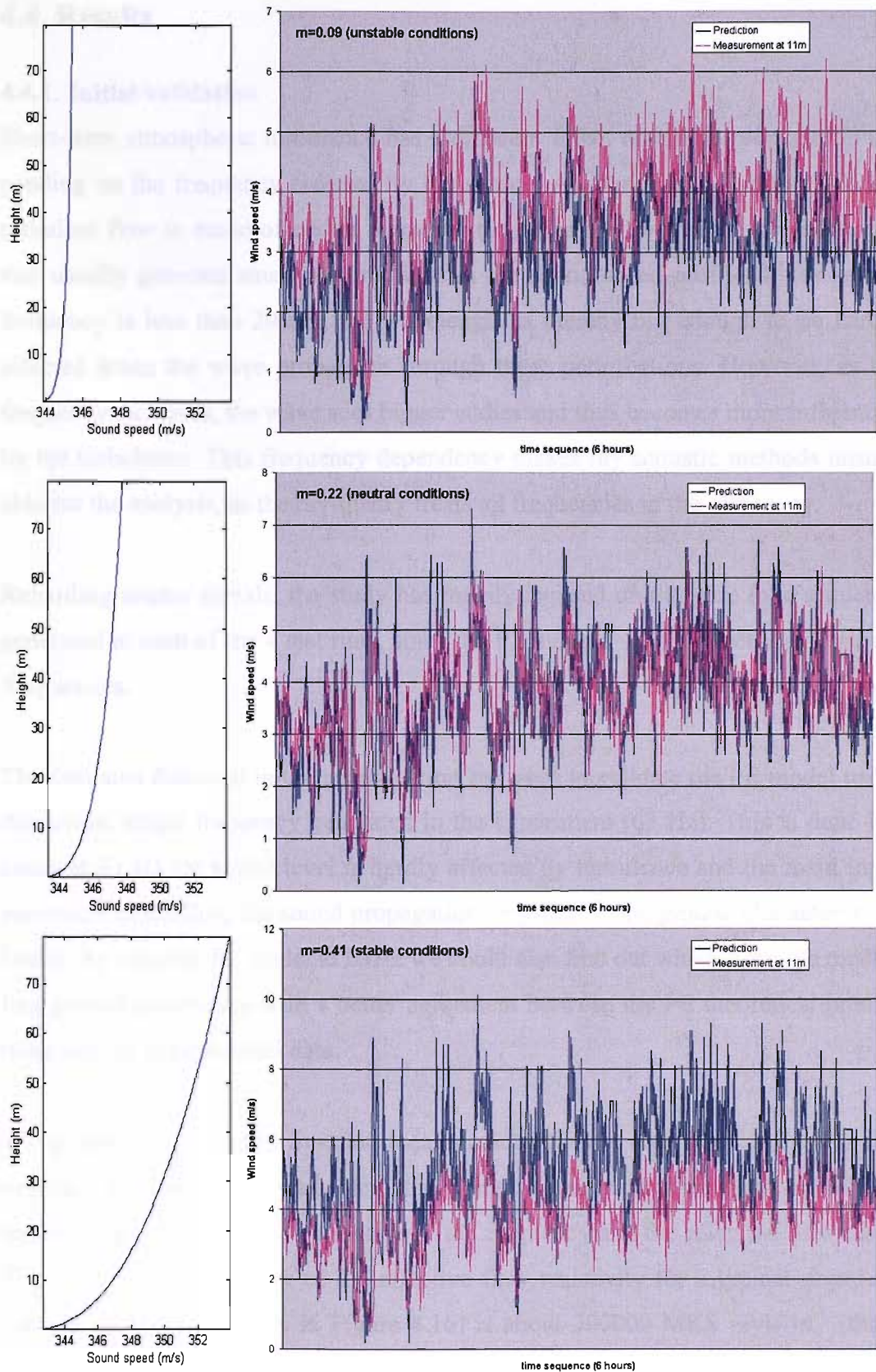
Figure 4.17 *Comparison between wind measured data at 11.2m height (red line) and extrapolated data using as a reference the data of the anemometer at 2m height. The extrapolation is done assuming different stability conditions.*

4.4. Results

4.4.1. Initial validation

Short-term atmospheric turbulence has a different effect on sound propagation depending on the frequency radiated by the source. As explained in section 4.2.1, a turbulent flow is made of eddies sizing of the order of few meters to centimetres that usually generate small perturbations in the sound speed profile. If the source frequency is less than 200Hz, the wavelength is thereby big enough to be hardly affected when the wave propagates through these perturbations. However, as the frequency increases, the wave sees bigger eddies and thus becomes more influenced by the turbulence. This frequency dependency makes ray acoustic methods unsuitable for the analysis, as the ray-theory treats all frequencies in the same way.

Regarding source signals, the study has mainly focused on the pure tone sequence generated at each of the 4 test runs, since the PE method works directly with single frequencies.

The first step followed in the investigation has been to validate the PE model using the lowest single frequency generated in the experiment (63 Hz). This is done because at 63 Hz the sound level is hardly affected by turbulence and the main input parameter controlling the sound propagation only lies on the ground characteristics. Hence, by running the model at 63Hz we could also find out which were the modelling ground parameters with a better agreement between the PE theoretical predictions and the experimental data.

The ground was modelled as a flat, locally reacting plane with a finite complex impedance. The impedance was calculated using the empirical formula (4.15) of (Attenbourough, K.), which is a function of the frequency and the effective flow resistivity, σ_e. A realistic value of the effective flow resistivity for a typical grassland surface (as the one shown in Figure 4.16) is about 300000 MKS rayls m^{-1} (these units are N s m^{-4}). As the σ_e was not measured experimentally, the transmission loss for this recommended value, plus for two other possible values (25×10^4 and 35×10^4 MKS) over and under the 300000 MKS, were predicted and compared against the measured transmission loss. The comparison is shown in Figure 4.18.
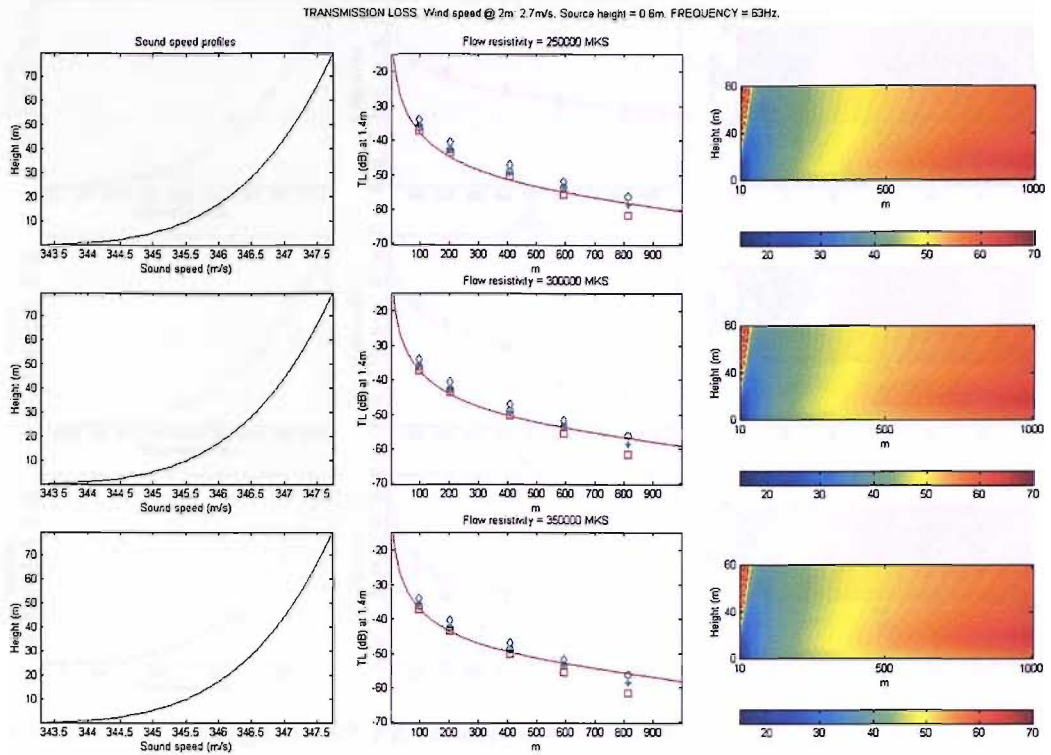
Figure 4.18 *PE validation for different values of effective flow resistivity at a frequency of 63 Hz.*

At a glance, the central column of Figure 4.18 shows a good general agreement between the PE predictions (red line) and the experimental data recorded at each of the 4 runs. There is not so much difference between the three theoretical predictions, but perhaps the $3x10^5$ MKS flow resistivity gives a better fit amongst the three. The plots at the left side of the figure represent the average sound speed profile during the 4 runs (assuming neutral conditions), whereas the last column shows the 2D noise maps for the three different surface types.

The effective flow resistivity for all further PE simulations was selected to be 300000 MKS units, since is the typical value used in the literature for grassland and, in particular, because it was the one to show the best agreement with the experimental data at 63 Hz. Nevertheless, to check its full validity, the transmission loss for all the other single tested frequencies (125, 250, 500, 1k and 2k Hz) was also calculated. Figure 4.19 shows this comparison for the lowest frequencies: 63, 125 and 250 Hz, whereas Figure 4.20 shows it for 500, 1k and 2kHz.
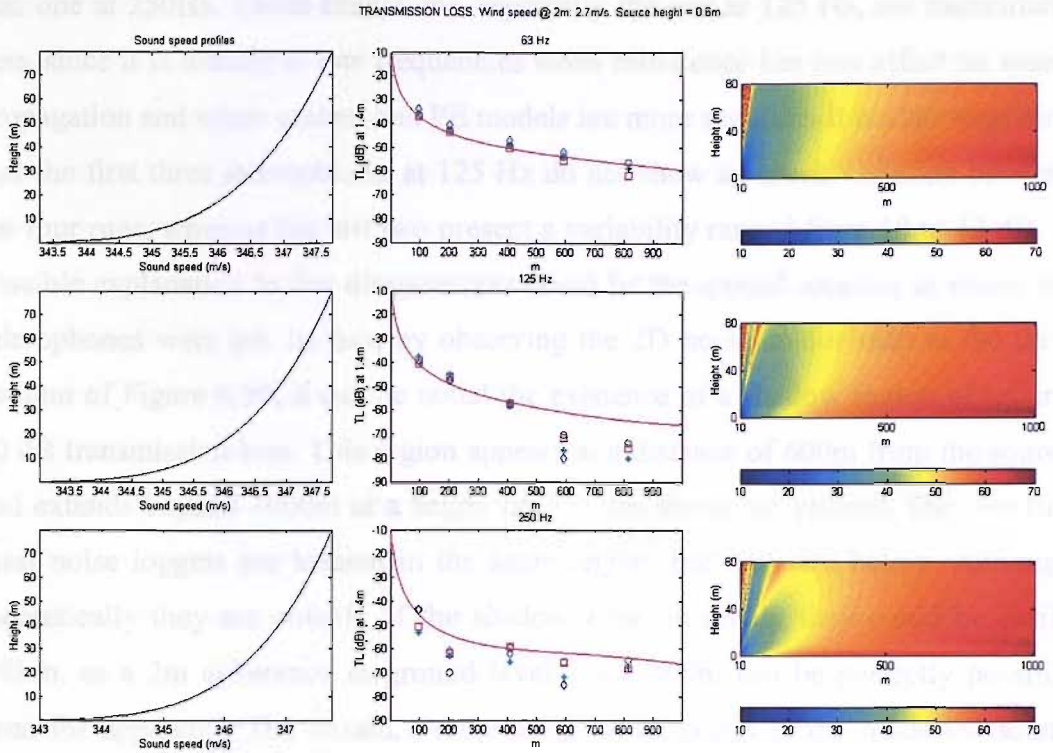
Figure 4.19 *PE validation for 63, 125 and 250 Hz.*
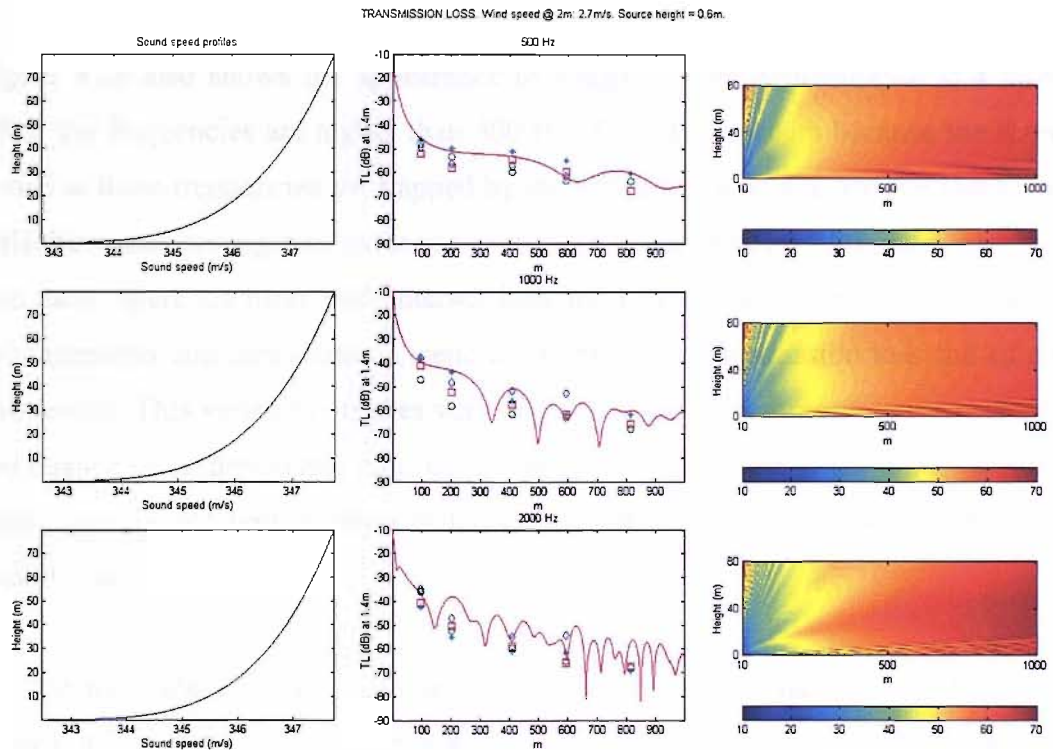
Figure 4.20 *PE validation for 500, 1k and 2k Hz.*

All frequencies show a good general agreement between the measured transmission loss and the PE calculations, except for the last two receivers at 125 Hz and the sec-

ond one at 250Hz. These exceptions, especially the one at 125 Hz, are particularly rare, since it is usually at low frequencies when turbulence has less effect on sound propagation and when ground and PE models are more accurate. It is also surprising that the first three microphones at 125 Hz do not show so much variation between the four runs, whereas the last two present a variability ranged from 10 to 12 dB. A possible explanation to this disagreement could be the special location in where the microphones were set. In fact, by observing the 2D noise colour map at the third column of Figure 6.10, it can be noted the existence of a shadow region of around 70 dB transmission loss. This region appears at a distance of 600m from the source and extends beyond 1000m at a height of 3 to 4m above the ground. The two furthest noise loggers are located in the same region, but only 2m below. Although theoretically they are outside of the shadow zone, in reality they could be easily within, as a 2m difference in ground level along 600m can be perfectly possible even for apparently flat terrain. Furthermore, small errors in the modelled sound speed profile or in other atmospheric variables might make this predicted shadow area move towards the noise monitoring points and then reach a better agreement.

Figure 4.20 also shows the appearance of wiggles in the transmission loss curve when the frequencies are higher than 500 Hz. This effect occurs because the sound waves at these frequencies get trapped by the sound speed profile and the number of reflections and propagation paths increase close to the ground. With more propagation paths, there are more path intersections and consequently more sound pressure enhancements and cancellations, generating thereby a transmission loss full of ups and downs. This variability makes very difficult to obtain a representative comparison against the experimental data, since a slight change in one of the input variables might yield a different position of the peaks and dips, changing considerably the output result.

For the particular objective of this thesis, the level of accuracy of the PE model shown in Figure 4.19 and in Figure 4.20 is enough to study the noise level variability. The agreement reached between the averaged measured and predicted levels ensures a correct PE central tendency for subsequent modelling of the noise variation.

4.4.2. Turbulence model

As explained in section 4.2.3, the PE model works as a marching algorithm; the medium of propagation is divided in vertical lines and the sound field at any of these lines is determined from the field calculated at the preceding one. Furthermore, at each of these lines, the marching algorithm requires having information about the vertical sound speed profile and the ground impedance that can be the same throughout the propagation range or that can change with distance. Up to now, all the PE simulations have been run using a constant sound speed profile; however the possibility of including different sound speed profiles in each of the marching steps seems ideal for computing atmospheric turbulence. Indeed, turbulence can be included as small fluctuations of the sound speed profile and hence computed straightforward by the PE model. Mathematically this can be expressed as:

$$n = \bar{n} + \mu \qquad (4.36)$$

Here n represents the acoustic refractive-index, which is equivalent to the sound speed ($n = c_0/c$), $\bar{n}$ is the average value of the refractive-index and μ denotes the fluctuation representing the turbulence (with $\mu << \bar{n}$ and $\bar{\mu} = 0$).

The first assumption adopted to define the turbulence field μ, is that the medium does not change as the sound waves propagate through it. This approach is known as the frozen medium approach, and is based on the fact that sound waves take less time to travel from source to receiver than the sound speed profile to fluctuate. This means that each realization is like a "snapshot" of the turbulent atmosphere.

The mathematical function describing the turbulence has been built considering that the fluctuation part of the index of refraction $\mu(r,z)$ has an autocorrelation function defined by:

$$C(s) \equiv \langle \mu(R+s) \cdot \mu(R) \rangle \qquad (4.37)$$

The symbol $< >$ has been used to denote an ensemble average over many realizations of μ, R=(x,y,z) to designate a position vector and s to represent some spatial separation distance in the r-z plane. According to a number of different authors, (Daigle, G.A.) or (Gilbert, K. E, et al.), for small-scale turbulence near the ground, C(s) can be approximated by a Gaussian distribution. However, other authors (Wilson, D.K. et al., or Salomons E.M) state that the values required by the Gaussian

parameters to give an empirical good 'fit' are not well justified from a meteorological point of view, and that other models for the turbulence spectrum, such as the Kolmogorov or the von Kármán spectra (details in Ostashev, V.E), are more realistic. Despite this debate, it is generally accepted that the Gaussian spectrum, with proper values of the parameters, agrees with both the von Kármán and Kolmogorov spectra in a frequency range which is relevant for most acoustic applications (20-2000Hz). Since this frequency range covers the frequencies investigated in the Salisbury Plain database and the equations for the Gaussian correlation and spectral functions are more easily obtainable, the Gaussian model has been applied in this work. Hence, for our two-dimensional turbulence model we use:

$$C(s) = \mu_0^2 e^{-s^2/l^2} \tag{4.38}$$

Here μ_0 is the root-mean-square fluctuation of $\mu(r,z)$ and l is the correlation length. (Daigle, Gilbert or Salomons recommend orders of magnitude for μ_0 and l of about 10^{-3} and $1m$, respectively).

The wavenumber spectrum $W(k_1,k_2)$ of the turbulence is defined as the Fourier transform of the autocorrelation function,

$$W(k_1, k_2) = \iint e^{i(k_1 s_1 + k_2 s_2)} C(s_1, s_2) ds_1 ds_2 \tag{4.39}$$

The two variables k_1 and k_2 are, respectively, the radial and vertical components of the wavenumber, and s_1 and s_2 are, respectively the radial and vertical components of the spatial separation. To obtain realizations of $\mu(r,z)$ from the wavenumber spectrum we multiplied $\sqrt{W}$ by a random phase function $\exp(i\emptyset(k_1,k_2))$ and calculated the inverse Fourier transform. Hence, for a given trial, we computed:

$$\mu(r, z) = N \iint \sqrt{W(k_1, k_2)} \cdot e^{-i(k_1 r + k_2 z)} \cdot e^{i\phi(k_1, k_2)} \frac{dk_1 dk_2}{(2\pi)^2} \tag{4.40}$$

The normalization factor N is the square root of the area over which $\mu(r,z)$ is defined in equation (4.39). To make μ real valued, there are two options: either requiring that $W \rightarrow +W$ and $\emptyset \rightarrow -\emptyset$ for negative values of k_1 or k_2, or calculating the standard deviation of the real part, $std(\mu)$, and then multiplying the real part of μ by the factor $\mu_0/ std(\mu)$ to ensure that μ satisfies equation (4.38).

Another important assumption considered in this model is that according with Figure 4.2, atmospheric turbulence decay with height, reaching a null value above

100 m in some cases. This feature has been taken into account by modulating the μ function with an exponential function, which takes the unity at the surface and decreases as height increases.

Figure 4.21 shows an example of a realization of μ(r,z). Note that the correlation length and average amplitude of the fluctuations are roughly 1m and 10^{-3}, following the recommendations of Daigle and Gilbert.

Figure 4.21 *A 150x150m sample of the stochastic part of the index of refraction μ(r,z) for a given realization. The root-mean square amplitude, $μ_0$, is $1.42x10^{-3}$ and the correlation length is 1.4m.*

Our primary objective is now to calculate the sound level variability generated by a turbulent atmosphere so that we can compare this variability against the measured standard deviation. In order to undertake this comparison, we have calculated 100 realizations of the above turbulence model. On each of these realizations, the turbulence field is different in detail than the sample shown in Fig. 4.21, but has the same properties as defined above. Fig. 4.22 shows the measured and the predicted sound level variability for all the different frequencies under study. The measured variability corresponds to the calculated standard deviation of the 30 continuous LAeq1s measurements taken for each of the 6 plotted frequencies. Within the 30s recording period, the met gauges took two average met measurements (wind, temperature...) of 15s at the two heights specified in section 4.3. Assuming neutral stability conditions, the average sound speed profile was extrapolated using these met values.

Figure 4.22 *TL variability for 63, 125, 250, 500, 1k and 2kHz. Predicted variability has been obtained with 100 isotropic turbulence realizations of 1.4m correlation length*

The left column of Figure 4.22 shows a comparison between the predicted and the measured standard deviation as a function of distance, and the right column compares both the average and the variability of measured and calculated sound levels. It is interesting to note that in contrast to the results of the Joule database, sound level variability does not show a clear trend as function of distance. One can see a general increase in sound level variability with distance, especially at low-mid frequencies, but even at those frequencies the trend is abrupt and unpredictable. In terms of agreement, curves do not perfectly match, but deviations are never further than 3-4 dB (regardless the two last receivers at 125 Hz, whose particularities were discussed in page 105).

Searching for a better agreement, we reviewed the statistical properties of the turbulence model. According to the explanation of page 78, a turbulent atmosphere often contains loops of air particles, which are called eddies. The size of these eddies is variable depending on the height from one is observing; Close to the ground, authors recommend a correlation length of about 1-2m., but when one is considering a 150m vertical profile, the existing turbulent eddies could be larger. Based on this reasoning, we have repeated the calculations, but with a higher turbulence correlation length (7m.). A sample of this new assumption is shown in Figure 4.23.
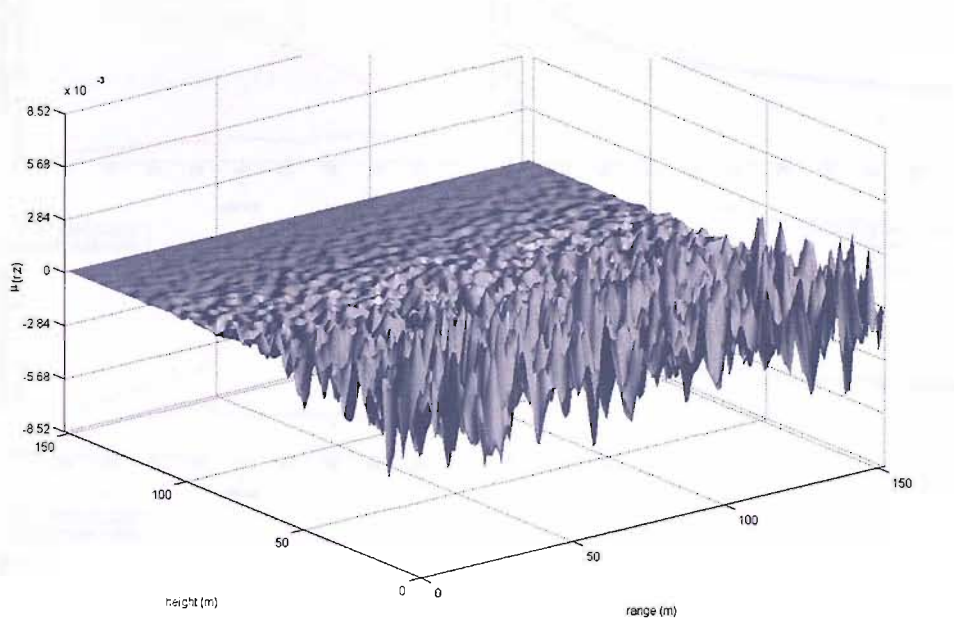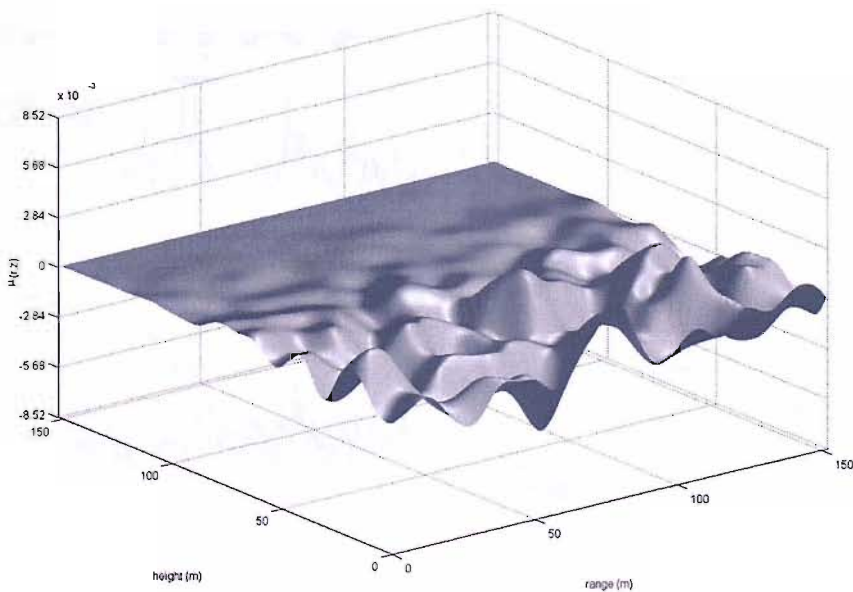

Figure 4.23 *A 150x150m sample of the stochastic part of the index of refraction μ(r,z) for a given realization. The root-mean square amplitude, μ_0, is $1.42x10^{-3}$ and the correlation length is 7m.*

111

Figure 4.24 *TL variability for 63, 125, 250, 500, 1k and 2kHz, obtained with 100 iso-tropic turbulence realizations of 7m correlation length*

Figure 4.24 shows the comparison between measured and predicted noise level variability when the isotropic turbulence model has a correlation length of 7m. As in the previous case, the agreement is not exact, having deviations ranging from 2 to 4-5 dB. The predicted standard deviation is slightly lower than Figure 4.22, understandably due to the smoother and larger variations of the assumed turbulent field. Predicted sound level variability of frequencies 250 and 500 Hz are particularly below the experimental values and measured average levels are slightly outside of the predicted standard deviation area depicted by the grey regions of the figures in the right column. It is particularly interesting to compare the predicted average noise levels at 1000Hz and 2000Hz. In the first case, there are large undulations in the predicted average and TL variability, whereas at 2000 Hz, the predicted transmission loss seems to have a smoother trend. This suggests that the calculated turbulent field is able to diffuse the sound energy at 2kHz, whilst at 1kHz, there are still undulations (cancellations and enhancements) up to about 700m (in where the field starts being more diffuse).

Our last trial is to assume that the characteristics of the turbulent field are not isotropic. This idea arises from observing the turbulence properties of another fluid: the ocean. In this medium, the correlation factor existing between the measured turbulence at two points separated 10m vertically is often of the same order of magnitude as the correlation factor of one of these sites and another located 1000m horizontally apart (Jensen et al.). This suggests that the correlation lengths of the oceanic turbulent field keep a relation of 1:100 between the y-axis and the x-axis.

Testing the above feature in our atmospheric sound propagation exercise, we calculated the correlation factors between the wind speed projections at the two heights (2-11m) of one of the met towers and between the two highest anemometer locations of the two met towers separated 1km apart. The correlation factors were respectively 0.7 and 0.35. These values do not fully satisfy the oceanic turbulence properties, but the not inconsiderable value of the second correlation factor could possibly indicate a vertical-horizontal relation between 1:1 and 1:100.

Searching for a more concrete answer in the literature, we find that in the theoretical development of the anisotropic Gaussian correlation and spectral functions under-

taken by (Wilson, DK, "Calculated..."), the author obtains a relation of approximately 1:10 between what he calls the "along-wind" and "cross-wind" extinction distances (which in our particular exercise are equivalent to our y and x correlation lengths). Since this ratio is well within the range predicted in the above paragraph, a y-x correlation length relation of 1:10 was assumed for the Gaussian anisotropic model adopted here.

Like Wilson, other authors (see Ostashev, V.E. et al.) have theoretically developed the different equations that stand for the correlation and spectral functions of a variety of anisotropic turbulence models (Gaussian, von Kármán, Mann's, etc...), however their equations have not yet been compared against experimental data. Therefore, the work carried out here is also a good opportunity to establish and quantify the true importance of the developed anisotropic models as compared to a real field experiment.

Figure 4.25 shows a 150x150m sample of the adopted anisotropic turbulent field. It can be noted that the variations are not homogeneous: The correlation length in the y-axis is 1.41m (as in Figure 4.21) and the correlation length in the x-axis is 14.1m.
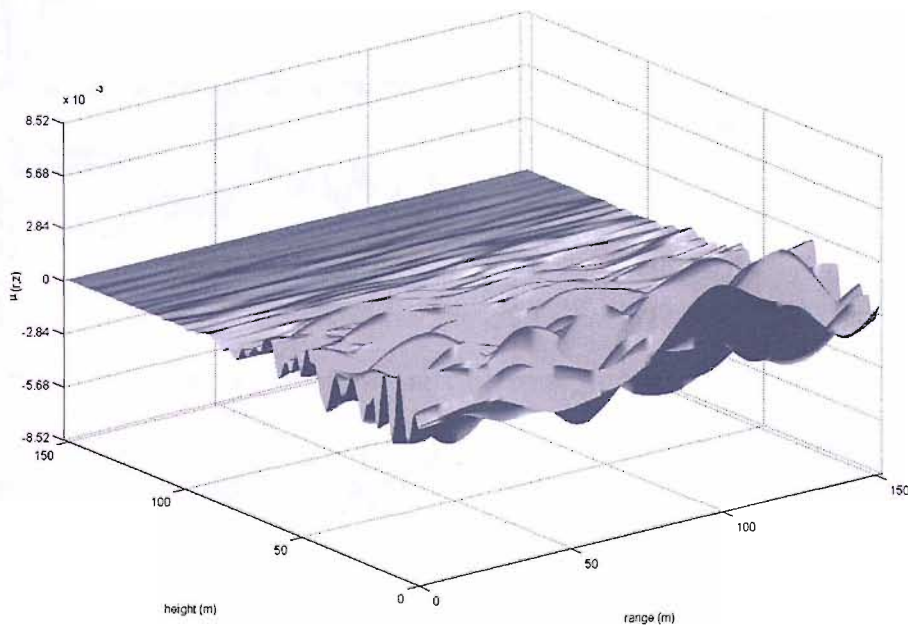
Figure 4.25 *A 150x150m sample of the stochastic part of the index of refraction μ(r,z) for a given anisotropic turbulence realization. The RMS amplitude μ_0, is $1.42x10^{-3}$ and the vertical and horizontal correlation lengths are 1.4m and 14m respectively.*
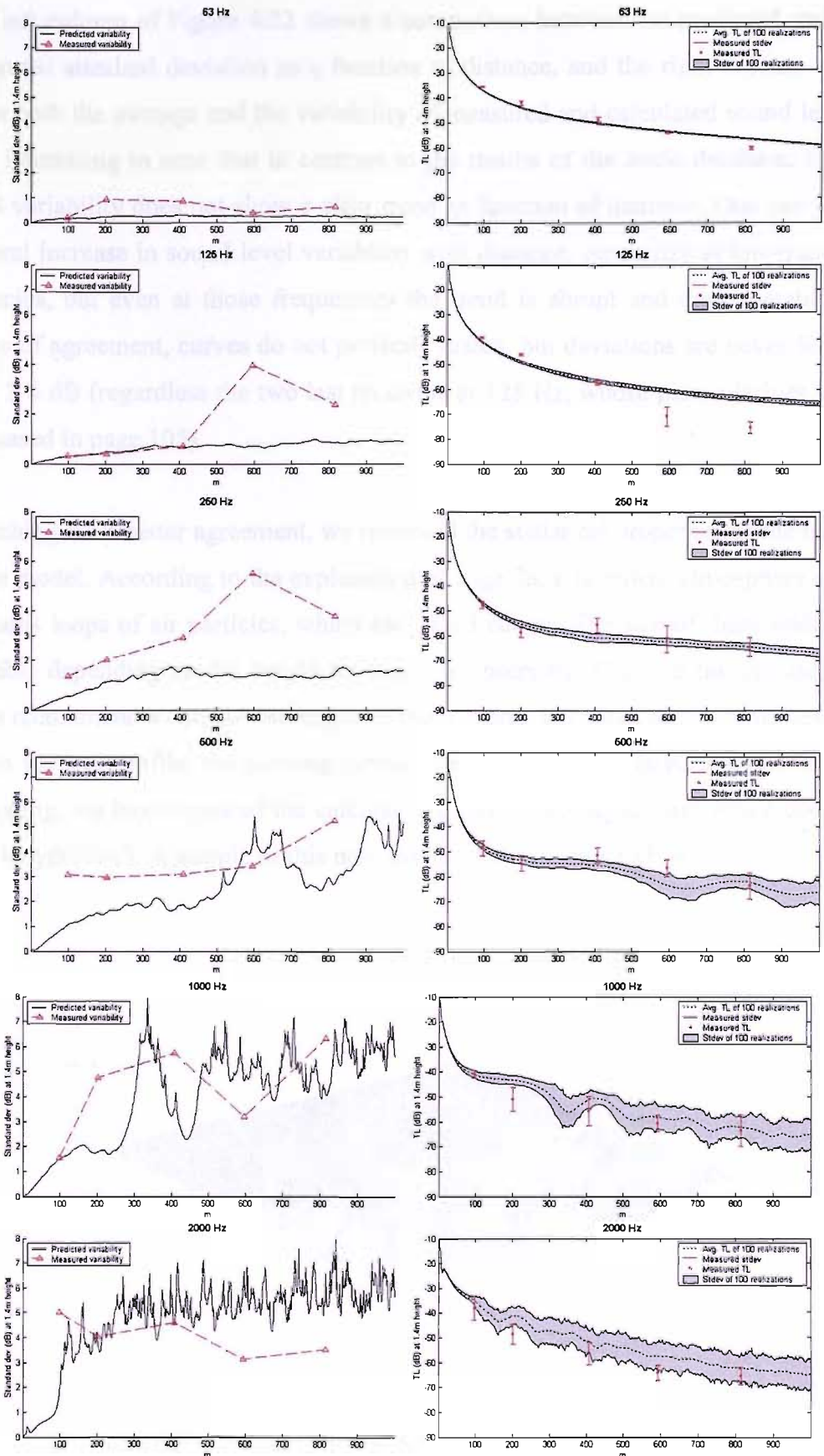
114
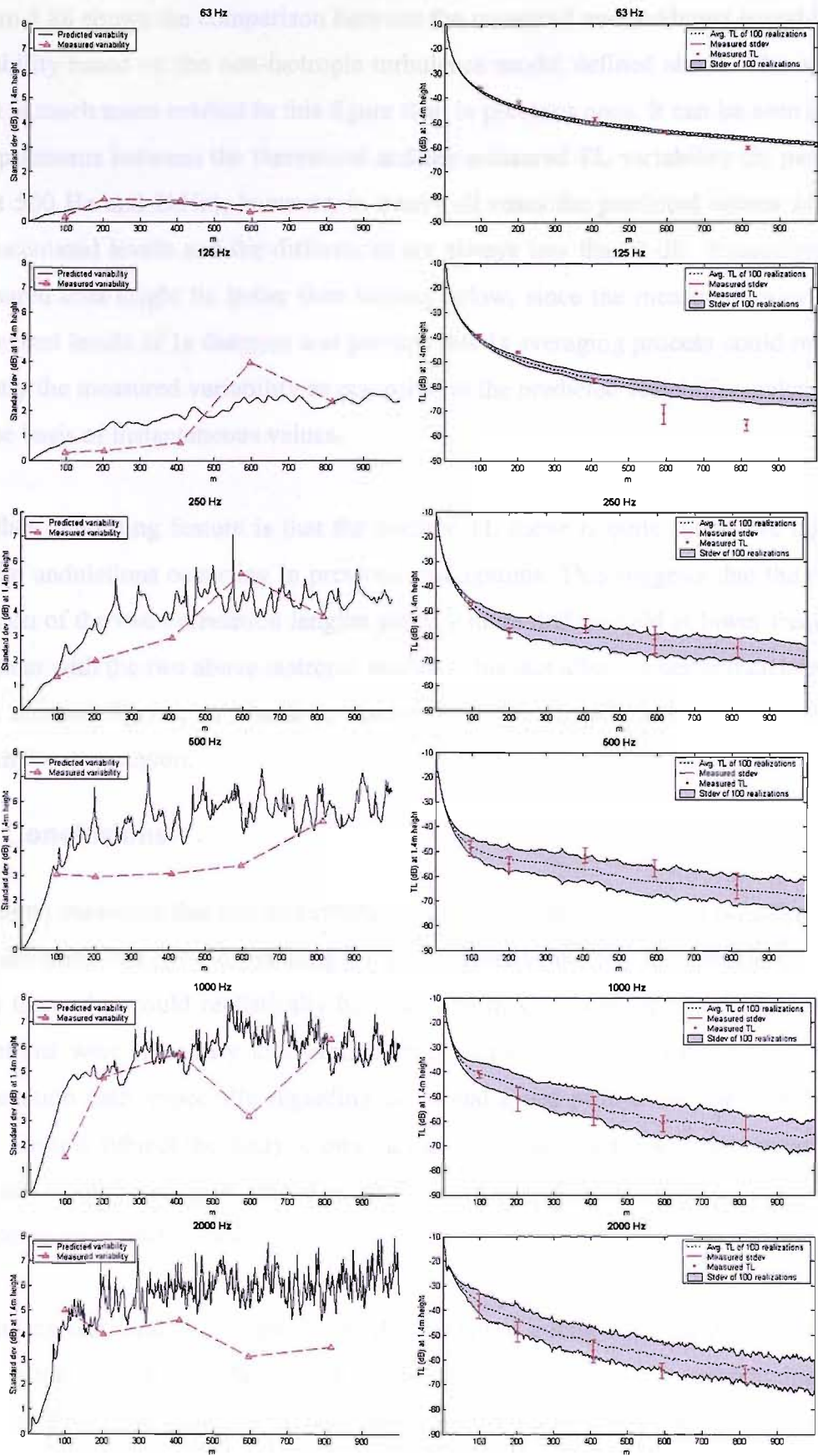
Figure 4.26 *TL variability for 63, 125, 250, 500, 1k and 2kHz, obtained with 100 anisotropic turbulence realizations of 1.4m & 14m vertical and horizontal correlation lengths.*

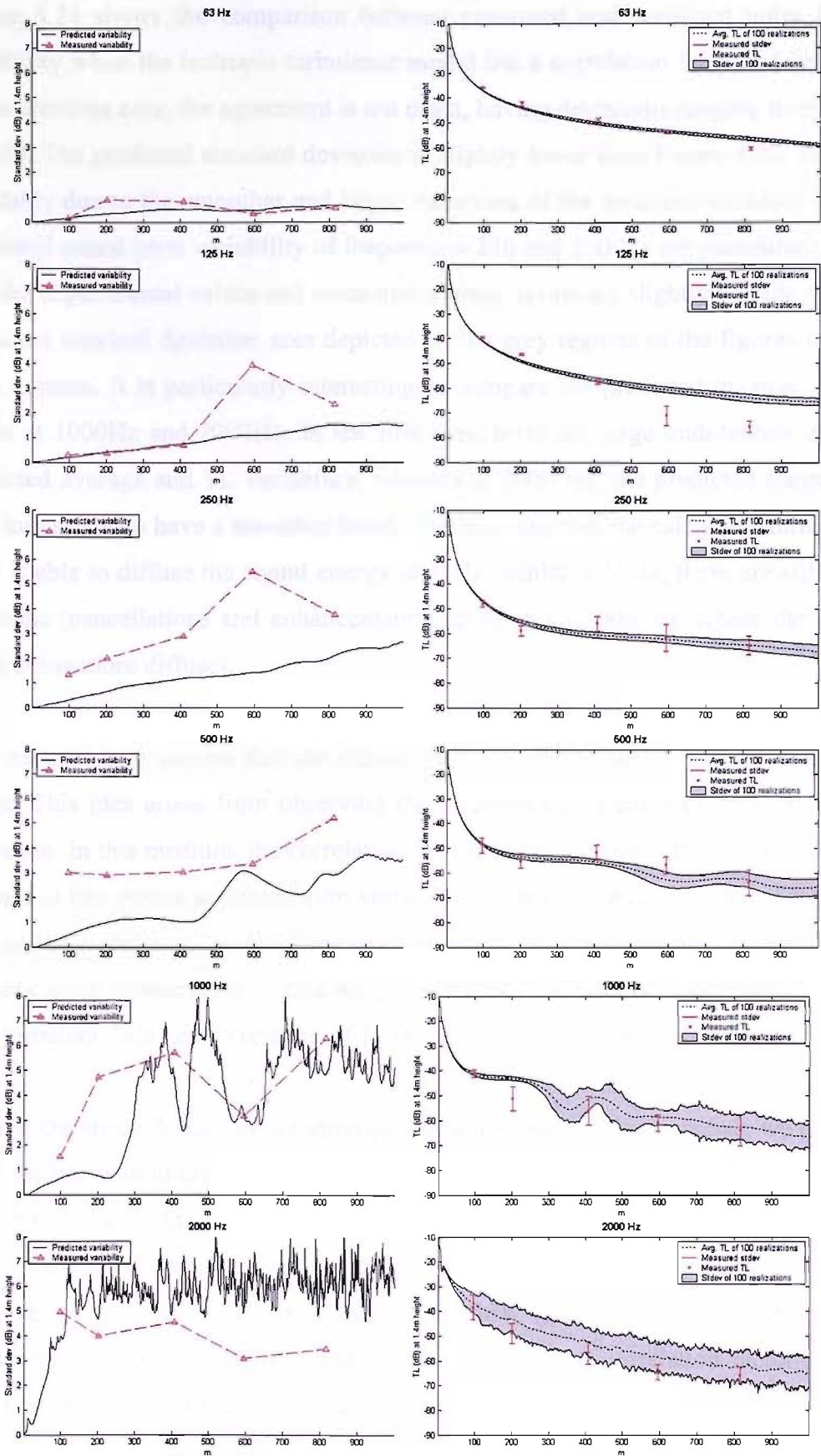Figure 4.26 shows the comparison between the measured and predicted sound level variability based on the non-isotropic turbulence model defined above. The agreement is much more evident in this figure than in previous ones. It can be seen some disagreements between the theoretical and the measured TL variability (in particular at 500 Hz and 2kHz), however, in nearly all cases the predicted values exceed the calculated levels and the differences are always less than 2 dB. Exceeding the measured data might be better than staying below, since the measured values are equivalent levels of 1s duration and perhaps this 1s averaging process could reduce slightly the measured variability as compared to the predicted variability, calculated on the basis of instantaneous values.

Another interesting feature is that the average TL curve is quite stable, we do not see the undulations occurring in previous assumptions. This suggests that the combination of the two correlation lengths yields a more diffuse field at lower frequencies than with the two above isotropic models. This fact allows a better match in the right column figures, in where is observed that nearly all measured values are within the grey region.

4.5. Conclusions

The first conclusion that can be extracted from this comparison is that the PE model was accurate, but very demanding in input environmental data, sometimes even more than what could realistically be measured in-situ. A number of different assumptions were necessary to reproduce the microclimate occurring at the sound propagation path, especially regarding the sound speed profile and the turbulence field. On this subject the study allows validating the assumptions against measured data and understanding in greater depth the meteorological parameters controlling the sound level fluctuations.

Regarding technical issues, the PE method required a long computational time for completing the calculations. The PE algorithm was optimised for reproducing the sound field as faster as possible, reaching calculation times of few seconds for up to 500Hz and few minutes for 1 and 2 kHz. However minutes in one simulation means hours in 100 realizations, which is still a lot for being implemented in practical ap-

plications or for calculating broad-band frequency spectrums. There are currently some research groups working on direct methods to obtain sound level variability by only one simulation (Blanc-Benon et al.), and others that are trying to improve the speed and accuracy of the PE model (Lingevitch, J. F., et al), but their work is still under development and its technical interest is out of the scope of this thesis.

A part from the technical appreciations, the Salisbury plain database shows the short-term sound level fluctuations arising from atmospheric turbulence. Contrarily to what happens in long-term fluctuations caused by migratory pressure systems, turbulence does not yield a sound level variability exponentially or linearly related with distance. There is, nevertheless, a general increase in the standard deviation as a function of distance and frequency.

All the 2D turbulence models used above showed a good agreement with measured data, in particular when using the non-isotropic turbulence assumption. The models provided a better understanding of the general properties involving atmospheric turbulence, avoiding the impracticable task of measuring the turbulence field in-situ. Predictions showed that other assumptions to those commonly used in the literature might also be possible. The inclusion of an exponential decay of atmospheric turbulence as a function of height (based on Heimann's observations) and the different correlation length values adopted in the model reached a better match than literature recommendations. This opens a research possibility to find better descriptors of the air turbulent flow and more appropriate statistical parameters of the atmospheric turbulence distribution.

Chapter 5

Conclusions

5.1. Thesis results

Based on a comprehensive analysis of three different outdoor noise measurement databases, the thesis provides qualitative and quantitative answers as to how measured noise levels vary in a range of common environmental situations.

The 50 site database covers a considerable amount of environmental noise sources and random situations within different types of suburban and rural residential areas, in where no theoretical modelling was practicable. Despite the unpredictable conditions and the low level of measuring details, the analysis revealed some order within the disorder: A strong inverse relationship between measured standard deviations and mean noise levels. Measured noise variability increased from typical standard deviations of around 1.5 dB at overall average noise levels of around 70 dB and above to around 4.5 dB at lower average noise levels of around 50 dB.

Both the Joule and Salisbury Plain databases were designed to find a quantitative explanation of the relationship found in the 50 site database. The Joule measuring exercise focused on the mid-term meteorological effects on noise level variability, while the Salibury Plain acoustical test concentrated on the influence of atmospheric turbulence on received sound pressure levels. Both exercises were recorded

under controlled conditions and at a sufficient level of detail to undertake theoretical modelling.

The analysis of Joule database showed that over a 2 week period and at short ranges the sound propagation was most influenced by small changes in atmospheric absorption rates, while at increasing distances the atmospheric refraction effects became increasingly dominant as compared to other factors. The trend resulting from adding all variability contributions agreed with that obtained in the 50 site database: Standard deviations of the recorded LAeq values increased exponentially at increasingly long distances to the source. In addition, the ray theoretical modelling developed for this analysis provided a useful tool for the explanation and prediction of the observed relationship.

The Salisbury Plain database explained the short-term sound level fluctuations arising from atmospheric turbulence. In contrast to previous databases, Salisbury Plain database showed that turbulence does not yield a sound level variability exponentially or linearly related with distance, although it does produce a general increase in the standard deviation as frequencies and source-receiver distances increase. The PE model developed for the analysis introduced some technical improvements over other PE solution schemes and provided the possibility to investigate the validity of different assumptions for modelling actual atmospheric turbulence.

In sum, the main result lies on the found inverse correlation between standard deviations and average noise levels. Other found relationships and related theoretical modelling are also relevant for different practical and technical reasons, but in the context of the thesis, are especially significant for justifying partially or totally the relationship observed in the 50 site database.

5.2. Applicability

In Chapter 1, the thesis clarifies that the noise mapping technique widely used in common practical applications is not as precise as most users could expect. Its colourful representation looks tidy and professional, but when extracting noise level information or when validating calculated data against measured levels, the colour-

noise conversion becomes very ambiguous in reality. Furthermore, and more importantly, noise mapping models and current noise policies focus on the determination of a single noise value that could represent the full range of noise conditions over a 'relevant year'; when, as the thesis shows, that kind of indication could only be completely representative by providing additional information on noise level variability over the averaged period.

When studying the noise level variability, the Joule database confirms that for any fixed propagation path of constant noise level source, the most important feature affecting the sound level variability involves the variation of the sound speed profiles above the ground. This variation can be considered in a range of different time-scales:

-When long-term variation is of interest, the meteorological phenomena dominating the change of sound speed profiles is related to the pass-by of weather systems and additionally to the diurnal and nocturnal changes of the atmospheric properties. The vertical profiles are in this case smooth functions of height and averaged over a period that could range between 10 min to 2 hours (according to the spectral gap shown in Figure 4.1). The large dimension of the weather systems as compared to the dimension of our field experiments allows assuming the same sound speed profile along the propagation path (i.e. range-independent conditions).

-When short-term variation is of interest, atmospheric turbulence is the dominant factor. The turbulence variability is much quicker than the fluctuating rate of the bulk of the wind flow, and the physical size of the turbulent eddies is usually much smaller than the propagation path; this yields to a variety of different and irregular vertical profiles along the source-receiver distance (i.e. range-dependent propagation).

The above classification is not only supported by the 3 different databases investigated throughout the thesis, but also by some evidences in the literature. It is remarkable, for example, the contribution of (Heimann D and Salomons E.M) about long-term variability. Using averaged sound speed profiles of consecutive 6-h intervals during one year, they calculate the sound pressure levels at 20, 200 and 1000m

from the source. Based on PE calculations, they limited the 1452 measured meteorological situations over one year to 121 representative meteorological conditions. While it is debatable that 121 meteorological situations is still a large number to be used in practical applications, the conclusion which has a lot in common with the work reported here is the exponential increase of noise level variability with distance: they obtained that their predicted levels varied up to 2 dB (20m), 18 dB (200m) and 42 dB (1000m) for rigid ground and approximately halved in the case of absorbing ground. Their variability ranges are then in good agreement with those found in the Joule database.

In terms of practical applicability, do these conclusions support the use of a 'worse case' noise approach commonly adopted by many practical engineering methods like ISO 9613? It is evident that the sound variability is large; however both the 50 site and the Joule databases show that the noise level distribution is skewed to the minimum values. Hence, in the 50 site database, we see that in both plots of Figure 2.11, the bulk of the points affected by meteorological conditions (high standard deviation) lay down the central trend line, and in the Joule database, Table 3.2 and Table 3.3 clearly show larger corrections for upwind than downwind conditions. All this suggests that the average levels are much closer to the maximum values than to the minimum levels and consequently, a 'worse case' approach might not be as misguided for an indication of a long-term average as one could initially expect.

The above reasoning also explains partly why the ISO 9613 A-weighted predictions agreed with the average noise measured levels of the Joule database (Figure 3.14). These evidences show that the ISO 9613 predictions might be helpful as an estimation of average long-term levels; however, there are cases in which a worse case approach might not be enough to cover other aspects of the noise level distribution:

-There can be situations in where the prevailing wind is unfavourable to propagation. In this situation then, a generic worse case approach is likely to provide much higher values than the long-term average noise levels.

-There are also cases in where it is important to know for how long and under which meteorological conditions the noise level from a source vanishes into the

background noise level. In this situation, a more detailed method is required than the 'worse case' approach applied in most of practical engineering methods.

In the above situations, the noise level variability becomes very important, and (Heimann and Salomons)'s approach or this thesis approach could be in theory more suitable for tackling the posed problems, because of the much greater level of detail provided.

In sum, the thesis gives three different solutions as to how to take into account noise level variability in practice according to the particular situation that the user is facing:

-If the noise environmental assessment covers a big area with a broad range of uncontrolled noise sources and with limited time and resources to measure, the results of the 50 site database could be applied. Such results indicate the order of magnitude and the main contributions factors affecting the noise level variability. They could act as an estimative tool for predicting the noise level variability in measurements; this additional information might be essential to complete the representativeness of measured or calculated averaged noise levels. Subject to the caveat that extrapolation of the '50 site database' results to conditions not generically represented in the overall measurement database may be of dubious value, the general finding of relevance to the estimation of variability in noise measurements is that measured road traffic noise variability increases from typical standard deviations of one minute LAeqs of around 1.5 dB at overall average noise levels of around 70 LAeq and above to around 4.5 dB at lower average noise levels of around 50 LAeq.

-If the meteorological conditions are controlled in a sufficient level of detail and the interest is focused on the mid-term met effects on noise levels, the thesis suggests a method for estimating the noise level variability based on calculating the dominant influence of the atmospheric refraction effects. In this case, the Joule database confirms that over the shorter source to receiver distances, small changes in measured source sound power output and predicted changes in atmospheric absorption rates were the most important controlling factors. At increasing source to receiver distances, predicted differences in either upwards or downwards sound ray curvature

associated with differences in wind speed and air temperature profiles above the ground became increasingly dominant. Additionally, both the noise level statistical distributions obtained in the '50 site' and 'Joule' databases support the use of a 'worse case' noise approach to environmental noise impact when no level of detail is required.

-For a more detailed information about short-term noise level fluctuations, the work reported here proposes the use of a PE model for taken into account the effects of atmospheric turbulence on sound propagation. By applying this model to the Salisbury Plain database, results show that turbulence does not yield a smooth function of noise variability with distance, as happened in previous cases. However, results show that there is a general increase in the standard deviation as a function of distance and frequency. The anisotropic turbulence model was found to be in much better agreement with field measurements than the different isotropic models investigated in the thesis.

References

Alberola, J., Flindell, I. H., Bullmore, A. J., Peral, R., "Variability of Outdoor Sound Propagation Arising Under Different Meteorological Conditions" 11th International Congress on Sound and Vibration, St Petersburg (2004)

Alberola-Asensio, J., Mendoza-Lopez, J., Bullmore A. J., Flindell, I. H, "Noise mapping: Uncertainties", *Forum Acusticum* Sevilla (2002)

ANSI S1.26, Method for the Calculation of the Absorption of Sound by the Atmosphere. - 1978, American National Standard.

Attenborough, K., "Acoustical Impedance Models for Outdoor Ground Surfaces", *Journal of Sound and Vibration* **99** (4), pp. 521-544 (1985)

Attenborough, K., "Review of Ground Effects on Outdoor Sound Propagation from Continuous Broadband Sources", *Applied Acoustics* **24**, pp. 289-319 (1988)

Bass, J. H., Bullmore, A. J., Sloth E., "Development of a Wind Farm Noise Propagation Prediction Model", Non-Nuclear Energy Programme Joule III. JOR3-CT95-0051

Berry, A., Daigle, G. A., "Controlled Experiments of the Diffraction of Sound by a Curved Surface", *J. Acoust. Soc. Am.* **83** (6), pp. 2047-2058 (1985)

Blanc-Benon, Ph., Dallois, L., Juvé, D., "Long Rage Sound Propagation in a Turbulent Atmosphere Within the Parabolic Approximation", *Acustica-Acta Acustica* **87**, pp. 659-669 (2001)

Bradley, S. G., "Vertical structures of wind, temperature, precipitation and turbulence and their influence on sound propagation". *IOA conference*: "Weather or not to measure..." 2002.

Chen, C., Lin Y., Lee, D., "A three-dimensional azimuthal wide-angle model for the parabolic wave equation", *Journal of Computational Acoustics*, **7**, pp. 269-286 (1999)

Chessel, C. I., "Propagation of Noise Along a Finite Impedance Boundary", *J. Acoustic. Soc. Am.*, **62**, pp. 62-68 (1977)

CONCAWE report No. 4/81, The Propagation of Noise from Petroleum and Petrochemical Complexes to Neighbouring Communities (1981)

Craven N. J., Kerry G., A "Good Practice Guide on the Sources and Magnitude of Uncertainty Arising in the Practical Measurement of Environmental Noise". *DTI Project: 2.2.1 – National Measurement System.* Programme for Acoustical Metrology.

CRTN, Calculation of Road Traffic Noise. Department of Transport - Welsh Office (1988)

Daigle, G. A. "Effects of Atmospheric Turbulence on the Interference of Sound Waves above a Hard Boundary", *J. Acoust. Soc. Am.* **64** (2), pp. 622-630, (1978)

DEFRA (Department for Environment, Food and Rural Affairs), "Towards a National Ambient Noise Strategy" A Consultation Paper from the Air and Environmental Quality Division. (November 2001).

Delany, M. E., Bazley, E. N., "Acoustical Properties of Fibrous Absorbent Materials", *Applied Acoustics*, 3, pp 105-116 (1970)

Delrieux Y., Malbéqui, P., "Atmospheric sound propagation using a three-dimensional parabolic equation", Proc. Fifth Symposium on Long-Range Sound Propagation, Milton Keynes, England, 147-157 (1992)

Embleton, T. F. W., "Tutorial on Sound Propagation Outdoors", *Journal of the Acoustic Society of America*, 100 (1), pp. 31-48 (1996)

Embleton, T. F. W., Piercy, J. E., Olson, N., "Outdoor Sound Propagation Over Ground Of Finite Impedance", *J. Acoustic. Soc. Am.*, 77 (4), pp. 267-277 (1976)

Embleton, T. F. W., Thiessen, G. J., Piercy, J. E., "Propagation in an Inversion and Reflections at the Ground", *J. Acoust. Soc. Am.*, 59, No. 2, pp. 278-282, (1976)

European Commission, "Environmental Noise Directive 2002/49/EC", *Official Journal of the European Communities* L189, pp. 12-25 (June 2002).

European Commission, "Green Paper on Future Noise Policy" November 1996

Farrelly, F. A., Brambilla, G., "Determination of Uncertainty in Environmental Noise Measurements by Bootstrap Method", *Journal of Sound and Vibration,* 268, pp. 167-175 (2003)

Gaja, E., Giménez, A., Sancho S., "Sampling techniques for the estimation of the annual equivalent noise level under urban traffic conditions". *Applied Acoustics*; 64 (1): 43-53 (2003)

Gilbert, K. E., White, M. J., "Application of the Parabolic Equation to Sound Propagation in a Refracting Atmosphere", *J. Acoust. Soc. Am.* 85 (2), pp. 630-637, (1989)

Gilbert, K.E., Di, X. "A fast Green's function method for one-way sound propagation in the atmosphere" *J. Acoust. Soc. Am.* 94, pp. 2343-2352, (1993)

Gilbert, K.E., Raspet, R., Di X. "Calculation of Turbulence Effects in an Upward-Refracting Atmosphere", *J. Acoust. Soc. Am.* 87 (6), pp. 2428-2437, (1990)

Hardin, R. H., Tappert F. D., "Applications of the Split-Step Fourier Method to the Numerical Solution of Nonlinear and Variable Coefficient Wave Equations", *SIAM* Rev. 15, 423 (1973)

Heimann, D., "Influence of Meteorological Parameters on Outdoor Sound Propagation" *Euronoise Conference*, Naples 2003.

Heimann, D., "Meteorological Aspects in Modelling Noise Propagation Outdoors" *Euronoise Conference*, Naples 2003.

Heimann, D., Salomons, E.M., "Testing meteorological classifications for the prediction of long-term average sound levels" *Applied Acoustics* 65, pp. 925-950, (2004)

Holtslag, A. A. M., "Estimates of Diabatic Wind Speed Profiles form Near-Surface Weather Observations" *Boundary-Layer Meteorology* **29**, pp. 225-250 (1984)

IEC International Standard 61400-11, Wind turbine generator systems – Part 11: Acoustic noise measurement techniques, IEC 61400-11:1998(E)

ISO 9613-1, Acoustics – Attenuation of Sound During Propagation Outdoors – Part 1: Calculation of the Absorption of Sound by the Atmosphere, ISO 9613-1:1996, International Standards Organisation.

ISO 9613-2, Acoustics – Attenuation of Sound During Propagation Outdoors – Part 2: General Method of Calculation, ISO 9613-2:1996, International Standards Organisation.

ISO Publication 6461-3:1995.General Metrology – Part 3: Guide to the Expression of Uncertainty in Measurement (GUM), BIPM / IEC / IFCC / ISO / IUPAC / IUPAP / OIML, 1995.

Jensen, F. B., Kuperman, W. A., Porter, M. B., Schmidt, H., "Computational Ocean Acoustics" American Institute of Physics Press, New York, 605 pages. (1994)

Kühner, D., "Excess attenuation due to meteorological influences and ground impedance", *Acustica – Acta Acustica* **84**, pp. 870-883 (1998)

Larsson, C., "Atmospheric Absorption Conditions for Horizontal Sound Propagation" *Applied Acoustics* **50** (3), pp. 231-245, (1997)

Lee, D., Pierce, A. D., Shang, E., "Parabolic Equation Development in the Twentieth Century", *Journal of Computational Acoustics*, **8**, (4), pp. 527-637 (2000)

Lingevitch, JF, Collins, MD, Dacol, DK, Drob, DP, Rogers, JCW, Siegmann, WL, "A wide angle and high Mach number parabolic equation" *J. Acoust. Soc. Am.* **111** (2), pp. 729-734, (2002)

Maekawa, Z., "Noise Reduction by Screens", *Applied Acoustics* **1**, pp. 157-173 (1968)

Manvell D., Stapelfeldt H., Shilton S., "Matching Noise Maps with Reality – Reducing Error through Validation and Calibration", Institute of Acoustics meeting Noise Mapping – Which way now?, London (February 2002)

McDaniel, S. T., "Propagation of Normal Mode in the Parabolic Approximation" *J. Acoust. Soc. Am.* **57**, pp. 307-311 (1975).

McKenzie, A., Bullmore, A. J., Flindell, I. H., "The Effects of Weather on Ambient and Background Noise in the Sub-Urban Environment", Conference held by *Institute of Acoustics*: "Weather or not to measure..." Leicester (2002)

Ostashev, V.E., "Acoustics in Moving Inhomogeneous Media", E&FN Spon, London (1997)

Ostashev, V.E., Wilson, D.K., Goedecke, G.H., "Spherical wave propagation through inhomogeneous, anisotropic turbulence: Log-amplitude and phase correlations" *J. Acoust. Soc. Am.* **115** (1), pp. 120-130, (2004)

Piercy, J. E., Embleton, T. F. W., Daigle, G. A., "Atmospheric Propagation of Sound: Progress in Understanding Basic Mechanisms" *11th ICA*, pp. 37-46, (Paris 1983)

Probst W., Donner U., "The Uncertainty of Sound Pressure Levels calculated with Noise Prediction Programs" Cadna A web page.

Rudnick, I., "Propagation of Sound in the Open Air" in *Handbook of Noise Control*, edited by C. M. Harris (McGrawHill, New York, 1957), **Chap. 3**.

Sack, R.A., West, M., "The Lagrange Padé parabolic equation (LP-PE) for the prediction of long range sound propagation in the atmosphere" *Applied Acoustics* **49**, pp. 105-125, (1996)

Salomons E.M., "Computational Atmospheric Acoustics", Kluwer Academic Publishers, Dordrecht, 335 pages (2001).

Van der Hoven, I., "Power Spectrum of Horizontal Wind Speed in the Frequency Range from 0.0007 to 900 Cycles per Hour", *Journal of Meteorology* **14**, pp. 160-164 (1956)

White, P. R., Class notes – Chapter 4; Modelling of Sound Propagation in the Ocean. ISVR. University of Southampton.

Wilson, D.K., Brasseur, J.G., Gilbert, K.E., "Acoustic scattering and the spectrum of atmospheric turbulence" *J. Acoust. Soc. Am.* **105**, pp. 30-34, (1999)

Wilson, D.K., Thomson, D.W., "Calculated coherence and extinction of sound waves propagating through anisotropic, shear-induced turbulent velocity fluctuations" *J. Acoust. Soc. Am.* **105**, pp. 658-671, (1999)

Wolde, T. T., "The EU Noise Policy and Its Research Needs", *Revista de Acústica* **23**, No.3-4, pp. 15-20, (2002).

Young, H. D., "Statistical Treatment of Experimental Data. An Introduction to Statistical Methods", McGraw-Hill (1962)

Appendix

CAUSES

Single vehicle

Road Noise Origin

Multiple vehicles

▶ Air interaction ◀

Description

Noise produced by the vehicle when moving against air particles. Especially important with high speed and low aerodynamic of vehicles.

Variables

- Speed
- Vehicle aerodynamic

Wind

▶ Vehicle mechanisms ◀

Description

Noise produced basically by three ways: Engine ventilation (important at low speed: urban traffic), transmission and gearbox, and engine.

Variables

- Speed
- Gradient
- Type of vehicle (HGV)

▶ Wheel-road interaction ◀

Description

Wheel vibrations and pressure fluctuations of air inside tyre drawings, bring about noise emissions which are particularly significant for light vehicles at high speed.

Variables

| - Speed | |
| - Surface type | Tyre type |

VARIABLES

Traffic Flow

Noise for multiple vehicles

Converts single vehicle noise into line sources. The more traffic, the more accurate these line sources are. Noise seems to increase logarithmically with this parameter.

Speed interaction

The more traffic the less speed vehicles can develop.

Variables

- Time of the day
- Road type

Time of the day

Traffic Flow interaction

Depending on the time of the day, traffic flows change, reaching maximum and minimum peaks at day and night times respectively.

Variables

- Country

Country

Time of the day interaction

According to the costumes of each country time peaks will be different

Speed

Tyre interaction

High velocities (>70 Km/h) in standard vehicles can make this noise source comparable with engine noise or even louder.

Engine noise interaction

Low velocities make engine ventilation work and radiate noise. For high speed engine noise remains nearly constant.

Aerodynamic interaction

Aerodynamic noise variation law doesn't have a proportional tend. The relationship is quite complex: Speed variations at less than 50Km/h have small effects, whilst at more than 70 Km/h effects are pretty noticeable.

Variables

| - Traffic flow | Gradient |
| - Road type | Atmospheric factors |

Road type

Traffic flow interaction

Traffic usually has same proportions according to road types.

Speed interaction

Road type represents a constraint for vehicle speed, because of speed limits.

Surface type interaction

High quality materials will usually correspond to important roads (Motorways, A)

HGV

Engine noise interaction

This is the main noise source for this kind of vehicles at any range of speed. This noise has to be considered apart from the noise produced by standard vehicles.

Gradient

Engine noise interaction

Road slope will modify the number of revolutions developed by the engine and consequently will vary the noise emission.

Speed interaction

Downward or upward slopes might increase or reduce speed respectively.

Surface type

Tyre interaction

Reductions up to 9 dBA could be reached by the application of porous asphalt instead of a pavement without any treatment

Variables

Road type
Rain

▶ Atmospheric factors ◀

Wind

Wind effect has similar consequences in noise emission than when vehicle moves against air. Wind might easily reach speeds of 50 km/h.

Rain on asphalt

Wet pavements increase noise radiation from wheel-road surface interaction (2-4dBA). However, porous asphalts suffer a minor enhancement than conventional pavements.

Rain, snow, fog

Adverse atmospheric conditions generate a more careful driving, and subsequently a reduction in the average speed.
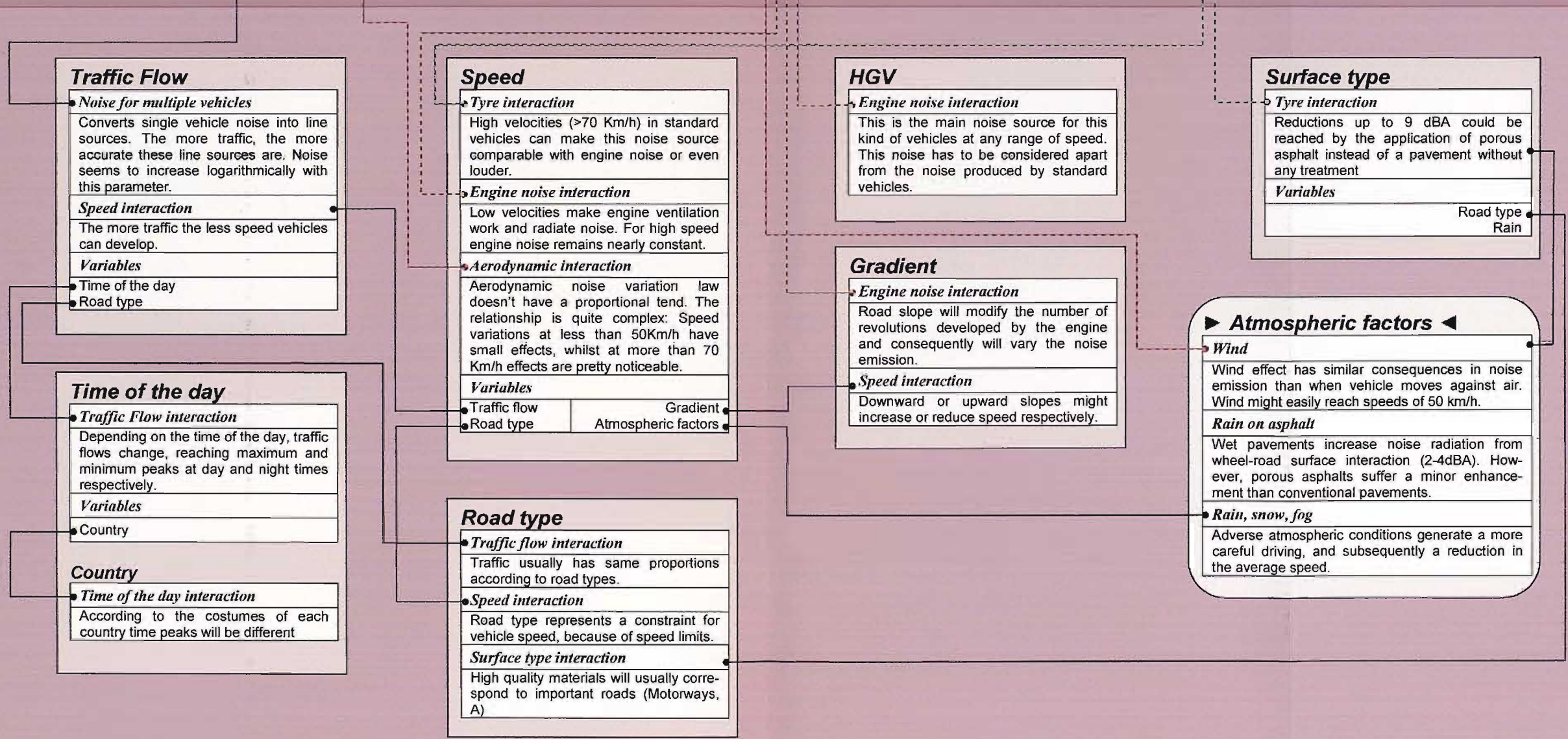
Figure A.1 *Flow diagram representing the most relevant causes of road traffic noise and the variables that make this noise louder or quieter.*